# EFFECTS OF PATTERNED TOPOGRAPHY ON BIOFILM FORMATION

By

RAVIKUMAR VASUDEVAN

A DISSERTATION PRESENTED TO THE GRADUATE SCHOOL
OF THE UNIVERSITY OF FLORIDA IN PARTIAL FULFILLMENT
OF THE REQUIREMENTS FOR THE DEGREE OF
DOCTOR OF PHILOSOPHY

UNIVERSITY OF FLORIDA

2011

To my beloved parents and family
To my cherished gurus
To my dearest wife

ACKNOWLEDGMENTS

I am deeply indebted to Dr. Ronald Baney and Alan Kennedy for the providing me with the unique experience of pursuing a doctoral degree. I would like to thank Prof. Wolfgang Sigmund for introducing me to Dr. Ronald Baney and a research environment at this University. I would also like to thank my committee members Prof. Christopher Batich and Prof. Brij Moudgil for their inspirational teaching and advice. I am grateful to external committee member Prof. Ben Koopman for his support and encouragement.

I would like to extend special thanks to Dr. Priscilla Phillips for her unstinting support in performing biofilm research and Dr. Edward Mckenna for his part in our collaborative wetting research. I would also like to thank them for their company, the extensive discussions about problems in research and some such. I would like to thank Megan Merritt for providing *enterobacter cloacae* growth data over the 48 hour period.

I would like to recognize the help of all the staff members from the nanoscale research facility (NRF), major analytical instrumentation center (MAIC) and particle engineering research center (PERC) for making this research possible.

I would like to thank Dr.Gregory Schultz for his advice and for allowing me to use his lab space for the biofilm experiments. I would also like to thank Afifa Hamad, Qinping Yang and Angel for their advice relating to biofilm research.

I would also like to thank the Baney research group members Edward McKenna, Sunhwan Yeo, Drs.Le Song, Lewin Jin, Chunghao Shih, Ting Cheng and Aniket Selarka for their critical suggestions.

I would like to express my heartfelt gratitude to my high school chemistry teacher Prof. K. Nagarajan who whet my appetite for the sciences and kindled my interest in pursuing a scientific career.

I would like to thank my parents, Vasumathi and Vasudevan, my wife Sowmya, my kin, Rajesh, Sukanya, Bhanumathi, Sankaran and Siddharth; without their support and encouragement I would not have made it to my defense. Also, not to say the least my heart goes out to Satyajit, Sonalika, Sundararaman and all my friends who have made my life so joyous and enjoyable through their company.

Finally, I would like to thank that big pot of possibilities ‘chance’.

TABLE OF CONTENTS

page

ACKNOWLEDGMENTS ..... 4

LIST OF TABLES ..... 9

LIST OF FIGURES ..... 10

LIST OF ABBREVIATIONS ..... 15

ABSTRACT ..... 17

CHAPTER

1 INTRODUCTION ..... 19

Research Approaches Used In This Dissertation ..... 23
Gap Analysis ..... 23
The Confinement Approach ..... 27
Topography group 1: pit and pillar type hexagons ..... 28
Topography group 2: cross topography ..... 29
The Wetting Approach ..... 29
Rationale for Scale of Chosen Topography ..... 31

2 LITERATURE REVIEW ..... 34

Eukaryotic Cell Topography Interactions ..... 35
Response of Algal Spores to Topographical Surfaces ..... 39
Biofilm Formation on Surfaces ..... 43
Defining Biofilms ..... 44
Structure and Function of Biofilms ..... 44
Biofilms in the Environment ..... 46
Medical Biofilms ..... 47
Quorum sensing ..... 48
Catheter associated urinary tract infections (CAUTI) ..... 50
Bacterial Adhesion ..... 53
Forces involved in bacterial adhesion ..... 53
Studies on attachment to surfaces ..... 56
Biofilm Growth Protocols ..... 59
Bacterial Nutrient Conditions ..... 60
Characterization of Bacterial Colonization ..... 61
Microscopy ..... 61
Quantification of biofilm growth ..... 62
Wetting Effects of Patterned Topographical Surface Designs for Inhibiting Biofilm Formation ..... 65

Fabrication Strategies for Nonwetting Surfaces ..... 65
Modeling Contact Angle Hysteresis ..... 70

3 MATERIALS AND METHODS ..... 77

Materials ..... 77
Materials Used for the Confinement Approach ..... 77
Nutrient medium ..... 77
Test material ..... 78
Bacterial test species ..... 78
Materials Used For The Wetting Approach ..... 79
Methods Used for the Confinement Approach ..... 79
Duration of the Test ..... 79
Fabrication of Patterned Topography for the Confinement Approach ..... 80
Scanning Electron Microscopy ..... 81
Profilometry ..... 82
Primers Used in the Study for polymerase chain reactions (PCR) ..... 83
Biofilm Growth Protocol ..... 83
Confocal Laser Scanning Microscopy (CLSM) ..... 84
Plate Counts ..... 85
Bio-Timer Assay (BTA) ..... 86
Calibration curve ..... 86
Image analysis ..... 87
Antibiotic Susceptibility ..... 87
Quantitative Polymerase Chain Reaction (qPCR) sample preparation ..... 88
Standard curve ..... 89
Quantitative real time PCR (qPCR) plate preparation ..... 90
Quantitative Reverse Transcriptase PCR (RT-qPCR) sample preparation ..... 91
Methods Used for the Wetting Approach ..... 93
Fabrication of Undercut Topographical Surfaces for the Wetting Approach ..... 93
Breakthrough Pressure Measurement ..... 94
Imaging and Measurement of Static and Dynamic Water Contact Angles ..... 95
Statistical Methods ..... 96

4 RESULTS AND DISCUSSION ..... 98

The Confinement Approach ..... 98
Characteristics of the Test Topography ..... 98
*Pseudomonas Aeruginosa* Biofilm Formation ..... 102
Morphology of biofilms on patterned topography ..... 102
Quantitative and phenotypic evaluation of patterned topography on biofilm formation ..... 103
*Staphylococcus Aureus* Biofilm Formation ..... 109
Morphology of biofilms on patterned topography ..... 109
Quantitative and phenotypic evaluation of patterned topography on biofilm formation ..... 115
*Enterobacter Cloacae* Biofilm Morphology ..... 123

The Wetting Approach ..... 126
Characteristics of Test Topography ..... 127
Breakthrough Pressure Analysis ..... 128
Triple Phase Contact Line Analysis ..... 129
Discussion ..... 134
The Confinement Approach ..... 134
The Wetting Approach ..... 142

5 CONCLUSIONS AND SUGGESTIONS FOR FUTURE WORK ..... 145

Conclusions ..... 145
Suggestions for Future Work ..... 146

APPENDIX

A SEM IMAGING OF SAMPLE WITH AND WITHOUT MECHANICAL TREATMENT FOR PLATE COUNT PROTOCOL FOR *PSEUDOMONAS AERUGINOSA* ..... 150

B *PSUEDOMONAS AERUGINOSA* ROCHESTER STRAIN BIOFILM FORMATION ..... 151

C MATLAB CODE FOR ANALYZING BTA IMAGES FOR COLOR CHANGE ..... 152

D POLYMERASE CHAIN REACTION DATA, GRAPHS AND GEL RESULTS ..... 154

LIST OF REFERENCES ..... 155

BIOGRAPHICAL SKETCH ..... 174

LIST OF TABLES


| Table | | page |
|---|---|---|
| 1-1 | Medical biofilms (*3*) | 19 |
| 3-1 | Primers used for the qPCR and RT-qPCR tests | 82 |
| 3-2 | Constituents and corresponding volumes for qPCR | 90 |
| 4-1 | Dimensions of topography used for bacterial testing | 98 |
| 4-2 | Material characteristics for the samples prepared for biofilm tests | 102 |
| 4-3 | Log reduction data from antibiotic susceptibility experiment along with corresponding inference for SH1000 biofilm formation | 118 |
| 4-4 | Example tests: material, bacterium, protocol and results | 144 |
| D-1 | Real-time PCR quantification data – SH1000 qPCR | 154 |

LIST OF FIGURES


Figure page

1-1 Total hospital acquired infections (1,195,142 outside of ICUs) ( for the year 2002, in the US, consisted of 4 major categories: blood stream infections..... 20

1-2 Sharklet™ response over 21 days (A,C,E,I) and (B,D,F,J) representing 2, 7, 14 and 21 days of static immersion in high nutrient conditions(*17*). ..... 25

1-3 Illustration of current major mechanisms of colonization ..... 26

1-4 Hexagonal pit and pillar type topography design ..... 27

1-5 Cross type topography design ..... 28

1-6 Parts of undercut patterned topography ..... 29

1-7 Effect of feature geometry on wetting ..... 31

2-1 Summary of literature review topics and interconnections..... 34

2-2 Types of topographies used in the algal spore tests. A, 5µm by 5µm spaced pilars; B, 5µm by 5µm spaced pits; C, 5µm by 20µm spaced channels; D, ..... 41

2-3 *Ulva linza* spore attachment reduction due to smaller size features ..... 43

2-4 Illustration of a hypothetical wound biofilm formation following the steps reversible attachment, EPS production and irreversible attachment ..... 45

2-5 SEM images of a mature PAO1 biofilm on pig skin post 24 hour (6 cycle) negative pressure therapy with saline instillation: a) PAO1 cells embedded ..... 47

2-6 Universal quorum sensing autoinducer 2 molecule for interspecies communication, originally isolated from *vibrio harveyi (101)* ..... 49

2-7 Potential problems in a Foley catheter (*18*) ..... 51

2-8 Usage nutrient media for testing biofilm formation on artificial surfaces, data synthesized from articles dating 1983 through 2011 ..... 60

2-9 Processes available for the fabrication of nonwetting surfaces (adapated from (*165*))..... 66

2-10 Examples of super-hydrophobic surfaces fabricated using various methods (A) SEM image of ZnO nanorods, insets showing XRD results <001>..... 67

2-11 Examples of patterned topographies used for testing wetting models with contact angle data (A) 1µm silicon pillars (*176*) (B) another example..... 68

2-12 Young equilibrium contact angle on a smooth surface ..... 70

2-13 Wenzel and Cassie-Baxter type wetting modes ..... 72

2-14 Variation of apparent contact angle on an alkyl ketene dimer surface with variation of the probing liquid: various ratios of 1,4-dioxane and water (*173*)..... 73

2-15 Gao-McCarthy thought Experiment: (A) Hypothetical question, how do forces at A and B affect force balance at C? (B) Demonstration that TPCL. ..... 74

3-1 Fabrication process schematic for fabricating patterned topography on PDMSe ..... 80

3-2 Growth protocol (A) petridish growth container with 20ml of TSB (B) sample arrangement within chamber to simulate near identical conditions for the ..... 83

3-3 Plate count protocol (A) petridish from which 8mm diameter circular pieces are punched out (B) punchouts are then placed in 5ml PBS. ..... 85

3-4 Fabrication process schematic for topographies for water wetting studies..... 94

3-5 Schematic view of the breakthrough pressure apparatus..... 95

3-6 Receding contact angle measurements (A) erroneous (B) correct method ..... 95

4-1 SEM images of the test topography on PDMSe. Representation: A&B - 2µm, C&D - 7µm E&F - 17µm hexagonal pits and G&H 2 micron cross..... 99

4-2 SEM images of the test topography on PDMSe. Representation: A&B - 5µm, C&D - 11µm E&F - 21µm hexagonal pillars and G&H Sharklet™..... 100

4-3 5 micron cross topography (A) Top down view of the 5µm wide, 25µm long intersecting beams spaced by 5µm S – spacing, E-E – edge to edge..... 101

4-4 Biofilm characterization methods used for topographies testing the confinement approach to inhibit biofilm formation..... 101

4-5 Plate count numbers following 7 day PAO1 biofilm growth on topography and smooth PDMSe surface. Error bars represent one standard deviation..... 103

4-6 Plot of total number of cells calculated from qPCR (hatched bars) and viable cells as plate counts CFU/ml (solid bars) for PAO1 on the various patterned .. 104

4-7 *P. Aeruginosa* bacterial morphology on smooth PDMSe after 7 days. (A) & (B) black arrow - dispersed cells (C) & (D) denser coverage..... 105

4-8 *P. Aeruginosa* bacterial morphology on 2µm pit topography after 7 days. (A) & (B) dispersed cells (black arrow) (C) & (D) disperse coverage..... 105

4-9 *P. Aeruginosa* bacterial morphology on the 7µm pit topography after 7 days (A) & (B) dispersed cells (black arrow) (C) & (D) black arrow – gradual ..... 106

4-10 *P. Aeruginosa* bacterial morphology on the 17µm pit topography after 7 days (A), (B) & (C) dispersed cells (black arrow) (D) black arrow – gradual change 106

4-11 *P. Aeruginosa* bacterial morphology on the 5µm pillar topography after 7 days (A), (B) & (C) dispersed cells (black arrow) (D) black arrow – gradual..... 107

4-12 *P. Aeruginosa* bacterial morphology on the 11µm pillar topography after 7 days (A), (B) & (C) dispersed cells (black arrow) (D) black arrow – gradua ..... 107

4-13 *P. Aeruginosa* bacterial morphology on the 21µm pillar topography after 7 days (A), (B) black arrow - dispersed cells; red arrow - cell curving over ..... 108

4-14 *P. Aeruginosa* bacterial morphology on the 2µm cross topography after 7 days (A) & (B) black arrow - dispersed cells; red arrow - cell curving over..... 108

4-15 *P. Aeruginosa* bacterial morphology on the Sharklet™ topography after 7 days (A) black arrow - dispersed cells; black circles – bending and attached .. 109

4-16 *S. aureus* bacterial morphology on smooth PDMSe after 7 days (A) & (B) black arrow – dense coverage; red arrow – cells curving over curvature ..... 110

4-17 *S. aureus* bacterial morphology on the 2µm pit topography after 7 days (A) & (B) black arrow – dense coverage (C) & (D) black arrow - isolated cells..... 110

4-18 *S. aureus* bacterial morphology on the 7µm pit topography after 7 days (A) & (B) black arrow – dense coverage; red arrow – cells curving over curvature ... 111

4-19 *S. aureus* bacterial morphology on the 17µm pit topography after 7 days (A) & (B) black arrow – dense coverage; red arrow – cells curving over curvature 111

4-20 *S. aureus* bacterial morphology on the 5µm pillar topography after 7 days (A), (B), (C) & (D) black arrow – isolated cells; red arrow – small cluster ..... 112

4-21 *S. aureus* bacterial morphology on the 11µm pillar topography after 7 days (A) & (B) black arrow – dense coverage; red arrow – cells curving over ..... 112

4-22 *S. aureus* bacterial morphology on the 21µm pillar topography after 7 days (A) & (B) black arrow – dense coverage; red arrow – cells curving over ..... 113

4-23 *S. aureus* bacterial morphology on the 2µm cross topography after 7 days (A) & (B) black arrow – dense coverage; red arrow – cells curving over ..... 113

4-24 *S. aureus* bacterial morphology on the Sharklet™ topography after 7 days (A) & (B) black arrow – dense coverage; red arrow – cells on the top..... 114

4-25 Example biofilm images on PDMSe tympanostomy tubes (A) *p. aeruginosa* biofilm and (B) *s. aureus* biofilm. Black arrow – dense coverage ..... 114

4-26 Biotimer assay results post 7 days of *s. aureus* SH1000 growth protocol in terms of mean PE CFU/ml. Error bars represent one standard deviation..... 116

4-27 Biotimer assay results post 7 days of *s. aureus* SH1000 growth protocol in terms of colour change time. Error bars represent one standard deviation. ..... 116

4-28 The correlations of log CFU/ml versus time required for color switch from red to yellow for planktonic s. aureus cultures used as calibration curves in BTA .. 117

4-29 Plot of total number of cells calculated from qPCR (hatched bars) and viable cells as mean PE CFU/ml (solid bars) for *Staphylococcus aureus* SH1000 ..... 119

4-30 Relative arcA gene expression levels on patterned topography and smooth PDMSe (normalized with 16S rRNA expression) represented as a ratio..... 120

4-31 Real-time PCR fluorescence intensity amplification chart – SH1000 qPCR. Top red box indicates fluorescence intensity of 16s planktonic expression..... 121

4-32 Oxacillin susceptibility results in terms of mean PE CFU/ml versus apparent contact angle. Displays no significant trend..... 122

4-33 Oxacillin susceptibility results in terms of mean PE CFU/ml versus recessed area fraction. Only in the case of hexagonal pillars. ..... 123

4-34 Confocal images of *e. cloacae* growth on silicone elastomer (courtesy: Megan Merritt, ERDC, MS)..... 124

4-35 Confocal images *enterobacter cloacae* growth silicone elastomer over a 48 hour period (courtesy: Megan Merritt, ERDC, MS) A: 11µm hexagonal pillars, 124

4-36 Confocal images *enterobacter cloacae* growth silicone elastomer over a 48 hour period (courtesy: Megan Merritt, ERDC, MS) A: 11µm hexagonal pillars, 125

4-37 Confocal images *enterobacter cloacae* growth silicone elastomer over a 48 hour period (courtesy: Megan Merritt, ERDC, MS) A: 2µm cross pattern..... 126

4-38 Example image: 10µm wide hexagonal array spaced by 3µm..... 127

4-39 Classification of samples based on extent of under and height of features..... 128

4-40 Collected view of the breakthrough pressure data on all the undercut patterned topography tested. ..... 1289

4-41 Average (30µm through 100µm) breakthrough pressure versus etch type; A and B represent statistically significantly different groups. ..... 131

4-42 Average (20µm by 6µm-24µm) breakthrough pressure versus etch type; A, B and C represent statistically significantly different groups. ..... 131

4-43 Comparison of breakthrough pressure on 10&20µm samples versus etch condition; asterisk represents statistically significant difference ..... 131

4-44 Advancing and receding water contact angles on 10µm through 100µm wide surfaces spaced apart by 3µm. Error on all data points is within 2 degrees. .... 132

4-45 Advancing and receding water contact angles on 20µm wide surfaces spaced apart by 3µm through 96µm. ..... 133

4-46 Advancing water contact angles versus solid wetted area fraction on the normal wafer, with theoretical predictions for 20µm spaced apart samples..... 133

4-47 Advancing water contact angles versus solid wetted area fraction on the normal wafer, with theoretical predictions for 20µm spaced apart samples..... 134

4-48 Previous study biotimer assay results post 7 days of SA growth protocol. Error bars represent one standard deviations(*131*) ..... 136

4-49 5µm hexagonal pillar perspective view, black dimension arrow – indicates artifact of etching, about 0.69µm in diameter..... 137

4-50 Hypothetical snapshot of the biofilm formation process on day 7. Topography influences bacterial adhesion within a certain size scale..... 142

4-51 Contact angle images for 20µm spaced by 24µm with a $\varphi_S$ of 0.19 (A) 15° on cleaned, (B) 144° on surface coated with $C_4F_8$ plasma ..... 143

A-1 Sample areas on the 10µm honeycomb pattern: 1) with sonication and vortexing; 2) without sonication and vortexing..... 150

B-1 Number of colony forming units following 21 day biofilm growth on hexagonal pit, pillar, cross pattern, Sharklet$^{TM}$, and smooth PDMSe surface. ..... 151

LIST OF ABBREVIATIONS

| | |
|---|---|
| AB | Acid-base |
| BSI | Blood stream infections |
| BTA | Bio-timer assay |
| BT-PR | Biotimer phenol red |
| CAUTI | Catheter associated urinary tract infection |
| CB | Cassie-Baxter |
| CF | Cystic fibrosis |
| CFU | Colony forming units |
| DLVO | Derjaguin-Landau-Verwey-Overbeek |
| DNA | Deoxyribonucleic acid |
| DNase | Deoxyribonuclease |
| *E. Cloacae* | *Enterobacter cloacae* |
| EL | Electrical double layer |
| ELP | Early log phase |
| $ERI_{II}$ | Engineered roughness index |
| HAI | Healthcare associated infections |
| IAEA | Image analyzed epifluorescence microscopy |
| ICU | Intensive care unit |
| LV | Liquid-Vapour |
| LW | Lifshitz-van der Waals |
| MRSA | Methicillin-resistant Staphylococcus aureus |
| NCBI | National Center for Biotechnology Information |
| NHDS | National hospital discharge survey |
| NS | Non-specific interactions |

| | |
|---|---|
| NVE | Native valve endocarditis |
| OM | Otitis media |
| *P. Aeruginosa* | *Pseudomonas aeruginosa* |
| PDMSe | Polydimethylsiloxane elastomer |
| PE | Planktonic equivalent |
| PEO | Polyethylene oxide |
| PNEU | Pneumonia |
| PTFE® | Polytetrafluoroethylene |
| qPCR | Quantitative real time polymerase chain reaction |
| RNA | Ribonucleic acid |
| RNase | Ribonuclease |
| RT-qPCR | Reverse transcriptase real time polymerase chain reaction |
| S | Specific interactions |
| SEM | Scanning electron microscope |
| SL | Solid-Liquid |
| SV | Solid-Vapour |
| *S. Aureus* | *Staphylococcus aureus* |
| SSI | Surgical site infections |
| TPCL | Triple phase contact line |
| UTI | Urinary tract infections |
| UV | Ultra violet |
| W | Wenzel |
| Y | Young |

Abstract of Dissertation Presented to the Graduate School
of the University of Florida in Partial Fulfillment of the
Requirements for the Degree of Doctor of Philosophy

# EFFECTS OF PATTERNED TOPOGRAPHY ON BIOFILM FORMATION

By

Ravikumar Vasudevan

December 2011

Chair: Ronald H. Baney
Major: Materials Science and Engineering

Bacterial biofilms are a population of bacteria attached to each other and irreversibly to a surface, enclosed in a matrix of self-secreted polymers, among others polysaccharides, proteins, DNA. Biofilms cause persisting infections associated with implanted medical devices and hospital acquired (nosocomial) infections. Catheter-associated urinary tract infections (CAUTIs) are the most common type of nosocomial infections accounting for up to 40% of all hospital acquired infections.

Several different strategies, including use of antibacterial agents and genetic cues, quorum sensing, have been adopted for inhibiting biofilm formation relevant to CAUTI surfaces. Each of these methods pertains to certain types of bacteria, processes and has shortcomings. Based on eukaryotic cell topography interaction studies and *Ulva linza* spore studies, topographical surfaces were suggested as a benign control method for biofilm formation. However, topographies tested so far have not included a systematic variation of size across basic topography shapes.

In this study patterned topography was systematically varied in size and shape according to two approaches 1) confinement and 2) wetting. For the confinement approach, using scanning electron microscopy and confocal microscopy, orienting

effects of tested topography based on *staphylococcus aureus* (*s. aureus*) (SH1000) and *enterobacter cloacae* (*e. cloacae*) (ATCC 700258) bacterial models were identified on features of up to 10 times the size of the bacterium. *Psuedomonas aeruginosa* (*p. aeruginosa*) (PAO1) did not show any orientational effects, under the test conditions. Another important factor in medical biofilms is the identification and quantification of phenotypic state which has not been discussed in the literature concerning bacteria topography characterizations. This was done based on antibiotic susceptibility evaluation and also based on gene expression analysis. Although orientational effects occur, phenotypically no difference was observed between the patterned topography tested.

Another potential strategy for biofilm control through patterned topography is based on the design of robust non-wetting surfaces with undercut feature geometries, characterized by 1) breakthrough pressure and 2) triple phase contact line model. It was found that height and presence of undercut had statistically significant effects, directly proportional to breakthrough pressures, whereas extent of undercut did not. A predictive triple phase contact line model was also developed.

# CHAPTER 1
# INTRODUCTION

Bacterial biofilms are a major problem in several areas because they resist antibiotic treatments even at very high concentrations (*1*). They can serve as a nidus of infection, resulting in recurring (often chronic) infection and colonization of distal sites within a specimen/organism. This is especially true in organisms with a compromised immune system (*2*).

Table 1-1. Medical biofilms (*3*)

| Human infections | Medical devices |
|---|---|
| Native valve endocarditis (NVE) – vascular endothelium<br>mitral, tricuspid and pulmonic valves | Prosthetic heart valves and vascular grafts (NVE/Prosthetic VE) |
| Otitis media (OM) – inflammation of mucoperiosteal lining | Tympanostomy tubes (OM) |
| Chronic bacterial prostatis – infection of the prostate gland | Endotracheal tubes (CF) |
| Cystic fibrosis – infection of the lungs due to improper mucus production | Venous catheters (BSI)<br>Urinary catheters (UTI) |
| Urinary tract infection (UTI) | Orthopaedic implants |
| Blood stream infections (BSI) | Dental implants (periodontitis) |
| Periodontitis | Contact lenses |

Bacterial biofilms also impact functioning of industrial systems. They can foul pipelines, thus increasing pressure head needed for pumping important fluids such water, oil, and even contaminate them in the process (*4*). They can also be a basis for fouling on ship hulls, leading to excess drag and in increase in fuel costs (*5*). Biofilm formation on ships leads to an estimated 20% increase in fuel costs (*6*). Bacterial biofilms thus represent a major economic and quality of life problem and therefore provide the incentive for studying methods to prevent their formation. Healthcare costs due to pathogenic/opportunistic biofilms are on the rise. Medical biofilms can be broadly divided in to two categories 1) human infections involving biofilms and 2) biofilms on

medical devices (*3*). Table 1-1 summarizes the major types of healthcare associated infections. It has been estimated that in US hospitals, in the year 2002 alone, 1.7 million HAIs occurred with 98,987 casualties (*7*). The overall healthcare cost associated with such infections is estimated at $4.5 billion (*8*). The total estimate is based on the hospital acquired infections (HAIs) reported to national nosocomial infections surveillance (NNIS) obtained from 283 hospitals with 678 intensive care units (ICUs). The national hospital discharge survey (NHDS) data was obtained from 445 participating hospitals. In addition to these, the American hospital association survey supplied data from 5800 hospitals.

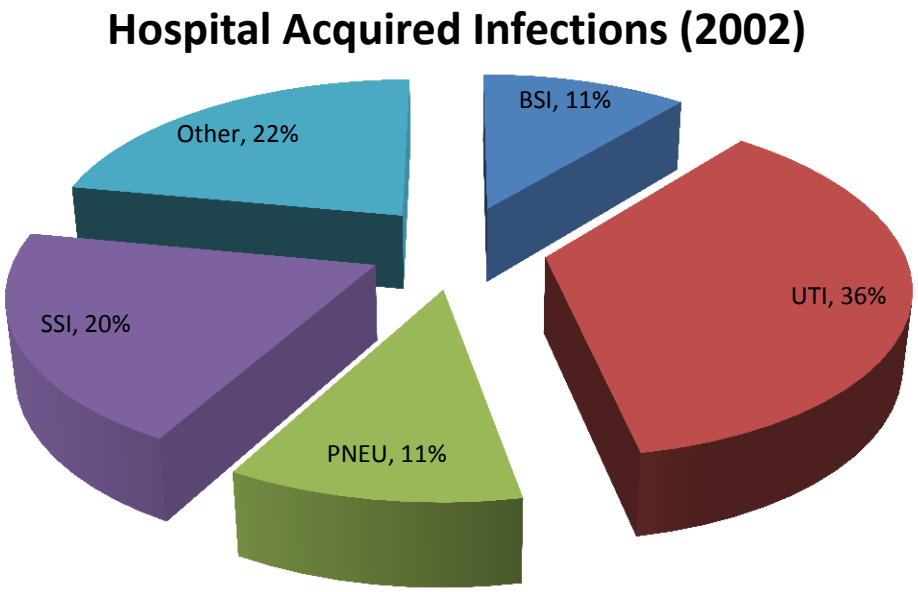


Figure 1-1. Total hospital acquired infections (1,195,142 outside of ICUs) ( for the year 2002, in the US, consisted of 4 major categories: blood stream infections (BSI), surgical site infections (SSI), pneumonia (PNEU), urinary tract infections (UTI) and 22% other infection types (adapted) (*7*).

Figure 1-1 shows a pi-chart of the various types of HAIs reported, data obtained from 1997-2004. Of specific interest to this study is the fact that urinary tract infections represented 36% of all HAIs in 2002 accounting for nearly 13,000 deaths. Of the nearly

99,000 fatalities, pneumonia (35,967) and blood stream infections (30,665) claimed the most casualties(*7*). Invasive medical implants, such as catheters and stents, are major infection sites. The annual cost for catheter related blood stream infections has been estimated to be $60 to $460 million (*9*). *Staphylococcus aureus* (*s. aureus)* (*7, 10*) and *pseudomonas aeruginosa (p. aeruginosa)* (*11*) are among leading causes of nosocomial infections and bacterial biofilm formation on implants.

From the general perspective of pathogenic and fouling bacterial biofilms on medical and industrial materials/devices, several approaches have been put forth in the attempt to solve these problems. One approach is to attach anti-bacterial molecules to surfaces of materials that kill bacteria on contact (*12*). But as bacteria get killed and coat the surface with a layer of dead bacteria, such a surface may become ineffective and get conditioned for further attachment and growth. Another approach is to use specific genetic cues such as quorum sensing, density depend chemical signaling between bacteria capable of acting as global biofilm regulators, to control biofilm growth and/or development (*13, 14*). For example, researchers have synthesized a halogenated furanone, based on macroalgal (seaweed), *desalia pulchra*, furanone extract, which shows enhanced quorum sensing inhibitory activity for some types of biofilm (depending on the species present) (*15*). This approach makes use of unique intercellular signals as a means to control biofilm formations and could present specific solutions to the bacterial biofouling problem. Another approach is to design environmentally benign surfaces based on modifications of surface chemistry/topography which are non-toxic. Polyethylene glycol and similar molecules capable of reducing protein adsorption have been shown in some studies to decrease biofouling (*16*). Recently, the Sharklet$^{TM}$

surface was reported as a potential strategy, using SEM characterization, to inhibit biofilm growth(*17*). In the particular arena of catheter associated urinary tract infections (CAUTIs) there are several complications. CAUTIs account for greater than 40% of all nosocomial infections(*18*). CAUTIs are also estimated to comprise the largest reservoir of nosocomial antibiotic-resistant pathogens(*19*). Urinary catheters have been constructed traditionally from natural rubber latex.

As an approach to prevent CAUTI, natural rubber has been incorporated with antimicrobials and disinfectants. One approach is to continuously drain the catheter, while adding antibacterial agent or disinfectant to the collection bag(*20*). Another possibility is to induce controlled release(*21*) of antimicrobials from glass type or polymeric materials (*22*). However, these interfere with its mechanical properties and biocompatibility and may also have toxicity issues(*23*). Therefore, coatings have been developed as alternatives for the same purpose and these include silver, silver oxide, PTFE® and silicone coatings. Silver and silver oxide based coatings have provided mixed results. In one study with catheterized male patients, an increase in the amount of staphylococcal infection was observed (*24*) and another study questioned the potential benefits silver coated catheters (*25*). A more recent study showed statistically significant differences based on the silver coated catheter use (*26*). PTFE® coated catheters, used mainly for the properties of lubricity and low surface energy, have been shown to be among the most toxic catheter materials (*27*). Hydrogel coatings have also been employed to increase ease of insertion and biocompatibility (*28, 29*). A comparison based on the mechanical properties, reported hydrogel catheters to be inept at handling the stresses that catheters are subjected to (*24*) and in some cases

have been reported to be prone to rapid encrustation (*23*). Polydimethylsiloxane (or silicone) has been used to construct all parts of the urinary catheters and is one of the major structural polymers used in making Foley catheters (*30*). Silicone too has had mixed reports in the literature with regard to its ability to prevent fouling. One report has shown that all silicone materials showed maximum bacterial fouling (*28*), whereas others tout such materials to be most favourable for the inhibition of bacterial adhesion (*23, 31, 32*). In all the materials and coatings used till date there still remain complications due to infection, encrustation and blocking due to bacterial contamination. There is a definite need for better materials for preventing biofilm formation and lengthening the life catheters.

## Research Approaches Used In This Dissertation

This study was undertaken in order to bridge the following scientific gaps found in the literature in relation to using patterned topography as an approach to solving the CAUTI problem.

### Gap Analysis

It has been suggested that the mechanism by which topography appears to inhibit biofilm formation is by disrupting colony formation(*17*). According to the experimental conditions used, there are two possible mechanisms by which the surface is colonized by bacteria:

- Random attachment: (A) reversible attachment leading to irreversible attachment/surface motility (B) irreversible attachment
- Growth subsequent to attachment (A) by replication (B) by motility

Random attachment is based partly on the basic forces governing the interaction of surface forces in a solvent. It is also based partly on the modification of the bacterial

response, gene expression regulation, to environmental stimuli. Growth subsequent to attachment mostly depends on genetic responses to environmental stimuli and the internal need to replicate, but physicochemical forces also play a role. Motility includes swimming, gliding and swarming (*33, 34*).

The proposition that biofilm formation is disrupted by colony formation, doesn't state whether one or all of these is/are impeded by the topography. The majority of biofilm formation studies, based on surface interactions, either consider initial colonization and modeling on initial attraction forces over short durations (within 48 hours).

Although this is an important problem, within time periods usually considered, differentiation of bacteria to a biofilm phenotype (Chapter 2: Defining Biofilms) may not have occurred. The findings of such tests might not directly apply to medical device problems.

Also, the nature of quantification is, in most of the cases, based only on microscopic analysis. This implies that a very small area that is probed and statistically significant results are obtained by sampling a number of different regions on very large sample (relatively). The sampling might not include regions with all the different extents of coverage and therefore the numbers might not reflect actual number of bacteria present.

The presence of "functional biofilms" (Chapter 2: Defining Biofilms) has not been part of the test criteria in most cases and definitely not been tested on any of the topographies. The phenotypic ability of bacteria in biofilms, to resist antibiotic treatment is of major importance when considering medical device biofilm studies.

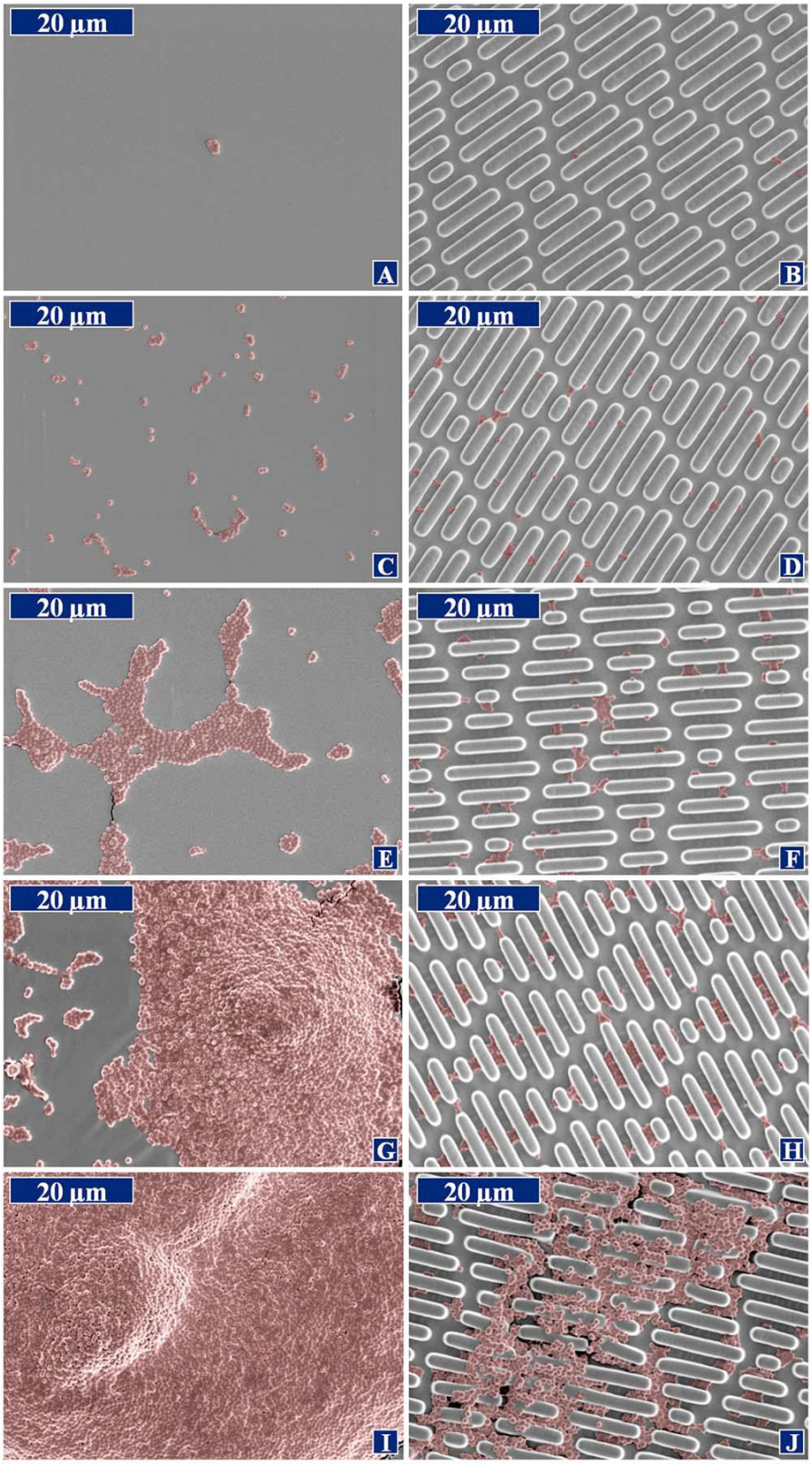


Figure 1-2. Sharklet™ response over 21 days (A,C,E,I) and (B,D,F,J) representing 2, 7, 14 and 21 days of static immersion in high nutrient conditions. Reprinted (adapted) from (*17*). Copyright © 2007, American Vacuum Society..

Another approach related to the use of patterned topography in biofilm inhibition, with potential applications in catheters, is the use of submerged non-wetting surfaces. It has been suggested that wettability or rather the lack of it may be used as a strategy for the inhibition of biofilm formation (*35, 36*). Before such a study can be undertaken, there is a need to ensure the stability of air pockets in the submerged surface. This is similar to the stability of Cassie-Baxter mode of wetting (a state where a droplet sits partial on the micro/nano structures of a surface and partially on air pockets). There are only a few accounts of the study of the stability of such non-wetting surfaces underwater and even those retain the property over very short periods of time, on the order of a few hours (*37, 38*).

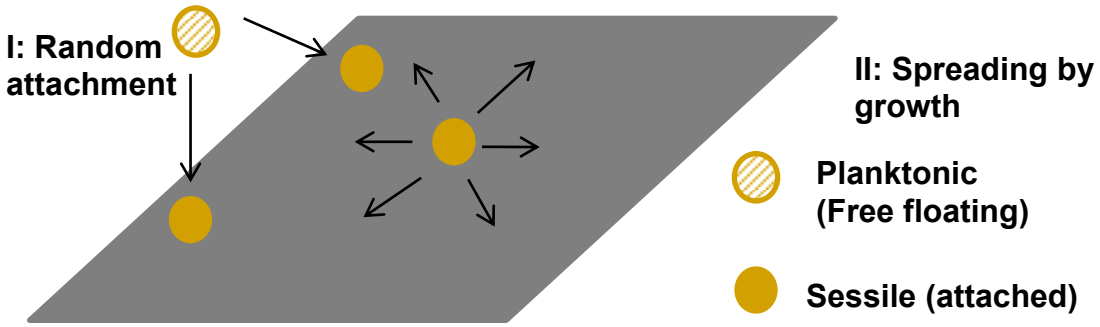


Figure 1-3. Illustration of current major mechanisms of colonization

The important questions for which answers are sought in this study are:

- Gap 1: Which mechanism of biofilm formation is affected by topography?
- Gap 2: Does microscale topography quantitatively reduce biofilm formation compared to the smooth surface for long test durations?
- Gap 3: How does microscale topography affect bacterial transitions to the biofilm phenotype?
- Gap 4: What size range of undercut patterned topography that would be effective at maintaining a stable non-wetted state? How effective will such a surface be in inhibiting biofilm formation?

- Gap 5: Can droplet pinning by discrete undercut patterned topography be predicted accurately? This may be used for future designs, tailored to prevent biofilm spreading, since biofilms depend on water wetting to spread.

The aim of this study is to determine the effectiveness of patterned topographical surfaces in controlling biofilm formation. For this two different approaches were considered. These approaches are explained in detail in the following sections.

- Approach 1: Confinement - Growth inhibition via physical barriers to growth
- Approach 2: Wetting - Inhibition by control of water wetting of surface

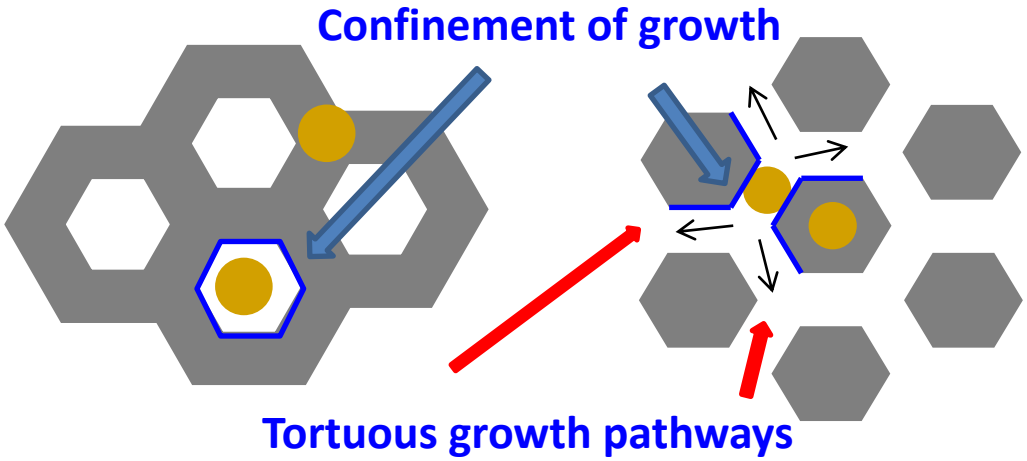


Figure 1-4. Hexagonal pit and pillar type topography design

**The Confinement Approach**

The confinement approach is intended for bridging Gap 1, Gap 2 and Gap 3 stated above. Bearing in mind the CAUTI application, microtopography that was used successfully for inhibition of *ulva linza* settlement was proposed as a solution for the inhibition of *s. aureus* settlement (Figure 1-2). This study was based on the results of SEM imaging indicated a significant decrease ($p<0.05$) in percentage areal *s. aureus* biofilm formation on the topography compared to the smooth surface. It is suggested that the growth of *s. aureus* colony was impeded due to the physical constraints of the topography. So, an initial hypothesis was proposed- “biofilm formation is disrupted by topographical features” (*17*) (Figure 1-3). This is modified and the “Confinement

Hypothesis" is proposed here as, "growing bacterial colonies are confined by abrupt changes in topography".

Based on the above described criteria, the following topographies have been proposed for testing the Confinement Hypothesis.

**Topography group 1: pit and pillar type hexagons**

The reason for selecting a hexagonal array of hexagons was due to the fact that pattern displays the maximum planar symmetry in structures, and therefore present the highest similarity based on bacterial landing site. Also, the original Sharklet$^{TM}$ structure is actually basic hexagonal pattern and this was chosen to both serve as a simpler study system and basis for comparison (Figure 1-4).

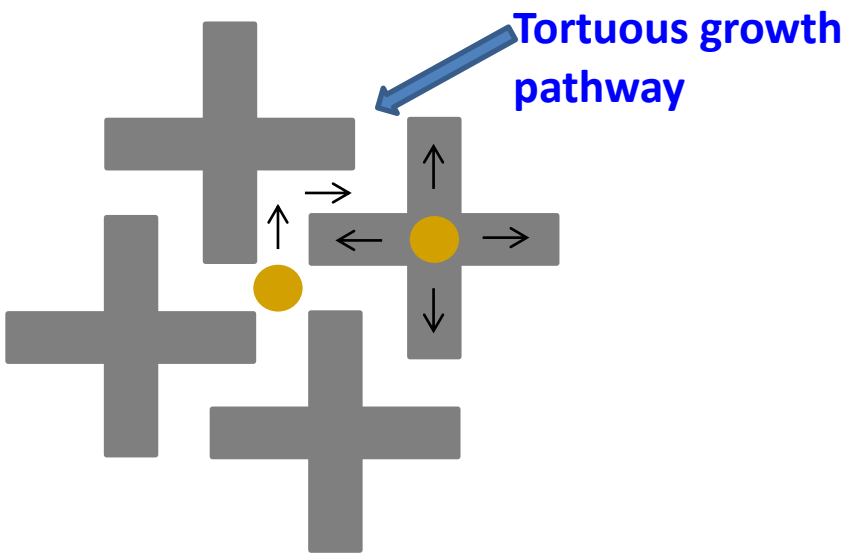


Figure 1-5. Cross type topography design

The reason for testing both pit type configuration in addition to the usual pillar type structures was to observe differences in the quantitative responses in biofilm formation. Previous studies with other microorganisms resulted in predominant valley settlement, as shown in the literature review. This might then provide a means to isolate bacteria in

smaller micro colonies using the pit topography. The quantification of phenotypic state can then be used to provide recommendations for future topography scales.

Only morphological observations have been conducted so far and therefore this would be important to discuss the efficacy of the coating in reducing biofilm based infection. The reason for going with larger aspect ratios was to answer the question, at what point topography doesn't prevent the cells from differentiating to the biofilm phenotype.

**Topography group 2: cross topography**

The cross topography was designed to present a tortuous path for the biofilm formation in addition to the discrete hexagonal array. The object of this topography was to observe whether the repeated change in direction of the topography any quantitative influence on the number of bacteria and their phenotypic state (Figure 1-5).

**The Wetting Approach**

The topography design for testing the wetting approach for bridging Gap 4 and Gap 5 is explained below. The effort reported here for this approach did not involve biological testing, although it was originally intended. Only fabrication and characterization of the wetting properties of novel undercut surfaces were conducted within the time frame that was available for this research study.

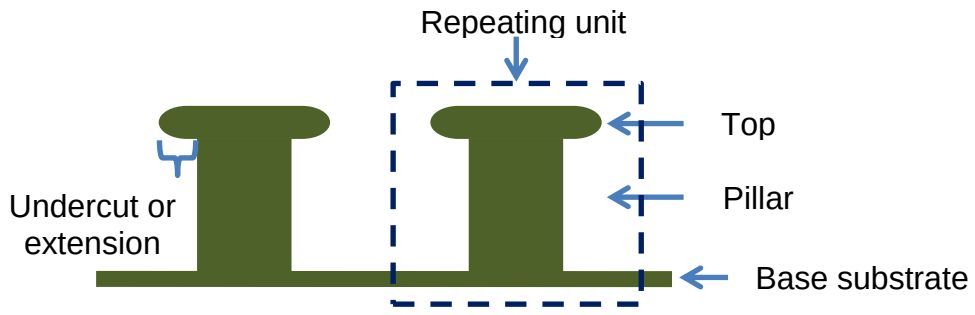


Figure 1-6. Parts of undercut patterned topography

**Topography group 1: non-wetting undercut hexagonal patterned topography:** Another potential strategy for biofilm control through patterned topography is based on the design of robust non-wetting surfaces. Non-wetting surfaces may be used as tools in inhibiting the formation of biofilms. Before this is directly tested, it would be fruitful to understand two specific aspects of non-wetting surfaces with potential applications in biofilm inhibition in mind:

- As stated earlier, the presence of robust submersed air pockets could reduce the area available for colonization by large amount: To what extent can undercut surfaces remain non-wetted under submersion?
- The ability to tailor the contact angle hysteresis of a surface so as to pin the medium of expansion of a colonizing biofilm. This control can be established by developing a predictive model for the contact angle hysteresis

Answers to these questions are explored in this study using patterned topographical surfaces with undercut geometries. An undercut microstructure is a microscale planar piece, top, which sits atop a pillar with portions of the top extending over the dimensions of the top of the pillar (Figure 1-6).

Undercut surfaces have been shown to be capable of displaying a robust Cassie state (*37, 39*). This translates to the stability of air pockets retained by the topography underwater. The manner in which the measurements are made is that, the entrapment of air within the topographies produces a mirror like interfaces due differences between the refractive index of air and silica tops. When the sample is submerged in water in a chamber fitted with a pressure gauge to a cylinder, as the pressure increases it moves from a large fraction of shimmer to no shimmer state.

Initially, a camera was positioned in many different positions to obtain pictures which were to be used to quantify the extent of shimmer due to the air pockets. This approach had to be abandoned because the images produced resulted in too much

noise and it was impossible to isolate the required data. Therefore, a qualitative human observation based study was conducted with two points represent initial and final breakthrough, points correspond initial appearance of no shimmer regions to a final point where there was no shimmer on the entire surface.

The second water wetting test involved the use of undercut microstructures for studying the dynamic apparent contact angles as a droplet advances and recedes on a surface. It would be useful to deconstruct effects due to partial penetration of droplet on to structures from effects due only to surface heterogeneity (Figure 1-7).

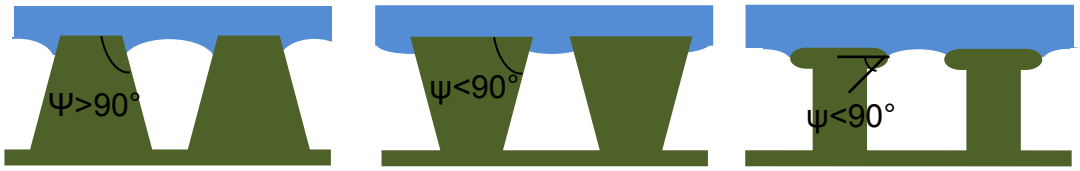


Figure 1-7. Effect of feature geometry on wetting

The pattern used was a symmetric hexagonal array of hexagons since the Cassie-Baxter equation works best in the symmetric case (least anisotropy) and would be a good pattern for comparison (*39*). It would be useful to obtain a predictive equation based on the linear fraction and compare and show that it works as well or even better than the Cassie-Baxter equation which is based on the areal fraction for such a system.

**Rationale for Scale of Chosen Topography**

For designing surfaces, through the confinement approach, for that inhibit biofilm formation, the application of topography as derived from the topographical approach would necessitate topography with submicron features. However, one potential problem is proposed here that, there is an additional concern that bacteria expressing the genes required for the production extracellular polymeric substances (EPS) following initial attachment may produce enough EPS to fill the gaps within ultrafine submicron

trenches, approaching the nanoscale, and thereby gaining a better state of attachment compared to the smooth surface combining mechanical interlocking and bonding. The energy expenditure needed to produce enough EPS to fill submicron trenches near one micron size and above sizes trenches can be expected to increase proportionally size of trenches that need to be filled. Therefore, a region in the micron scale feature size and spacing was selected for testing the inhibition of biofilm formation.

Following that argument, as the size of the feature increases, there should be a threshold value beyond which there is no observable effect on biofilm formation. Therefore, it was decided to conduct a biofilm formation test on systematically varying topography size. The lower limit was close to the size of a bacterium (500nm to 2µm) and the upper limit was as much as 20 times its size.

For designing surfaces through the wetting approach, which inhibit biofilm formation when a sample is completely submerged, the undercut surface design can robustly trap air-water interfaces within the surface of the material, such that less area is exposed for colonization. When the surfaces are not completely submerged, the mechanism of pinning of water droplets is made use of in preventing the advance of the biofilm over the entire surface, which again lessens area available for colonization drastically. For these purposes, the feature sizes have to be capable of supporting the top, while the undercut must be significant enough to display the desired effect (Figure 1-6). Tops equal to or lesser than 5µm were ill suited for this as the pillars were not able to support the tops. Thus top sizes from 10µm onwards through 100µm, approaching a smooth surface were tested and 20µm tops spaced by 6µm, 12µm, 24µm, 48µm and 96µm were chosen to explore the effects of varied spacing on the stability of the air

water interface. In addition, 5 different etch conditions were tested including short pillar, less undercut, normal undercut, thick top and tall pillar were studied (Figure 4-39).

CHAPTER 2
LITERATURE REVIEW

The literature review is organized in terms of the major topics required for understanding the contents of this field. Figure 2-1 summarizes the major topics covered in the literature review and identifies the connections between them. It clarifies the concepts from the three related topics of eukaryotic cell topography interactions, response of algal spores to topographical surfaces and effects of topographical surface on wetting applied to solving the problem of biofilm formation to surfaces.

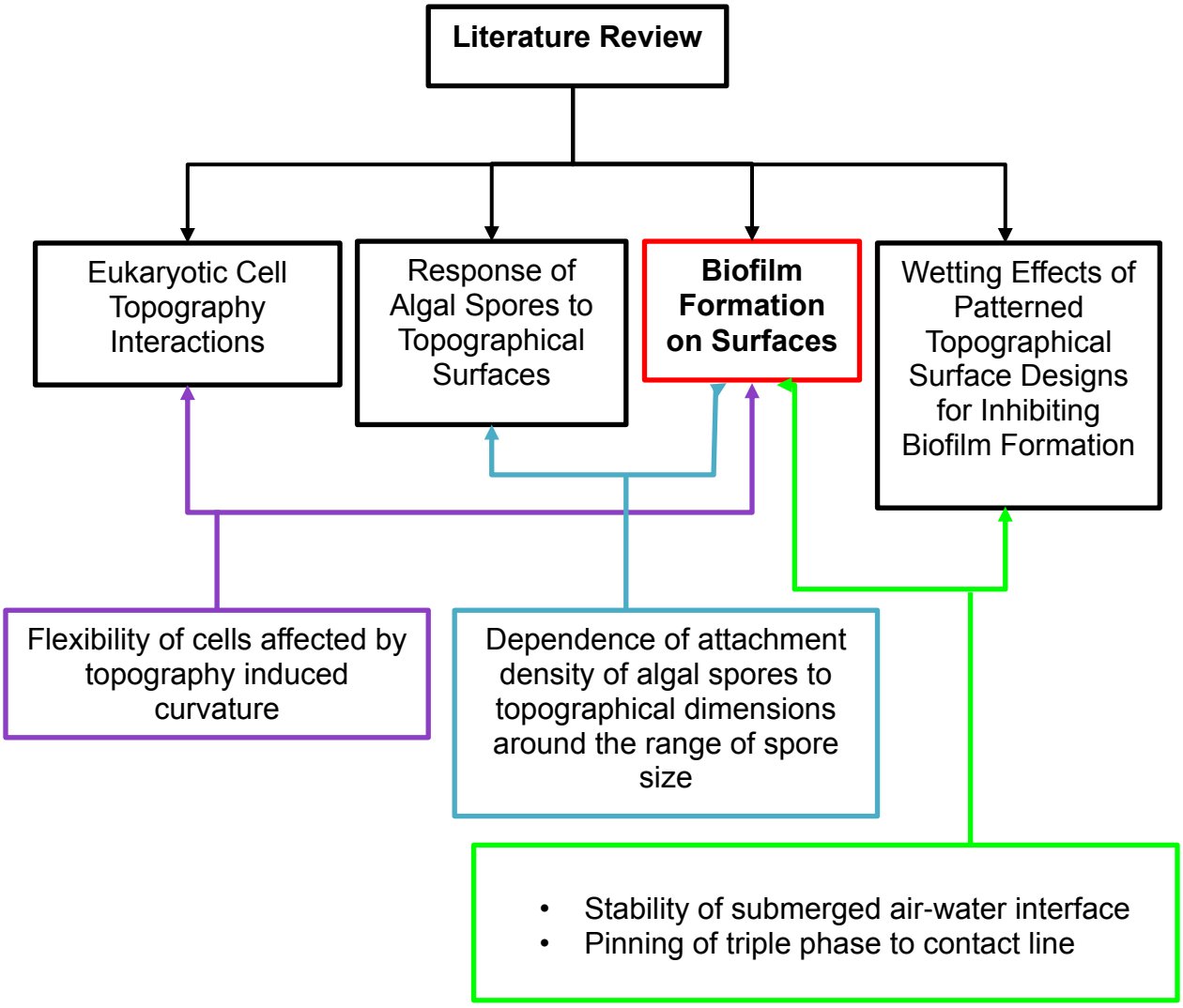


Figure 2-1. Summary of literature review topics and interconnections

## Eukaryotic Cell Topography Interactions

Harrison first showed that nerve cells were capable of growing directionally on closely woven spider web fibers (*40*). The term ‘contact guidance’ was coined by Weiss to describe the guided movement of cells on such fibrous materials (*41*). Patterns of varying adhesiveness were also found to influence the direction of cell locomotion. The orientation of Schwann cells on glass fibers of 13µm diameter was suggested to be due to the spreading of colloidal exudate by capillary action, with fibrous elements of the exudate becoming oriented by shear stresses (*41*). However, it was found that chick heart fibroblasts oriented themselves along the axis of glass fibers of 5µm to 15µm diameter without detectable colloidal exudate (*42*). This suggested that the response of chick heart fibroblasts must be due mainly to the shape of the substratum. In order to avoid the complication of tissue explants, dissociated chick and mouse fibroblasts were shown to align based on cylindrical grooved surfaces (*43*). This helped strengthen the reasoning that substratum shape and not oriented protein adsorption was the main reason for the orientation of the cells. Curvatures of the lesser than 100µm was shown to have an effect on the orientation of chick heart fibroblasts because greater curvatures are slight in comparison with the dimensions of the chick heart fibroblasts. This led to the hypothesis that linear elements of the cell locomotion is limited by curved substrate shape and relevant curvature will cause the cells to expand in the direction of the cell locomotion along unrestricted directions (*44*)

The presence of very close contacts of the order of 0.25µm to 0.5µm thick and 2µm to 10µm wide was observed and named focal contacts. They were observed under the peripheral ends of the discrete cytoplasmic fibres visible in the differential interference image. Interference reflexion microscopy was established as a useful

technique in determining relative separation distances under a cell and to track its movement on this basis (*45*).

Additional evidence for the Shape Hypothesis of contact guidance was advanced in a study where chick heart fibroblasts were cultured on hydrated, air-dried and acid treated collagen fibrils. It was observed that hydrated collagen, which has a 3D network, had bipolar strongly oriented growth whereas the air-dried and acid treated collagen, which have flattened 2D collagen network, showed random growth. The 3D network of collagen fibrils could distort the shape of the cell if the cells aren't aligned properly to the direction of alignment of the fibrils (*46*).

Microfilament bundles may be the reason why the cells are capable of bridging and retaining a stiff base while spreading over grooves. However, microfilament bundles alone are insufficient to explain why the cells orient themselves, even on features smaller than themselves. Another hypothesis was proposed that the maximization of the focal contacts, parts of the cell in direct contact with the substrate (0.25µm to 0.5µm wide and 2µm to 10µm long), probably determine orientation.

Focal contacts were found to be associated with the distal ends of microfilament bundles and it was found that microfilament bundles pass centripetally through the cytoplasm. Direct evidence was also provided to support that hypothesis that microfilament bundles form synchronously with the formation of focal contacts (*46*). Finer features limit focal contact formation in a direction perpendicular to ridge direction while being unrestricted along the ridge and therefore cells may orient themselves to increase adhesion in that direction. For describing cell growth/locomotion on curved

substrates, it may be necessary to include both micro-filament bundles and focal contacts (*47*).

New focal contacts are formed continually from existing ones through lamellipodia or microspikes. In 90% of the cases, cytoplasmic fibers form from the microspikes or lamellipodia and then extend out into while the focal contacts attach under the base of the lamellipodia. Thus, a primary role of the lamellipodia and microspikes is to extrend the cell margin, forming new adhesion and for the extension of cytoplasmic processes. Formation of new close contacts occur independent, both in time and space, of focal contacts and only occur when the extreme margin of the cell is extended for several microns free of the substrate, at 100nm separation, as a lamellipodium. Formation of close contact by lamellipodium is the result of movement of the cytoplasm in to the base of the lamellipodium resulting in an advance of the leading lamella, the required force being transmitted through close contact. Formation of focal contact and stress fibers and movement of cell body through forces developed in the stress fibers(*48*).

On a flat surface where there are no orientational effects, 46.2±1.9 was found to be the average angle of human gingival fibroblasts to an arbitrary axis. For a ridge type topography, for all the conditions regardless of the groove depth and groove/ridge width, the cell alignment was significantly less than 45 ($p<0.001$). Also, with the presence of the hierarchical patterning, the cells were found to orient themselves to the major grooves instead of the micro grooves. The cells were also capable of climbing over ridges and moving in to the grooves demonstrating considerable flexibility. The mechanism of contact guidance has been suggested to have two facets: 1) those with selective adhesion(*43*) 2) the mechanical properties of the system involved in cell

locomotion(*44*). Although insertions of microfilament bundles in to focal contacts and subsequent contractions have been shown to be important in the locomotion of some fibroblasts, other fibroblasts have been shown to be actively motile without either (*49-51*). It has also been suggested that microtubules which have been identified as the prime cytoskeletal element determining cell polarity(*52*), may be more important in contact guidance. It can be inferred from the flexibility of the cells in moving from ridges to grooves that the topography does not provide absolute barriers to cell locomotion (*53*).

It has also been shown that simple step type topographies may be efficient in guiding cells and that cell flexibility may increase the frequency of crossing across step type topographical features. The height of the steps considered is an important factor with heights less than 3µm showing little or no effect in comparison to both controls and the larger steps. The direction of approach also showed a significant effect with the crossover being lower in the ascent (from the bottom) compared to the descent (*54*).

Fluorescence microscopy revealed that given approximately the same amount of cell attachment, 100 percent of tested human fibroblast cells oriented themselves to 1 micron ridge type topography whereas they were randomly oriented on pure silicon. Using TEM it was inferred that additional attachment by mechanical interlocking enabled better attachment to substratum (*55*). Overall, the picture on contact guidance that emerges from a literature analysis suggests that, fine structured filaments and microtubules in a cell's cytoskeleton together with focal adhesion points sense the nature of the topography and likely to respond to it when there is variation that is equal to or larger in size scale compared to these elements. They also depend of the

abruptness of change in some of the curvature. It is important to notice that all studies on contact guidance consist of understand how topography affects cell locomotion than the expansion of colony of cells.

One type of eukaryotic cell which is commonly used for studying/modeling cell topography interactions is the fibroblast and its usual lifespan is about 57 days (*56*). This is extremely large compared to the lifespan of bacteria which multiplies every 57 minutes (*57*). Also, bacteria form biofilms well within this time period. Therefore the concepts explaining the nature of cell motility may not be directly applicable to bacterial interactions with topography.

That said, the flexibility of the exoskeleton of eukaryotic cells varies to a large extent and the ability of cells to crossover topographical barriers is proportional to their flexibility (*54*). Since, bacteria are less flexible compared to cells (*58*), the curvature effects seen for some of the cells which are also less flexible compared to others may be applicable to bacteria as well. The other important research area, which is potentially applicable to topography based research on biofilm inhibition, is the response of algal spore fouling of surfaces.

**Response of Algal Spores to Topographical Surfaces**

Micro-patterned topographies were made with dimensions 5µm, 10µm and 20µm spaced channels (*59*). The channels were 5µm deep and 10,000µm long. The attachment of zoospores of the plant *ulva linza* was test with this to understand the effect of topography. In another experiment, 5µm squares spaced 5µm apart with a 5µm depth was also studied. Attachment assay was performed according to the following procedure. Following the harvesting of *ulva* spores, quadriperm polystyrene culture dishes (Fisher Scientific) (26mm by 76mm leading to a total height of 5mm of culture

medium) were inoculated with 10ml of spore suspension, at a concentration of 2 x $10^6$ spores per ml, was added and incubated in the dark for 60 minutes. Based on these studies it was concluded that topography depth, spacing and type significantly affected the attachment of spores (*60*).

The Sharklet™ topography (Figure 2-2) along with a number of other topographies was tested for porcine vascular endothelial cell (PVEC) attachment and with *ulva linza* zoospores. The size of the features were explored from a minimum 2 µm width by 2 µm micron spacing to 5 µm (20 µm) width by 20 µm (5 µm) spacing. The height varied from a minimum of 1.5 µm to 5 µm. The algal spore assay was as described in the previous article discussion. The study concluded that, settlement was primarily in the valleys of the tested topography and as the spacing increased the settlement was closer to that of the smooth surface.

The Sharklet™ topography with dimensions lesser than that of the spore reduced attachment significantly. In accordance with previous observations, PVEC alignment was much higher on the ridges as well as the channels compared to the smooth surface(*59*).

$$ERI_I = \frac{(r \; x \; df)}{f_D} \tag{2-1}$$

Based on spore settlement data, from the above mentioned studies, an engineered roughness index, Equation 2-1 (a dimensionless ratio) was proposed to characterize patterned topographical surfaces (*61*). The variables are r representing Wenzel roughness, df representing degrees of freedom for movement on the surface and fD representing depressed surface fraction.

This equation was modified to Equation 2-2 in order to make it more predictive by including the number of distinct features (n) in the pattern instead of degrees of freedom which resulted in better correlation with experimental measurements for *ulva* spore settlement (*62*). This equation was used for characterizing biofilm test specimens to provide a basis for comparison of results in this work.

$$ERI_{II} = \frac{(r\ x\ n)}{f_D} \tag{2-2}$$

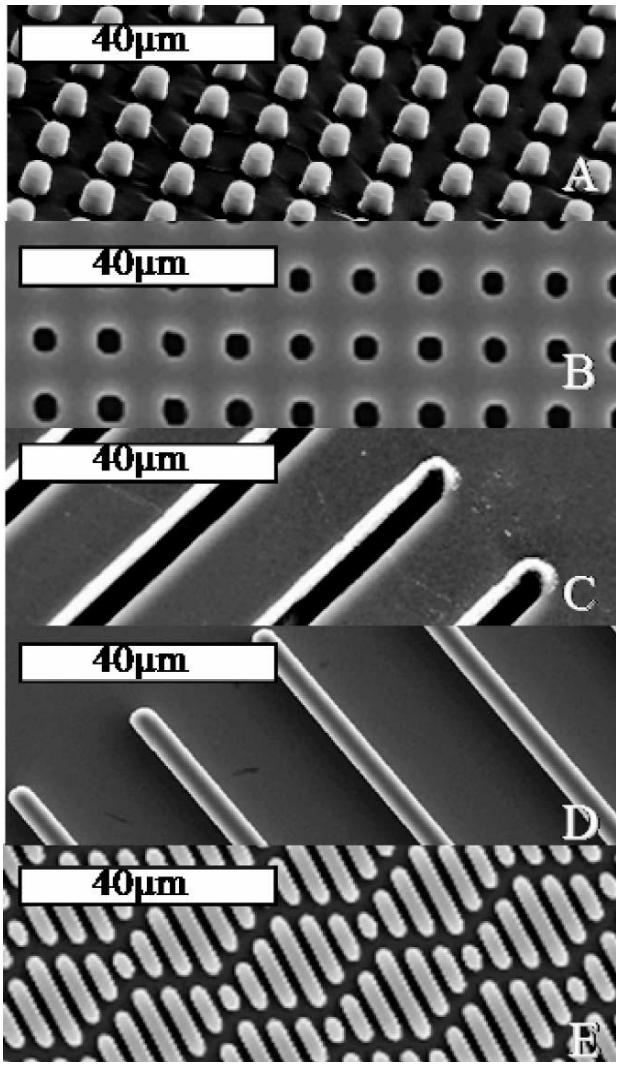


Figure 2-2. Types of topographies used in the algal spore tests. A, 5µm by 5µm spaced pilars; B, 5µm by 5µm spaced pits; C, 5µm by 20µm spaced channels; D, 5µm by 20µm spaced ridges and E; Sharklet™ topography. Reprinted (adapted) with permission from (*59*). Copyright © 2006, Taylor & Francis.

Although this equation empirically predicts settlement to some extent, the use of Wenzel roughness factor and depressed area fraction results in redundant use of areal parameters and can be reduced to a single fraction. It is also not clear how the factor n contributes to the mechanism of settlement inhibition. In systems with flow based on log and stationary phase *cobetia marina* (*c. marina*) settlement it was found that, in a 2 hour test period, there was statistically significantly lesser settlement on the topographies tested compared with the smooth surface. Apart from experimental results the study also proposed the inclusion of a Reynolds number component, based on the size and shape of the organism, to the original $ERI_{II}$ equation (Equation 2-2). A predictive model (Equation 2-3) was obtained by correlating both *ulva* spore and bacterial attachment to $ERII_{II}$ and Re ($R^2$ = 0.77). The predictive model is to serve as one model for different classes of organisms; algal spores and bacteria. In the test topographies used in this study, some features such as hexagonal array of pillars and the triangle-pillar array which are essentially hexagonal arrays have similar fluid flow patterns from every direction. Whereas, the Sharklet™, despite being a hexagonal array, and the ridge topography, have differences in flow pattern based on whether the features are oriented parallel or perpendicular to the flow direction. This wasn't addressed in the study, and thus it is may be incorrect to generalize on this one basis.

$$\log(\frac{A}{Ao}) = (ERI_{II}) * Re * 10^2 \quad (2\text{-}3)$$

Several studies (*59-61, 63*), with various patterned topography with *ulva linza* algal spores, were conducted following the same procedure as described for the spore attachment assay. Although the samples were immersed in nanopure water before the tests were conducted and were supposed to be fully wetted during the tests. The nature

of attachment of the algal spores to the valleys rather than the peaks could be 1) due to an increase in the attachment area and 2) due to signaling by the attached spores to enhance further attachment. Also, the fact that most attachment is observed to be in the valleys suggests that the samples were probably fully wetted. The reduction in the size of the features in at least one dimension (as in Sharklet$^{TM}$) reduced spore attachment. This has been suggested to be due to the reduction in the number of attachment sites (Figure 2-3). Despite the correlations obtained based on these analyses, it is not clear that the terms used in the correlation are causing the effect of decreased settlement.

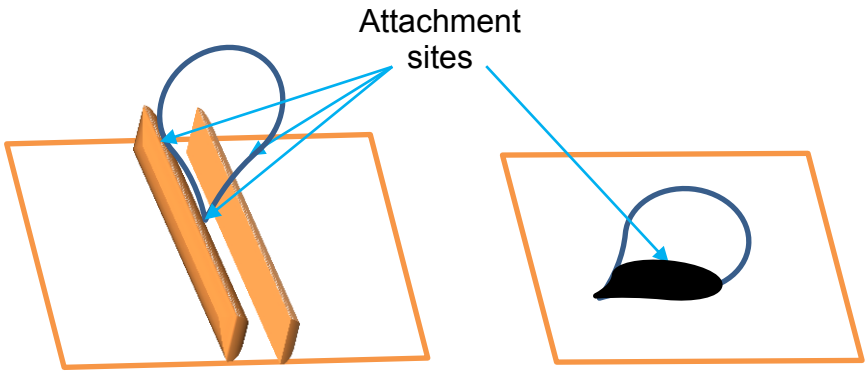


Figure 2-3. *Ulva linza* spore attachment reduction due to smaller size features

**Biofilm Formation on Surfaces**

Distinctly different characteristics between free floating (planktonic) and attached (sessile) bacterial biofilms were not fully appreciated and a great deal of our understanding of bacterial growth from Louis Pasteur and Robert Koch until relatively recently were understood based primarily on planktonic bacterial studies (*4, 64*). With the advent of wide scale computer use coupled with great advances in microscopy and imaging techniques and methods for studying biological molecular mechanisms, many groups have looked more closely into biofilms (*65-73*). Since then, accumulating

evidence clearly suggests that biofilms are a distinctly different form of bacterial existence in which bacteria co-operate to cope with environmental stresses.

**Defining Biofilms**

A generally accepted definition of bacterial biofilms is that biofilms are a population of bacteria enclosed in a matrix of self-secreted polymers (e.g, polysaccharides, DNA, proteins, etc.) attached to each other and irreversibly to a surface(*4*). Although this is widely accepted, another definition of biofilms namely “functional biofilms” has been advanced on the basis of resistance to antibiotics (*74*). In light of analysis of biomaterial colonization and infections, the latter might be more appropriate.

**Structure and Function of Biofilms**

In order to elucidate the now established fact that biofilms are not merely homogeneous biofilms, a uniform dispersion of bacterial cells embedded in a continuous extracellular polymeric substance (EPS) matrix, a number of experiments were carried out in several studies. In one study, micron sized fluorescent latex particles were allowed to settle on to a biofilm, many of which reach the bottom of the biofilms (*75, 76*). According to the original model (*77*), the latex particles should have been pushed out due to growth of bacteria from underneath and the presence of a continuous EPS matrix. This method is now used to determine flow rates within biofilms (*78, 79*).

Another interesting study on the structure of bacterial biofilm and its effect on surface materials were originally based on the hypothesis that microbe induced corrosion should decrease due to depleted oxygen levels near the substratum because of the continuous EPS matrix. However, accelerated corrosion due to formation of aeration cells by diffusion of oxygen through voids is one of the mechanisms of microbially induced corrosion (*80*).

Another particularly noteworthy study showed that chemical profiles obtained using microelectrodes show different values at different locations. This when viewed with confocal scanning laser microsocopy (CSLM), added evidence to the heterogeneity of biofilms (*65, 79*). Flow velocity distribution experiments observed using nuclear magnetic resonance imaging (NMRI) indicated that flow velocities reached zero only near the surface of substrate and not that of the biofilm (*81-83*).

To explain these and other such observations, a more realistic model of a heterogeneous biofilm developed. A heterogeneous biofilm consists of densely clustered micro-colonies covered in EPS, comprising most of the biomass, separated by large voids usually filled by water and strands of EPS known as streamers extending in the direction of flow. In natural and industrial environments they vary from dense, amorphous biofilms to well defined, structurally robust biofilms.

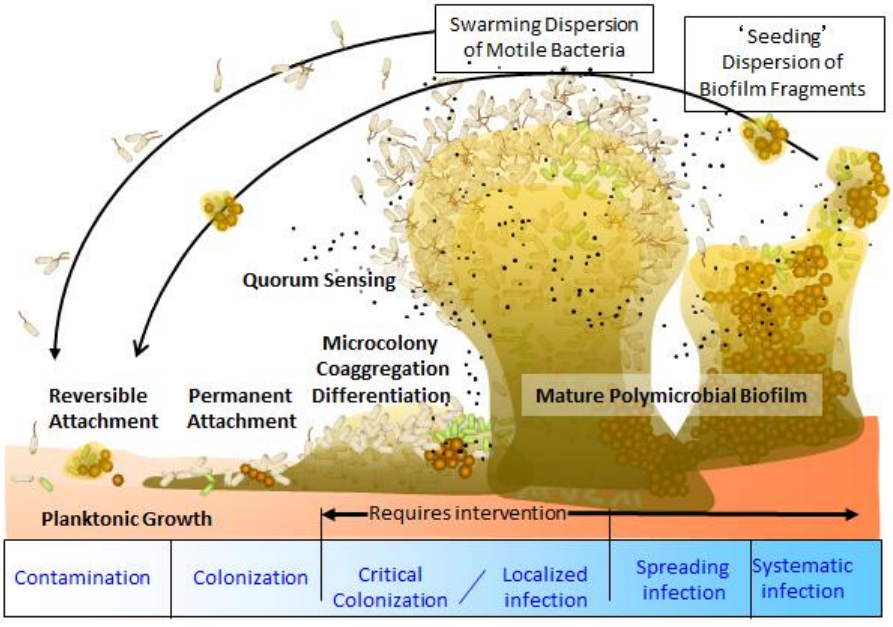


Figure 2-4. Illustration of a hypothetical wound biofilm formation following the steps reversible attachment, EPS production and irreversible attachment and replication, micro-colony formation, differentiation in to biofilm phenotype, release of planktonic cells for colonization of other areas (*84*).

As biofilms age, it has been found that the semi-continuous layer close to the substratum surface of attachment becomes denser and thicker, while the architecture of portions above remain relatively the same(7). It is not clear whether this is due to accumulation of debris or due to growth and accumulation at the bottom(*4*).

Hydrodynamics is very important in the biofilm growth processes, namely cell transport, attachment, growth and detachment. Hydrodynamics is responsible for mass transport to and within the biofilm, as well as biofilm erosion(*85*).

Based on this accumulated understanding, a general picture of biofilm formation has emerged. Figure 2-4 illustrates the process of a hypothetical wound biofilm formation. The details may differ but this is quite typical of most bacteria (*61, 86*).

The ability of bacteria to respond rapidly to changes in their environment is generally termed phenotypic plasticity. This is a major problem when it comes to implanted medical devices because all bodily fluids are abundant in nutrients; the surfaces provide a favorable breeding ground and a means to introduce pathogens into the body's fluid environment (*2, 4, 65, 87-94*). Example images of mature biofilms are given in Figure 2-5.

**Biofilms in the Environment**

It is universally accepted that the only absolute requirement for microbial growth, or any life as we know it for that matter, is water. Thus, there are few habitats that bacteria have not colonized. They have been shown to grow at any available intersection between water and nutrients, even in very harsh conditions such as low pH, high salt concentrations and high temperatures, characteristic of boiling hot spring waters (*88, 95-97*). The microflora of the human body is estimated to consist of nearly

ten to a hundred times the number of human cells (*98*). They are indispensable in many areas (*98*) and can be life threatening in others (*14, 99*).

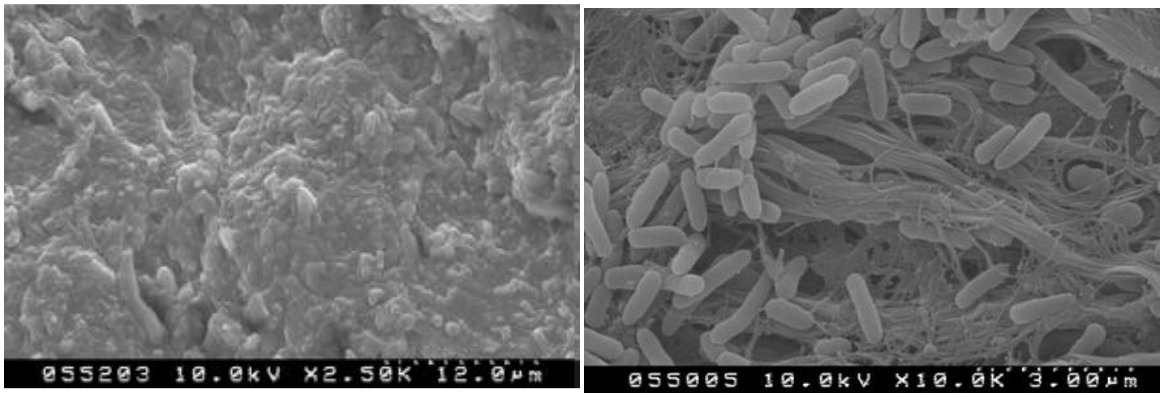


Figure 2-5. SEM images of a mature PAO1 biofilm on pig skin post 24 hour (6 cycle) negative pressure therapy with saline instillation: a) PAO1 cells embedded in EPS matrix attached to pig skin under the instillation port (12 µm scale). B) PAO1 cells attached to the surface of pig skin under the V.A.C.$^{TM}$ port (3 µm scale) (*74*)

**Medical Biofilms**

Bacterial biofilms cause persisting infections associated with implanted medical devices and nosocomial infections. In the formation of mature biofilms an important step involves cell to cell signaling, commonly referred to as quorum sensing. It has been found that bacterial signaling molecules, for example acyl homoserine lactones, are responsible for differentiation of attached sets of bacteria to biofilm phenotype when they reach a certain population density (*87*).

Biofilms offer robust protection to bacteria from antibiotic treatments and the minimum biofilm eradication concentration (MBECs) are typically about 100 to 1000 times the minimum inhibitory concentration (MIC) of planktonic bacteria (*2, 4*). One hypothesis for the increased tolerance of biofilms to antimicrobials is the ability of the extracellular polymeric substances to absorb and delay the passage of these agents. Another hypothesis suggests slower growth rate in biofilm cells could lead less

susceptibility(*3*). Biofilm growth on medical devices has been studied for nearly 3 decades with most of the investigation using basic techniques. They involve plate counting and scanning electron microscopy for the most part. A list of medical device colonization with respect to bacterial species involved is available in the literature. Nosocomial infections by *staphylococcus epidermis* (s. epidermis) and aureus infections lead to the colonization of suture, arteriovenous shunts, mechanical heart valves and catheters. Contact lenses are colonized by *p. aeruginosa* and gram-positive cocci. Endotracheal tubes are colonized a variety of bacteria and central venous catheters are colonized by s. epidermis and other bacteria (*2*).

Central venous catheters are used for administration of fluids, medicine and nutrients. Biofilms have been shown to occur on the outside as well as inner lumen of catheters. Many microorganisms have been identified on these devices including coagulase negative staphylococci (CoNS), *s. aureus, p. aeruginosa, klebsiella pneumoniae (k.pneumoniae)*, *enterococcus faecalis (e. faecalis)* and *candida albicans(c. albicans) (3)*.

**Quorum sensing**

Quorum sensing is the manner in which bacterial gene expression is regulated on the basis of population density. The regulation is carried out by small chemical molecules synthesized by bacteria following patterns of attachment or responses to environmental stimuli (*100*).

Bacterial cell-cell signaling has been shown to be important in the development of *p. aeruginosa* biofilms. Mutant bacteria incapable of producing differentiated biofilm phenotypes were produced by silencing expression of the *lasI* gene. When the autoinducer molecule, acyl homoserine lactone (AHL) was added to the system, it

restored the cells to a biofilm phenotype producing colonies similar to the wild type strain(*87*). It was also shown using a PAO1 model system that, synthetic furanones, based on a natural quorum sensing inhibitors, were capable of inhibiting biofilm formation (*13*). While specific quorum sensing mechanisms based on AHL or an auto-inducing peptide (AIP), found in *s. aureus* biofilms, are known to facilitate communication between bacteria of the same species, it has been found that another signaling molecule auto-inducer 2 (AI-2), appears to be universally responsible for interspecies communication (Figure 2-6) (*101*). Biofilm inhibitors may be designed using AI-2.

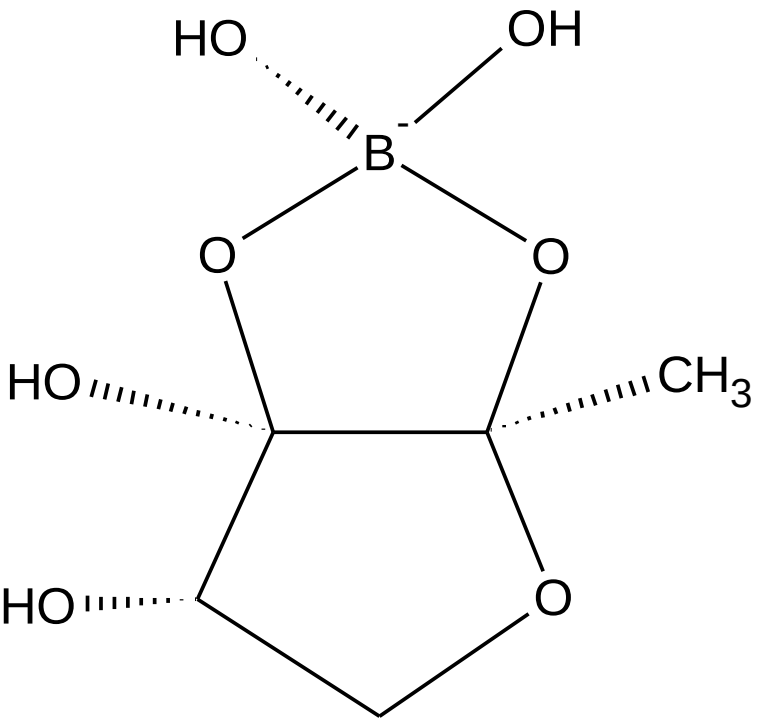


Figure 2-6. Universal quorum sensing autoinducer 2 molecule for interspecies communication, originally isolated from from *vibrio harveyi* (adaptation *(101)*)

Additionally, quorum sensing is not restricted only to communication between bacterial cells. Communication between hosts and microorganisms may also take place through quorum sensing molecules. Such signals are referred to as inter-kingdom

signaling (*102*). An understanding of these communication systems may allow for the development of biomaterials specifically for cell attachment and growth in preference to bacteria. Although there are studies where quorum sensing has been shown to be important, it may not play any apparent role under some conditions. The role of *agr* expression, touted to be an important factor for biofilm formation in *s.aureus* biofilms, under some conditions has no discernible influence. Its role in biofilm formation was found to be dependent on environmental conditions (*103*).

**Catheter associated urinary tract infections (CAUTI)**

Urinary catheters are used for the purpose of preventing urine retention, controlling urinary incontinence, collecting urine during surgery and to measure urine output. They are inserted into the bladder through the urethra. The numbers of patients in which urinary catheters are inserted exceed 5 million every year. Catheter-associated urinary tract infections are the most common type of nosocomial infections accounting for 40% of all hospital acquired infections (*104*). The rate of urinary catheter infection can increase at the rate of 10% per day of catheterization(*3*). *Escherichia coli (e. coli*) leads the list of pathogens causing 26% of nosocomial CAUTI in acute care hospitals, followed by enterococci and *p. aeruginosa* representing 16% and 12% each (*19*).

Short-term catheterization, up to a period of 7 days, results in 10% to 50% of patients having urinary tract infections (*105*). Infecting organisms may enter during insertion or intraluminally from the collection bag through the tube (*3*).

Long term catheterization (greater than 28 days): about 100,000 patients have urethral catheters in nursing homes and many are catheterized for several months. Most of these patients are bacteriuric, detection bacterial contamination in the urine because of infection, by the end of 30 days (*104*).

The Foley catheter, the most common type of catheter has an inflatable balloon to hold its place in the bladder. It was invented in 1936 by Frederick B. Foley (*106*). Despite the life-saving nature of this device and other catheters which perform similar functions, as stated earlier, they suffer from an array of complications (Figure 2-7).

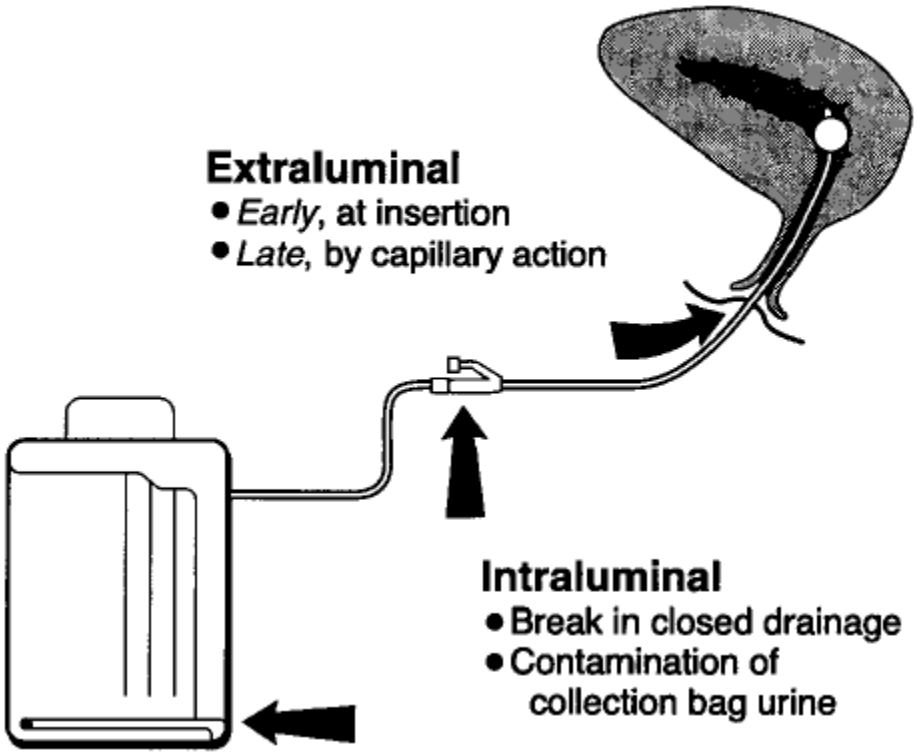


Figure 2-7. Potential problems in a Foley catheter. Reprinted (adapted) with permission from (*18*). Copyright © 2001, PubMed Central.

Among the type of catheters, since the invention of the latex catheter, several approaches have been put forward to solve the problem. PTFE® coated catheters have been shown to be among the most toxic catheter materials (*27*). Silicone is one of the most biocompatible synthetic materials. It also has excellent UV resistance and good chemical resistance. Silicone catheters also showed maximum time to blockage among commercially available catheters including, hydrogel/silver coated latex, which showed the least time and silicone coated latex (*24*).

CAUTI prevention has been approached by imbibing antimicrobials and disinfectant in natural rubber resins.

Continuous draining of catheters with the addition of antibacterial agent or disinfectant to the collection bag is an option (*20*), whereas, releasing antimicrobials from glass or polymeric materials in a controlled manner is another option (*21, 22*). Introducing antimicrobials in to materials may be toxic and may affect their biocompatibility and mechanical properties (*23*).

Silver, silver oxide, PTFE® and silicone coatings were proposed as alternative coatings for preventing biofilm formation. However silver and silver oxide coatings have been reported to have mixed results. One study reported the increase in the amount of staphylococcal infection (*24*), while another study question the potential benefits silver coated catheters (*25*). Statistically significant differences were observed in a study based on silver coated catheters (*26*).

Although, PTFE® coated catheters have high lubricity and low surface energy they have still been reported to be among the most toxic catheter materials (*27*). From the perspective of biocompatibility and increasing lubricity for ease of insertion hydrogel coatings have been employed for catheters (*28, 29*). Despite these advantages, hydrogel based catheters have poor mechanical performance (*24*) and have been shown to be prone to rapid encrustation (*23*). Most parts of the Foley catheter has been constructed from polydimethyl siloxane (or silicone) (*30*).

Literature reports consist of mixed reports in the prevention of biofilm formation on silicone catheters. Silicone materials have been reported to have maximum fouling prevention (*28*), while other studies indicate maximum bacterial adhesion (*23, 31, 32*).

Complications such as encrustation and blockage still exist as result of biofilm formation, in the materials and coatings used till date for making catheters.

A review article emphasizes the need for further research in to the development coatings or better materials for catheters. To quote from the article “although it has been 70 years since the Foley catheters were first introduced, the problems of infection and encrustation still remain”. It also states “little attention has been paid to the contributory effects of materials and design of urinary catheter” (*24*).

**Bacterial Adhesion**

Attempts to model bacterial adhesion was historically based on the thermodynamic approach. In an analysis based on 5 different bacteria on 4 different substrate materials, it was found that adhesion of bacteria followed a thermodynamic model to a considerable extent. Also, determination of the extent of adhesion was shown to potentially allow for the determination of bacterial surface tensions(*107*). The drawback with this system is that all adhesion assays were made within 30minutes and may not be applicable to systems where longer durations may be relevant.

The theory for stabilization of colloidal suspensions, namely the Derjaguin-Landau-Verwey-Overbeek (DLVO) theory has also been used for estimating attachment of bacteria to surfaces.

**Forces involved in bacterial adhesion**

The following bullet list is a summary of all the forces that have been described in the literature as playing a role in interfacial phenomena in biological systems (*108*). Non-specific interactions (NS), occur across the entire interacting surface and specific interactions (S) are short range forces arising from specific microscopic surface components on bacteria (*109*).

- Van der Waals (NS): London dispersion
- Van der Waals (NS): Debye induction
- Van der Waals (NS): Keesom orientation
- Electric double layer interaction (Coulombic ) (NS)
- Hydrogen bonding
- Hydrophobic interactions – attractive mode of hydrogen bonding
- Hydration pressure – repulsive mode of hydrogen bonding
- Brownian movement forces
- Osmotic pressure
- Disjoining pressure
- Structural forces
- Steric interactions
- Depletion interactions
- Entropy-driven interactions
- Enthalpy-driven interactions
- Cross-binding interactions
- Specific interactions (S): Short range, microscopic bacterial components

Although this list contains 17 different terms, some of the effects are actually manifestations of the primary forces or a combination of their effects. The primary forces can be summarized as follows (*108*),

- Lifshitz-van der Waals (LW) forces: can be attractive or repulsive depending on the surfaces and intervening medium under consideration (*110*).

- Electrical double layer interactions (EL): the forces here are repulsive due to charges of the same sign

- Lewis acid-base (AB) interactions: subsets of which include Bronsted acid-base and specific interactions described above

- Hydrogen bonding: is defined as “an attractive interaction between a hydrogen atom from a molecule or molecular fragment X-H in which X is more electronegative than H, and atom or a group of atoms in the same or a different molecule, in which there is evidence of bond formation”(*111*). Hydrogen bonding is a major contributor to the so called “hydration forces” and “hydrophobic effect”.

- Brownian energy: is the energy possessed by molecule or particle by virtue of thermal state of a system. For the same energy, the movement of molecules is rapid, keeping them in suspension, compared to particles of much larger diameters. Brownian movement was first described in colloidal particles as the random movement conferred by multiple collisions by molecules of the medium and thermal state of the particles.

Disjoining pressure is a summation effect of LW, EL and AB attractive or repulsive interactions within solvent layers adjoining surfaces during overlap (*112*). Osmotic pressure is described by a summation of a Brownian term and LW, EL and AB term for solutes in a medium. Structural forces are described on the basis of hydration or hydrophobic interactions due to structuring of water molecules around the interacting dimensions. Steric effect was used to explain the stabilization of hydrophobic particles in solution by non-ionic polymers or surfactants. It is essentially a summation of surface configurational entropy, osmotic pressure with an emphasis on the AB component and energy associated with the deforming the coiled chain, chain elasticity.

Hydrophobic materials tend to strongly attract each other in aqueous media and this is termed the “hydrophobic effect” (*113*). On the other hand, when two hydrophilic materials are brought in contact repulsive forces have been observed at the range of 1 nm. Examples include mica (*114*) and silica (*115*) surfaces. The repulsion is attributed to the energy needed to remove the adsorbed water layer. Hydration forces are caused by the orientation of water molecules on the strongly hydrogen accepting molecules. This is the motivation behind applying strongly hydrated polyethylene oxide (PEO) brush type surfaces (*116*).

The classic DLVO theory takes into account the LW and EL forces and is therefore unsuccessful at explaining bacterial interactions, which co-aggregate despite having similar surface charges hence similar zeta potentials. By taking into account polar interactions in the form of an extended DLVO (XDLVO) (*117*) theory, several groups have attempted to estimate initial bacterial adhesion of the same bacterial strain to

different substrata (*118-120*). Although this approach is more accurate it still assumes bacteria as inert particles.

Also, even though PEO based protein adsorption resistant surfaces work well in the preventing the adsorption of some bacterial strains, it has been shown that some strains of *p. aeruginosa* are capable of adhering even in such situations, reinforcing the dynamic nature of microbes. From a study with 3 adhesive and non-adhesive bacterial strains of *p. aeruginosa* it was found that, 1) It is supposed that surface active molecules (biosurfactants) such as may contribute to greater adhesion and 2) The cell surface hydrophobicity caused by cell surface proteins may cause the adherence to the hydrophobic portions of the PEO chains. From the observations made in the paper it is suggested that physicochemical factors alone cannot explain the interaction of bacteria with surfaces, and bacterial variability should be also considered (*121*). The important fact which challenges both thermodynamic (*122*) and DLVO based approaches is the fact that as living species, bacteria are capable of responding to changes in their environment according to their genetic code.

**Studies on attachment to surfaces**

Transportation of microorganisms to a surface may be through Brownian motion, gravitation, diffusion, convection and intrinsic motility (*109*). Initially reversibly attached microorganisms end up becoming irreversibly attached through exopolymeric substances or extracellular polymeric substances (EPS). The EPS may serve as a derived conditioning film, whose cohesiveness determines the strength of adhesion. Co-adhesion is used to represent two phenomena: 1) slowing down of planktonic organism by sessile organism and 2) through strong attractive interactions between sessile and planktonic species.

The differences in the acid-base character determine the hydrophobicity of the cells. Hydrophobicity of bacteria cannot be generalized on the basis of microbiological taxonomy (naming and classification of microbes) from contact angle data from a set of literature species or strains (*123*).

After attachment, the cells start to grow and multiply, which is supposed to be the major factor in the accumulation of the cells on the surface (*109*). Roughness has an influence on biofilm formation, but it is supposed to be a minor factor in initial adhesion. Microorganisms preferentially adhere to scratches and grooves. Roughness supports rapid re-growth of a biofilms, rendering cleaning attempts futile.

The process of biofilm formation has been described as primarily having the following 4 steps: transport to surface, initial attachment, irreversible attachment and maturation (*124*). Depending on the type of bacterium, the settlement of bacteria is controlled by the physico-chemical interactions between the bacterium and substratum surfaces in a medium to a significant extent. Bacteria such as S*taphylococcus aureus* usually falls under this category whereas, bacteria with flagella such as *Pseudomonas aeruginosa* are motile and capable of hunting for food sources. Interactions between a material surface and bacteria during the initial and irreversible attachment stages are, are relatively better understood and can be predicted based on some existing models (*107, 119, 125, 126*).

In such early growth stages it has been suggested that surface roughness contributes to a more significant extent compared to surface energy. However, mature biofilm growth, that is proliferation of bacteria following attachment to a surface and it's correlation to surface properties is very complicated and at present difficult to quantify.

Most of the previous studies, based on random roughness, suggest that the bacterial attachment to surfaces should increase with surface roughness. Bacterial attachment on rough surfaces has been studied in some detail. Results from restorative materials on the dependence of bacterial fouling on roughness seems to suggest a lower limit of 0.2 microns and generally increases with increase in roughness from that point on(*124*).

Minimizing the number of contact points available for bacteria is suggested for reducing fouling. It has also been found that bacteria more readily adhere to hydrophobic surfaces (*127*). It has been shown in almost all cases of bacterial attachment to rough surfaces, there is an increase in the number of bacteria attached. This increase bacterial attachment has been attributed to an increase in the total surface area available for attachment and, in flow systems, due to increased protection from shear forces (*128-130*). These results indicate that a rough, hydrophobic surface should increase attachment and proliferation of bacteria.

The novel patented Sharklet$^{TM}$ topography was devised based on finding that roughness on a surface leads to a statistically significant decrease, according areal coverage as measured from SEM images, in the amount of bacteria attached over a 21 day period (Figure 1-2) (*17*). Another study has reported that cylindrical nanometer sized polymer posts that were spaced apart at various distances showed specific alignment of PA cells at certain spacings (*131, 132*).

Surface attachment of bacteria is known to trigger changes in gene expression and leads to a biofilm phenotype that is very different from the planktonic phenotype (*133*). In a 7 day incubation time biofilm growth test, combined elastic modulus and

surface energy variations did not appear to have any effect on *s. aureus* (strain: ATCC 35556) biofilm formation (*134*).

In contrast, a 2 hour study suggested that surface stiffness could be a factor influencing the extent of colonization (*135*). Another 2 hour study reported a decrease in the extent of *Pseudomonas fluorescens* biofilm growth on sub-micron trench like features compared to smooth control (*136*).

**Biofilm Growth Protocols**

Biofilms are commonly grown in a flow cell reactor in biofilm characterization laboratory studies. This involves setting up a dedicated chamber for making many measurements such as micro-electrodes for local diffusivity measurements and optically sectioned images from confocal microscopy (*65, 137*).

Static biofilm formation models are accepted methods in the literature (*17, 134, 138, 139*). Besides picking the right method for biofilm growth based on the test specimens' application, it is imperative that growth conditions are standardized.

The comparison of biofilms based on test factors relies on the reproducible growth of biofilms. Environmental stimuli and growth conditions should be exactly the same in order to lay a basis for comparison between smooth and topographical test surfaces.

A number of studies were conducted based on confocal microscope images and image analysis using a computer program known as COMSTAT (*71, 72, 140*). Another program called Image Structure Analyzer (ISA) was also developed to look at various parameters in quantifying biofilm structure (*70, 141*). It would be useful to compare biofilm images using such programs to ensure the reproducibility of growth conditions.

**Bacterial Nutrient Conditions**

The following nutrient media have been used in the literature in bacterial attachment, growth and biofilm formation tests:

- Tryptic soy broth: 17g/l of enzymatic digest of casein and 3g/l liter of soya bean enzymatic digest among other things
- Luria-Bertani broth: 10g/l of tryptone and 5g/l of yeast extract - based on tryptone (assortment of peptides from a digest of casein by trypsin)
- Nutrient broth for microbiology used at 8g/l peptone from meat extract – based on the enzymatic digest of animal protein
- Mueller-Hinton broth: 17.5g/l acid casein peptone, 1.5g/l corn starch and 2g/l of beef infusion
- Minimum essential medium – contains no proteins or lipids or growth factors and has a sodium bicarbonate buffer system

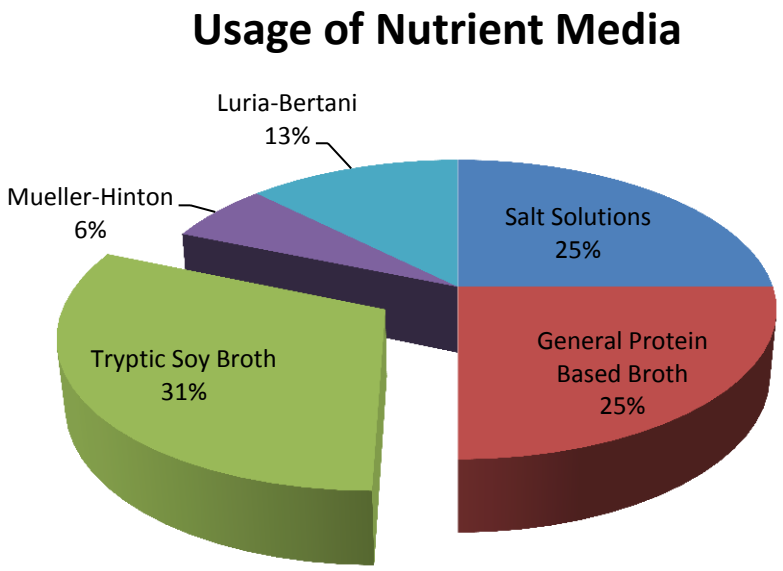


Figure 2-8. Usage nutrient media for testing biofilm formation on artificial surfaces, data synthesized from articles dating 1983 through 2011

From the nutrient media used in the literature, only a very few studies state the use of minimum essential medium. In most studies, 75%, the use of high protein sources for

test media is common practice. The data synthesized from literature articles dated 1983 through 2011 is shown in form of a pie chart (Figure 2-8) (*17, 107, 121, 136, 139, 142-148*).

**Characterization of Bacterial Colonization**

Out of the several unresolved questions with respect biofilm formation on patterned topography, the following characterizations form the focus of this part of the study. Identifying differences in long term biofilm growth, between patterned topographies of PDMSe smooth control would be pertinent to the problem of biofilm formation on catheters.

**Microscopy**

Qualitative visual analysis using microscopic techniques could provide an insight in to the arrangement of bacterial cells on topographical surfaces. Scanning electron microscopy (SEM) images has been used to visually assess biofilm growth on various artificial and human surfaces.

SEM can be used as a means to elucidate biofilm growth qualitatively. The high magnification and depth of field yield detailed images of the surface arrangement of biofilm on test surfaces. Despite their advantages, SEM measurements end up distorting the nature of the EPS matrix and introduce sample distortion and artifacts. Therefore, results should be interpreted with caution.

Image analyzed epifluorescence microscopy (IAEM) has been used for counting planktonic bacteria in natural waters (*149, 150*). IAEM is especially suited for enumeration of bacteria on opaque surfaces. The method was adapted to enumerate bacteria attached to biomaterial substrate using IAEM (*151*).

**Quantification of biofilm growth**

Quantifying biofilm formation reproducibly is important for identifying differences between topographical treatments. Several techniques have been applied to quantify biofilm formation in this study. The length of time for biofilm growth was chosen to be 7 days on the basis of earlier work (*134*) in which biofilm growth was observed on the smooth sample versus the Sharklet$^{TM}$ surface.

Plate counts have been used to quantify number of bacteria in solution since Robert Koch isolated bacterial colonies on solid nutrient plate and showed that microbes cause human disease (*64*). It is the most commonly used procedure for the determination of viable plate counts. Unfortunately, the recovery efficiency of such procedures needs to be specified (*3*). In the case of biofilm quantification, it was necessary to disperse the cells into a buffered saline solution (to keep the bacteria alive), following which they were serially diluted and spread on agar plates to determine the number of colony forming units present per specified volume, mass, or specimen. Although this method can be used in biofilm quantification, its usefulness depends on the type of bacterium. Diffused sonication and vortexing can be used to completely disburse *p. aeruginosa* (Appendix A) biofilms (*74*). However, individual cells from *s. aureus* biofilms were not easily separated from the surfaces to which they attached or from each other (*88, 152*). Vortexing and sonication parameters may be extended to separate the bulk of biofilm bacteria forcibly from the surface but these methods have problems as they typically don't completely remove the *s. aureus* cells from the surface nor disburse biofilm into separated single cell suspensions. Also, they may end up killing some percentage of the released bacteria due to the high shear rates (*1, 153*) Hence, plate counts were not used for enumerating *s. aureus* biofilms.

In this study, plate counts were used to compare *p. aeruginosa* biofilm growth on the patterned topography to the smooth control.

Bio-timer assay (BTA), an indirect metabolism based approach, was the primary method used for quantifying *s. aureus* biofilm on the patterned topography along with the smooth control. This method is based on the premise that each viable cell has a similar rate for metabolizing glucose on average in mature biofilm and that differences between samples reflect differences in the number of cells present (*154*). If grown under the same nutritional conditions over the same period of time, difference in metabolic rate as a whole should theoretically reflect differences in viable cells numbers in the biofilm in response to differences in pattern topography of the surface to which it attaches. Other methods used in this study employ indirect assays to comparatively quantitate the level of biofilm formed on each surface, including detecting ATP levels produced by viable cells (*155*) and colorimetric assays based on staining of biofilm mass (*152, 156*). Quantitative Polymerase Chain Reaction (qPCR) was used to quantify the total number of cells based on relative abundance (copy number) of target genes within the specimen in order to compare biofilm formation between different topography along with the smooth control, since quantifying with BTA used for the *s. aureus* biofilm depends on metabolic rate of viable cells. This method utilizes sonication, vortex and a high temperature to lyse the cells and extract the total DNA of the cells. The DNA pool from each specimen is then used in a real time PCR Experiment along with a standard series at known concentrations (and estimated gene copy number) of genomic DNA extracted from planktonically cultured bacteria. A standard curve is generated and used to estimate the number of cells that grew on each specimen.

Gene expression profiling gives more direct and specific results based on relative expression levels of specific genes that are reported to be expressed higher in biofilms compared to planktonic cells. Differentiation of bacteria from planktonic to biofilm phenotype significantly increases their tolerance against environmental stress. Both plate count and BTA tests were accompanied by antibiotic treatment so that tolerant biofilm cells can be differentiated from the susceptible planktonic cells and the percentage kill can be used to measure differences between the various patterns, thus its relative effect on the formation of tolerant biofilm. Antibiotic susceptibility is a useful indicator of the amount of biofilm cells present versus the total number of viable cells (*140, 157*). These are usually based on using specific antibiotics for the bacterium in question. Minimum concentrations for various stages such as minimum inhibitory concentration (MIC), minimum bactericidal concentration (MBC), minimum biofilm inhibitory concentration (MBIC) and minimum biofilm eradication concentration (MBEC) are determined. Minimum inhibitory and bactericidal concentrations represent the amount of antibiotics needed to deter growth of and kill planktonic bacteria. Minimum biofilm inhibitory and eradication concentrations represent the same for biofilms. . Post antibiotic treatment at MBC or MBEC levels, if the quantification tests yield viable colony forming units, this would then indicate that the planktonic bacteria in the test sample are dead and the remaining number of cells are the biofilm phenotype.

The parameters of this assay were chosen in the context that 1) only a certain concentration of antibiotics can be administered in a patient and 2) application of antibiotics at MIC levels is ineffective in device related and chronic infections (*4*) and 3) surface treatments capable of lowering the number of cells in the biofilm phenotype may

mitigate host infection. The understanding of the effect topographical surfaces on biofilm formation could be improved by the insights gleaned from studying their effects on wetting.

## Wetting Effects of Patterned Topographical Surface Designs for Inhibiting Biofilm Formation

Natural strategies utilize metastable water wetting states evolved to take advantage of wetting phenomena, such as superhydrophobicity observed in the lotus leaf effect. Several micro-/nano- structure and chemistry modifications allow for these special phenomena to occur in nature, some examples being the *nelumbo nucifera (lotus leaf)* (*158*), *gerris remigis (water strider)* (*159*), and *cicada orni (160)*. The lotus leaf is an example of a natural surface that has been extensively studied (*158, 161*). The lotus leaf is super-hydrophobic due to micron sized bumps spaced 20 to 40µm apart with nano sized wax cuticles. The water strider legs have microscale setae with nanoscale grooves on them. Such unique hierarchical microstructures lead these surfaces stable non-wetting states for water (*162*). *Cicada orni* achieves super-hydrophobic behaviour through nanopillar arrays alone (*160, 163*). Several reviews discuss in detail, the many methods that have been developed to produce microstructures that mimic nature (*36, 164-167*). Only a brief account of this is given in the next section.

### Fabrication Strategies for Nonwetting Surfaces

Many processes have been applied for inducing micron and nanoscale roughness for making non-wetting surfaces. These have been broadly classified under lithography, etching, deformation, deposition and transfer type processes (*168*) (Figure 2-9)

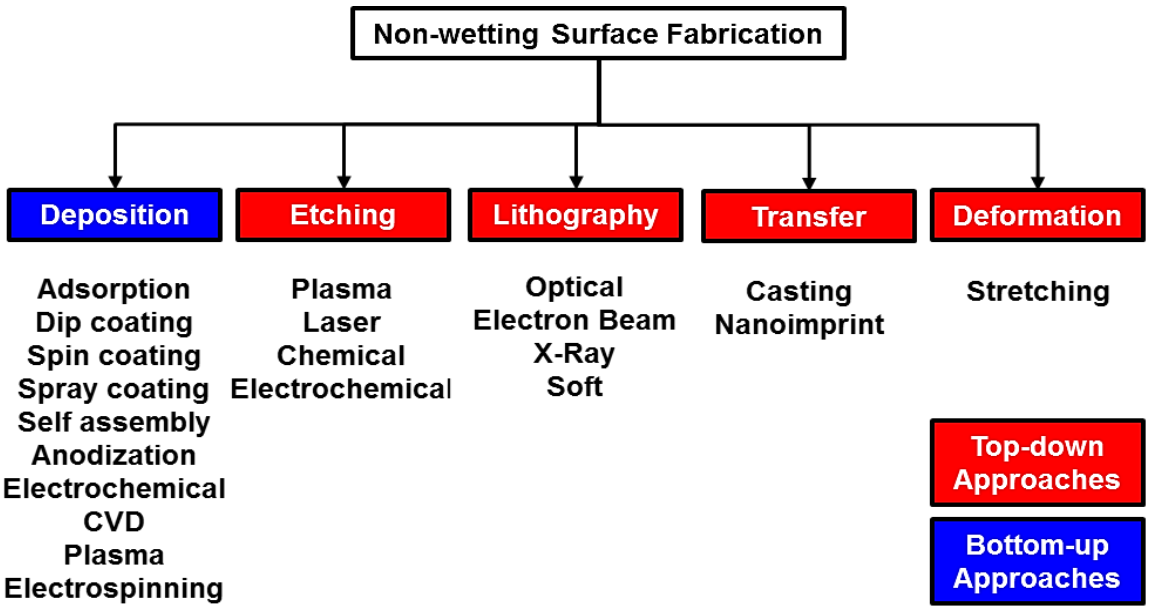


Figure 2-9. Processes available for the fabrication of nonwetting surfaces (adapated from (*168*))

Non-wetting surfaces, defined in terms of high liquid contact angles, made using the above described processes were, until recently, fabricated using two main strategies(*164*):

- Roughening of low energy surfaces
- Roughening a surface followed by reducing its surface energy

The first strategy uses materials such as Teflon®(*169*), silicones(*170*), organic polymers (polypropylene (*171*), polyethylene (*172*)), inorganic crystals (ZnO <001> facet (*173*), Figure 2-10 (A)) which are intrinsically low in surface energy and induce micron or nanoscale roughness. The second strategy roughens surfaces and tailors their surface energy through low surface energy coatings.

Another way to classify the processes used to make non-wetting surfaces is as follows:

- Top-down approach: represents the modification of bulk materials to obtain necessary surface face feature sizes, example: semiconductor processing techniques

- Bottom-up approach: using the physics and chemistry of molecular systems to build micron and nanoscale structures; examples: Polymerization(*174*), electrospinning (*175-177*) (Figure 2-10 B) and sol-gel techniques (*178*) (Figure 2-10 (C)).

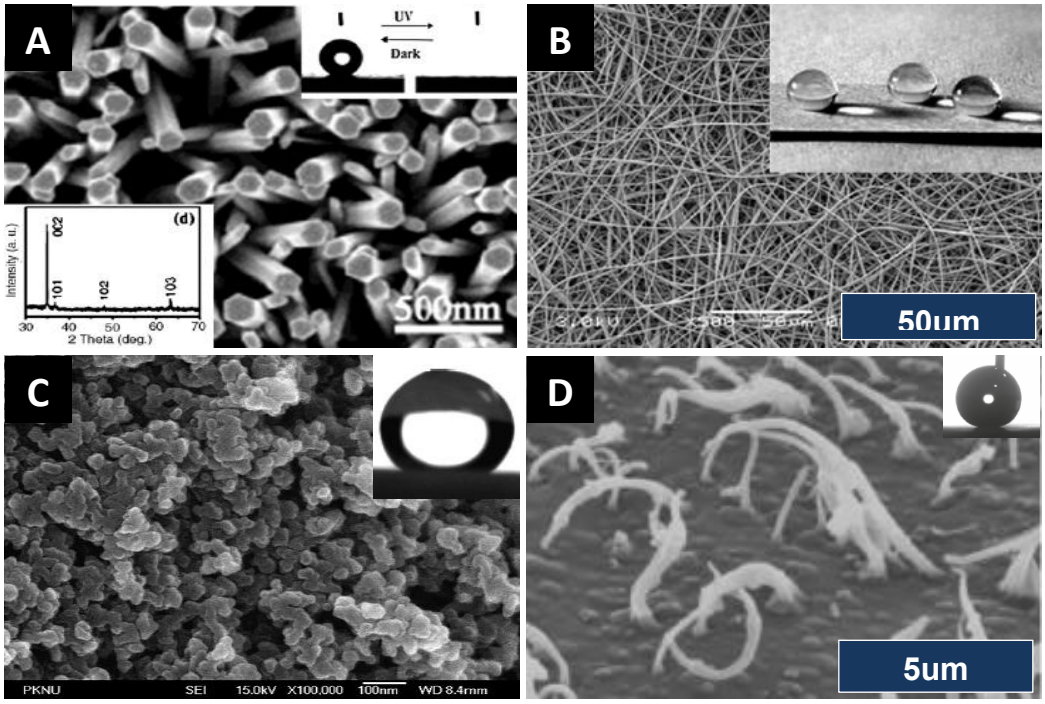


Figure 2-10. Examples of super-hydrophobic surfaces fabricated using various methods (A) SEM image of ZnO nanorods, insets showing XRD results <001> being the main crystal plane and the transition from non-wetted to fully wetted due to the electron-hole pair formation under UV light Reprinted (adapted) with permission from (*173*) Copyright © 2004 American Chemical Society. (B) electrospun poly(styrene-b-PDMS) copolymer Reprinted (adapted) with permission from (*175*) Copyright © 2005 American Chemical Society. (C) ambient pressure dried, MTMS xerogel (methanol solvent) with superhydrophobicity Reprinted with permission from (*178*). Copyright © 2007 Elsevier (D) sparsely distributed hair-like 600nm diameter polypropylene fibers with high contact angle (>170°) Reprinted (adapted) with permission from (*167*) Copyright © 2010 American Chemical Society.

The strategies mentioned so far, lead to the creation of metastable air-water interfaces due to scale of roughness involved. This is termed as the lotus-effect. Another category of surfaces with a nonwetting property make use of bendable nanofibers as seen in the water boatman insect, *notonecta glauca(179)*.

The super-hydrophobic property is achieved through what is known as the plastron effect. Plastron is defined as a metastable layer of air when a surface is submerged underwater, maintained by the dissipation of pressure fluctuations by the bending of submicron fibers(*180*). Figure 2-10 (D) is the SEM image of one such surface with sparse ($7 * 10^5$ pillars per $cm^2$) nanofiber superhydrophobic surface showing the plastron effect.

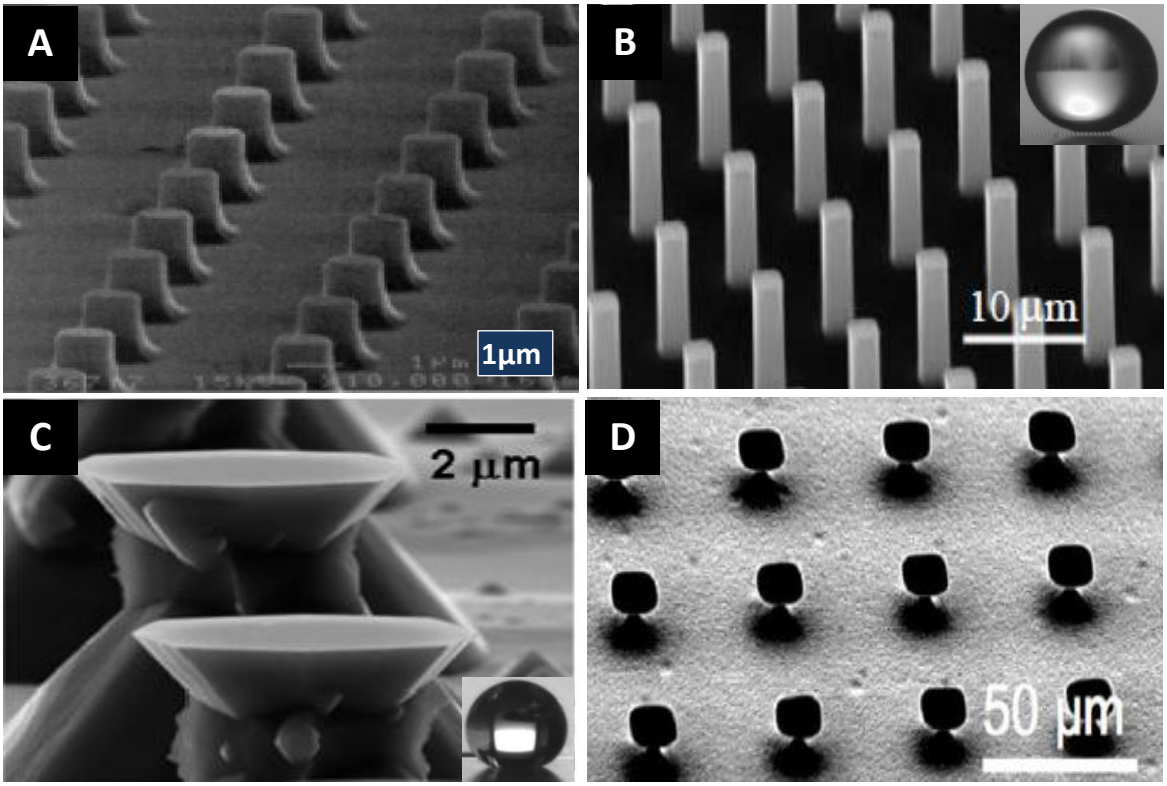


Figure 2-11. Examples of patterned topographies used for testing wetting models with contact angle data (A) 1µm silicon pillars (*181*) (B) another example of a regular array of etched silicon microposts Reprinted (adapted) with permission from (*182*) Copyright © 2008 Highwire Press. (C) undercut silicon microstructure with hydrophilic silica top exhibiting superhydrophobicity Reprinted (adapted) with permission from (*183*) Copyright © 2007 American Chemical Society. (D) undercut microstructure with silica top coated with fluorosilane capable of superoleophobicity Reprinted (adapted) with permission from (*184*) Copyright © 2008 National Academy of Sciences.

While there are many different methods to make superhydrophobic surfaces, the resultant surfaces are not easily, mathematically, definable. Therefore it is difficult to model the wetting effects observed via these surfaces. In order to overcome this disadvantage, using semiconductor processing based top-down approaches (Figure 2-9), for the purposes of modeling and testing existing wetting models, different patterned topographical surfaces have been fabricated (Figure 2-11).

The first important concept discussed, in the wetting approach, in this study, which is pertinent to biofilm formation, is the robustness of the submersed non-wetted state. A reduction in the area wetted could lead to a reduction in biofilm formation as bacteria depend on water for adhesion and survival (*185*). There are two reports for the characterization of breakthrough pressure measure. The first method uses CLSM scan images in combination with mass transfer measurements (*38*) and the second method uses changes in laser diffraction patterns through a translucent or transparent patterned material. The former requires the presence an elaborate setup with a tedious measurement procedure, however ends up being more informative. The latter, on the hand is easy to work with but is only applicable to translucent to transparent materials. Breakthrough pressure measurement represents the pressure needed to transition from a non-wetted to a wetted state. There are some accounts in boiling studies of undercut cavities (*186, 187*) on this and in recent publications on undercut topography for non-wetting applications (*37, 183, 184, 188*). However, there is a definite need for more data and analysis for understanding this phenomenon.

The second concept discussed here is the pinning of water by patterned topography. Apparent contact angle measurements, being reflective of the

inhomogeneity of a surface, provides a technique to characterize this pinning (*189*). Pinning leads to different apparent contact angles, termed dynamic contact angles, from the lowest called the 'receding contact angle' to the highest called the 'advancing contact angle'. The difference between the two is termed hysteresis and signifies energy lost in switching between metastable states (*190*).

**Modeling Contact Angle Hysteresis**

Many models have been put forward to predict the apparent contact angle observed on a surface (*189, 191-193*). There have also been arguments on the importance of the triple point contact line over the wetted area fraction of the solid surface for apparent contact angle prediction (*193-197*). Contact angle data on patterned topography with varying dimensions is necessary to illustrate the importance of the TPCL over the surface areal for predicting dynamic contact angles.

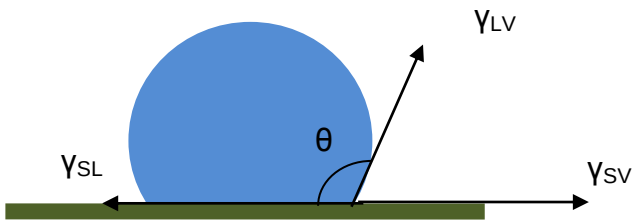


Figure 2-12. Young equilibrium contact angle on a smooth surface

A TPCL model was developed in collaborative work by a colleague (*198*) and the linear fractions ($\varphi_S$ advancing and receding) were employed in the analyses in this study. It is important to make clear the use of TPCL to model dynamic contact angles due to extent to which the Cassie-Baxter model is used in explaining wetting phenomena.

The basic models for explaining how wetting occurs are the Young-Dupre, Wenzel and Cassie-Baxter (*189, 191, 192*).

$$cos\theta_Y = \frac{\gamma_{SL} - \gamma_{SV}}{\gamma_{LV}} \quad (2\text{-}4)$$

The Young-Dupre (Equation 2-4) is derived from balance of forces between the liquid (L), solid (S) and vapour (V) interfaces with $\theta_Y$ representing equilibrium contact angle of the droplet on an ideal surface, shown in Figure 2-12. The equation is alternatively represented in terms of the work of adhesion where, the work of adhesion is a function of the solid-vapour and solid-liquid interfaces being destroyed and the solid-liquid interface being formed (Equation 2-5).

$$W_{SL} = \gamma_{LV}(1 + \cos\theta) \quad (2\text{-}5)$$

In the interest of understanding the nature of wetting on woven or knitted fabrics, Wenzel studied the resistance of solid surfaces to water wetting. The roughness ratio was proposed to characterize surfaces as the ratio of total surface area to the geometric area.

$$cos\theta_W^* = rcos\theta_Y \quad (2\text{-}6)$$

Wenzel concluded that the effect of a roughened surface would magnify the wetting property of the base material in proportion with the roughness of the material. By implication, the rough surface would be more wetting if the surface was originally prone to wetting and less so if it was not easily wetted. This effect is captured by Equation 2-6 where $\theta_W$ is the apparent Wenzel contact angle and r is the roughness factor (total surface area over planar area).

Although, there is significant agreement of measured contact angles for a lot of surfaces with the Wenzel model, several natural and artificial surfaces such as the lotus leaf and fabric surfaces showed much higher apparent contact angles than could be explained by only Wenzel roughness.

In order to explain these observations, Cassie and Baxter advanced a theoretical argument based on the inclusion of porosity and therefore effect of vapour entrapment on the surface under the droplet.

Figure 2-13 illustrates Wenzel and Cassie type wetting modes on hypothetical patterned substrates.

$$cos\theta^*_{CB} = f_s cos\theta_S + (1 - f_S) cos\theta_V \quad (2\text{-}7)$$

$\theta^*_{CB}$ is the apparent Cassie-Baxter contact angle and $\varphi_s$ is the solid area in contact with the liquid (Equation 2-7). When the vapour phase in contact with the liquid is air, the Cassie-Baxter equation becomes (Equation 2-8),

$$cos\theta^*_{CB} = -1 + f_S(1 + cos\theta_Y) \quad (2\text{-}8)$$

The Cassie-Baxter equation makes use of the areal solid wetted fraction and air pockets to account for the high apparent advancing and receding contact angles on fabric and natural surfaces.

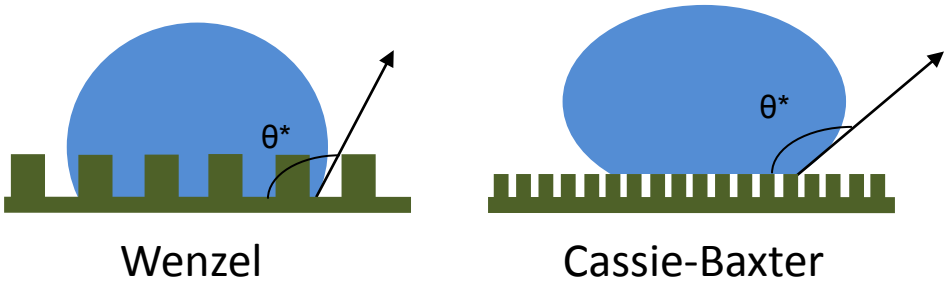


Figure 2-13. Wenzel and Cassie-Baxter type wetting modes

For hydrophobic surfaces, depending on the extent of increase in pinning sites and air pockets resulting from roughening, leads to an increase in the apparent contact angle. Base surfaces showing contact angles up from 90° show this effect. However, as a hydrophilic surface is roughened the apparent contact angle proportionally decreases till the roughness reaches dimensions where the apparent contact angle shoots up beyond 90° giving an apparent hydrophobic effect due to stable air pockets. This effect

can also be examined by varying the liquid surface energy systematically on a rough surface, as illustrated in Figure 2-14. This is why the lotus leaf and other surfaces such as cellulose based fabrics appear super-hydrophobic even if the underlying surface maybe hydrophilic. Once the stability of the air pockets is destroyed the lotus leaf loses its super-hydrophobic property (*199*).

An overwhelming majority of literature articles use the Wenel and Cassie-Baxter equations with areal solid wetted fractions to predict the nature of the wetting on surfaces. In order to argue for the use of the TPCL versus an areal approach, a simple thought Experiment was proposed by Gao-Mccarthy (*200*). Figure 2-15 (A) illustrates this, their idea is to pose the question of whether any forces at points P or Q affects force balance at R, i.e., along the TPCL. They demonstrate this by using puddles between and beyond nails on a surface as shown in Figure 2-15 (B) and remark on the similarity between the droplets in such a situation.

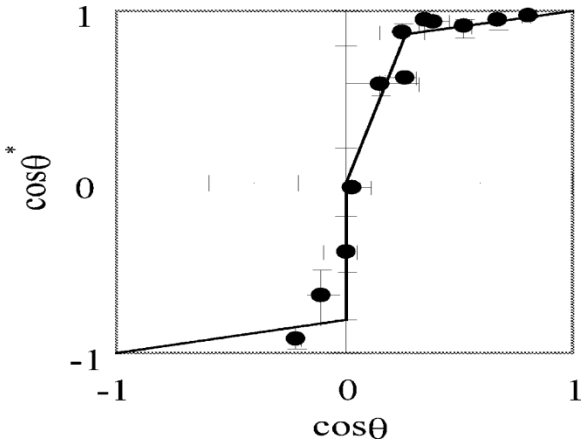


Figure 2-14. Variation of apparent contact angle on an alkyl ketene dimer surface with variation of the probing liquid: various ratios of 1,4-dioxane and water. Reprinted (adapted) with permission from (*174*). Copyright © 1996 American Chemical Society.

The presence of 3 significantly different contact angles surface was first noted by Bartell and co-workers (*201*). These were measured by carefully inserting into and

removing the plate surface in question from the liquid of choice. As opposed to previous areal fraction arguments, it was proposed that the balance of forces at the TPCL should dictate the liquid surface. The work of adhesion, needed to overcome or fill in the solid-vapour interface, needs to be minimized or maximized as the TPCL advances or recedes (*193*).

Good first discussed the possibility of metastable states, using experimental description provided by Bikerman(*202*), based on the existence of a ‘contortional’ energy barrier. This is defined as the energy spent in changing the liquid-vapour interface in order advance or recede. This is easily visualized on a rough surface peaks and valleys decrease the contortion of liquid-vapour interface would decrease leading to a decrease in hysteresis.

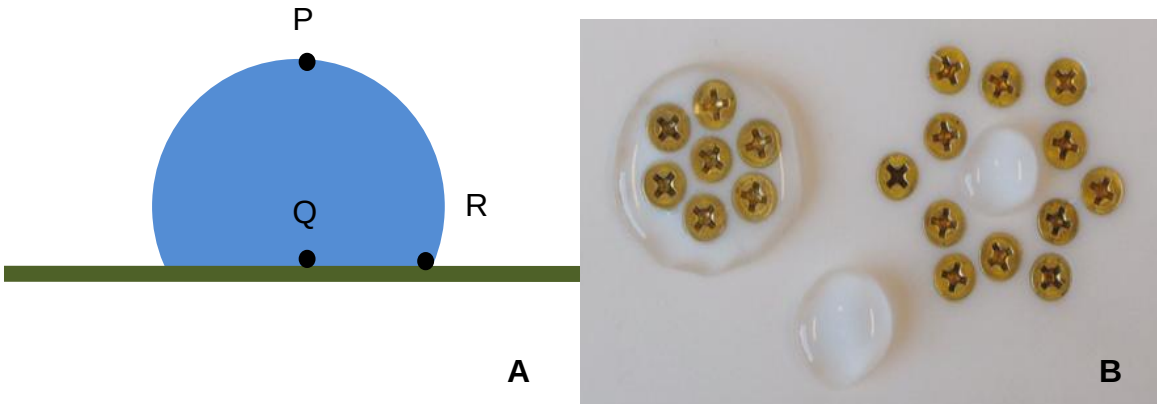


Figure 2-15. Gao-McCarthy thought Experiment: (A) Hypothetical question, how do forces at A and B affect force balance at C? (B) Demonstration that TPCL is unaffected by majority of the area within the droplet Reprinted (adapted) with permission from (*200*). Copyright © 2009 American Chemical Society.

A similar treatment on the basis of chemical surface inhomogeneity was also used to explain hysteresis on smooth surfaces. Based on this models were proposed by Johnson and Dettre and Joanny for contact angle hysteresis on a surface using the

difference in overall free energies between two metastable states along due to changes in surface area and defects along the TPCL(*203, 204*).

The results of the previously discussed hysteresis analyses some are based on surface area (conceptually incorrect) and others mathematically elaborate and are not easy to use. In order to overcome these problems, Extrand proposed the use of a criterion based on an undistorted TPCL. He developed a criterion for suspension or collapse by considering a balance of forces along TPCL. For suspended 'Cassie' droplets he describes a linear fraction of TPCL based equation for the direct determination of the apparent contact angle (*39*).

Recently, undercut surfaces were shown to be capable of maintaining a super-oleophobic state (meaning surfaces having a contact angle of any liquid to be above 150 degrees). A linear model was proposed to predict apparent contact angle based on $r_\varphi$, $\varphi_s$ and a separate model was proposed for estimating the stability of wetting states based on capillary pressure and $\varphi_s$ (*37, 188*).

The modified CB equation (Equation 2-9) (m-CB) involves the introduction of a differential parameter $\varphi_d$

$$cos\theta^*_{mCB} = r_\phi \phi_d cos\theta_1 + (1 - \phi_d) cos\theta_2 \quad (2\text{-}9)$$

The advancing and receding conditions are the locally stable maximum and minimum contact angles as the TPCL advances and recedes respectively. They correspond respectively to a minimum in $\varphi_{d,adv}$ and maximum in $\varphi_{d,rec}$ (Equation 2-10 and Equation 2-11).

$$cos\theta^*_{mCB,adv} = r_\phi \phi_{d,adv} cos\theta_1 + \left(1 - \phi_{d,adv}\right) cos\theta_2 \quad (2\text{-}10)$$

$$cos\theta^*_{mCB,rec} = r_\phi \phi_{d,rec} cos\theta_1 + \left(1 - \phi_{d,rec}\right) cos\theta_2 \quad (2\text{-}11)$$

It has been proposed that the advancing and receding angles may be predicted based on the maximization and minimization of respective $\varphi_d$. According to the model proposed $\varphi_{d,adv}$ value of zero should yield an apparent advancing angle of 180 degrees, but it is suggested that natural vibrations prevent this from showing on the apparent contact angle images (*188*).

# CHAPTER 3
# MATERIALS AND METHODS

## Materials

### Materials Used for the Confinement Approach

The materials required for fabrication and testing include n-type silicon wafer (University Wafer Inc., Boston, MA), Silastic T-2 polymer base and curing agent (Dow Corning Corp.,). Bacterial cultures were grown in tryptic soy broth (Sigma-Aldrich corp.). Washing solutions consisted of distilled water and 1X phosphate buffered solution (PBS) (Sigma-Aldrich corp.).

Gentamicin (Sigma-Aldrich corp.), oxacillin (Sigma-Aldrich corp., St. Louis, MO), molecular biology grade absolute ethanol (Sigma-Aldrich corp. , St. Louis, MO), tryptic soy broth (Sigma-Aldrich corp. , St. Louis, MO), tryptic soy agar (Fisher Scientific), Muller Hinton broth (Sigma-Aldrich corp., St. Louis, MO), phenol red, PBS (pH 7.4), PCR primers (IDT-DNA, Coralville, IA), DNA extraction kit (Invitrogen, Carlsbad, CA), RNA extraction kit (Invitrogen, Carlsbad, CA), superscript III RT-PCR kit (Invitrogen, Carlsbad, CA), glycogen, nuclease free water, acid-phenol:chloroform with isoamyl-alcohol (125:24:1, pH 4.5), PCR microtube plates, 96-well microplates, crystal violet were also used in the microbial testing process.

### Nutrient medium

The nutrient medium used for biofilm formation was 30 grams per litre of tryptic soy broth so as to provide maximum nutrient availability to the bacteria for growth. This was chosen to make the conditions most difficult to for the inhibition of biofilm formation. Also, literature review showed that up to 75% of biofilm studies use protein rich media (Chapter 2: Biofilm formation on surfaces: Bacterial nutrient conditions).

**Test material**

**A silicone elastomer** was chosen for two reasons, 1) it is a frequently used catheter material and therefore would be appropriate for test an approach to solving the CAUTI problem and 2) it is an excellent moldable material with the ability to replicate submicron features.

The Silastic brand (Dow Corning Corp., Midland, MI) is commonly used for Foley, central venous catheters, kidney dialysis tubing and shunts for movement of fluid in the brain. Polydimethyl siloxane is also the material used in mammary prostheses, orthopedic finger joints and testicular implants (*205*).

**Silicon wafer and octafluorocyclobutylene** are materials regular process in the electronics industry and have been optimized for use with conventional processing machines. A silicon wafer is usually used in semiconductor manufacturing and is compatible with the standard process machine used to produce deep pattern etches, surface technology systems deep reactive ion etching (STS DRIE, San Jose, CA). Octafluorocyclobutylene is a reactive gas capable of producing a passivation (passive to silicon etch mixture sulphur hexafluoride and oxygen) coating which aids in an anisotropic etch.

**Bacterial test species**

*S. aureus* and *p. aeruginosa* were chosen as the model species as in both cases they have extensively studied for biofilm formation characteristics and they are also known opportunistic pathogens that are commonly reported as the major contributor of medical implant associated infections (*7, 10, 11*).

The *s. aureus* wild type strain SH1000 was used in this study. This laboratory strain has been used in numerous reported biofilm studies and its genome sequence

was found to match very closely(*206*) to the publically available sequence of its parent strain *s. aureus* strain NCTC 8325 (NCBI genebank). *s. aureus* is a natural constituent of human skin microflora of which several notoriously pathogenic strains have evolved that are commonly associated with nosocomial and outbreaks of community acquired infections with increasing prevalence (i.e., Methicillin Resistant Staphylococcus Aureus MRSA).

The *P. aeruginosa* wild type strain PAO1 (ATCC 15692) was chosen because it is the most widely used laboratory *P. aeruginosa* strain and its sequence is publically available (NCBI genebank). *P. aeruginosa* is ubiquitously found in soil and water and is an increasingly prevalent, nosocomial, opportunistic pathogen that is capable of forming biofilms on wounds, in cystic fibrosis patients(*2*), and the lining of catheters(*11*). Another *P. aeruginosa* strain, *P. aeruginosa* Rochester, was also used.

*E. cloacae,* strain ATCC 700258, biofilm formation tests were conducted and CSLM images were obtained at the Engineers Research and Development Corps (ERDC) by Megan Merritt.

**Materials Used For The Wetting Approach**

Following is a bullet list of materials used:

- Silicon wafers (n-type, <001>, test grade, University Wafer Inc., Boston, MA)
- Octafluorobutylene (STS DRIE, Newport, UK)
- Sulphur hexafluoride (STS DRIE, Newport, UK)

## Methods Used for the Confinement Approach

**Duration of the Test**

The duration of the tests was chosen to be 7 days due to its relevance in catheter studies. Catheters are used for varying durations with 7 days signifies an average

duration for catheter applications. The results from this study would therefore be of direct interest to problem that is being addressed here. Also, initial tests with both *p. aeruginosa* (PAO1) and *s. aureus* (SH1000) indicated that there was very little overall growth up 5 days even on the smooth surface, with growth protocol used. A third reason for choosing 7 days was so that comparisons can be made with previous work with *s. aureus* biofilm formation on patterned topography.

**Fabrication of Patterned Topography for the Confinement Approach**

The fabrication process is as follows (Figure 3-1): in order to obtain multiple individual wafer molds the following process was employed using a single patterned mask. Firstly, a 4 inch diameter wafer was heated at 120°C for 5 minutes and coated for 45 seconds with a stream of hexamethyl di silazane (HMDS) at 90°C. It was then spun coated with a positive photoresist (S1813, Microposit, Shipley, Dow Chemical Co.) and soft baked at 105°C for 2 minutes. The wafer was then cleaved in to several small pieces each above 1.15 cm by 1.15 cm in dimensions.

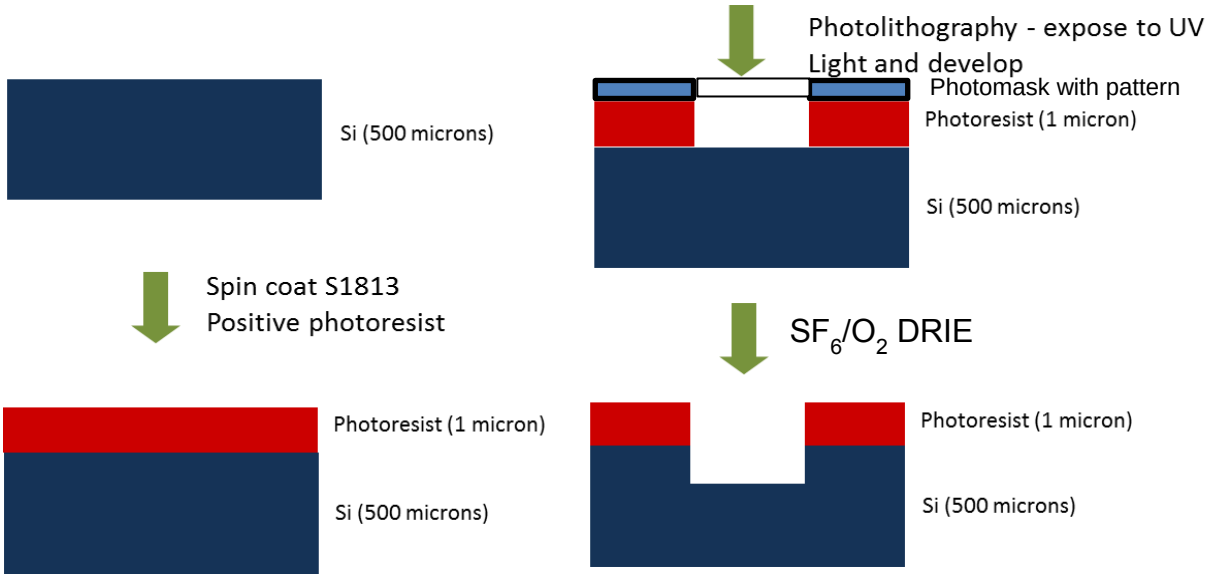


Figure 3-1. Fabrication process schematic for fabricating patterned topography on PDMSe

The samples were then exposed through the patterned mask for 21 seconds, followed by development for 1 minute and 30 seconds for pillar topographies. For the pit topographies following the 21 seconds exposure to UV light, the samples were exposed for 20minutes to ammonia reversing the image of the original exposure followed by 52.5 seconds of the flood exposure to UV (no mask) and development for 1 minute and 30 seconds. The samples were then hard baked at 125°C for 3 minutes and etched under different etch conditions to obtain similar heights. The Sharklet$^{TM}$ samples were made using silicon wafer molds provided by Liwen Jin (courtesy of Dr. Anthony Brennan, University of Florida).

**Casting topography on PDMSe:** The test specimens were made using platinum catalyzed PDMSe Silastic T-2 (Dow Corning Corporation) base and curing agent according to manufacturer's recommendations. A pre-polymer mix consisting of 10 weight percent curing agent to base was hand mixed in a plastic container for 3 minutes following which it was degassed twice at -25 in Hg pressure and room temperature for 3.5 minutes each time. Samples were peeled after 24 hours. The peel should be performed with a small unidirectional force.

**Scanning Electron Microscopy**

This was chosen as one of the methods to assay the 7 day biofilm growth because the method is excellent in adequate depth of field and high resolution images for analyzing the morphology of the biofilm.

Microstructure images were obtained using the scanning electron microscope (SEM). JEOL SEMs (JEOL 6400 – MAIC, JEOL 5700 – PERC) (thermal) were used to obtain the SEM images for this section of the study. Silicon samples were image without

any additional treatments in the secondary electron mode. All non-conductive samples were coated with gold-palladium and imaged in the secondary electron mode.

Following the final rinses, according to the growth protocol, the samples that were to be prepared for SEM analysis were immersed in 20ml of 10mM cetyl pyridinium chloride solution to fix the bacterial cells. After a 24 hour incubation period, the solution was aspirated and allowed to dry overnight. The entire sample (1.1cm by 1.1cm) was then placed on a SEM chuck ($\phi$ = 1 inch) with double sided adhesive copper tape. The SEM chucks were then placed in a vacuum chamber with mounted gold-palladium target and coated with plasma making the samples conductive. The samples were then imaged using a JEOL 6400 SEM in the secondary electron scanning mode.

Table 3-1. Primers used for the qPCR and RT-qPCR tests

| Species | Primer Type | Primer Sequence |
|---|---|---|
| PAO1 & SH1000 | 16S rRNA Forward | 5'-TCGTCAGCTCGTGTCGTGAG |
| | 16S rRNA Reverse | 5'-CATTGTAGCACGTGTGTAGCCC |
| SH1000 | arcA Forward | 5'-GTGCAGATGTACGTTCTGAAACGC |
| | arcA Reverse | 5'-CTGGAGAGCACGACGACGAGA |

**Profilometry**

To determine the height of surface features, a profilometer (Wyko NT 1000 Profiler, Veeco Instruments Inc., Tucson, AZ, U.S.A) was used. This optical profiler uses non-contact vertical scanning interferometry, based on reflected light interference signals. Sensors identify the top plane of a topographical surface and scan downward until the lower plane of the topography is reached. The height of the features is reported as the difference in height between the top surface and bottom surface planes. This was conducted at 5 different locations on the sample in order to obtain an average height.

**Primers Used in the Study for polymerase chain reactions (PCR)**

PCR primers for estimating total cell counts were designed on the basis of constitutively expressed genes (Table 3-1). Global gene expression has been studied previously and the housekeeping gene arcA (arginine deiminase), involved in arginine catabolism during anaerobic conditions and nutritional limitation, has been shown to be one of the genes that are expressed in large amounts in *s. aureus* biofilm cells compared to planktonic cells after 48 hour growth(*207*).

**Biofilm Growth Protocol**

Biofilm phenotypic characteristics can be very different with variations in growth conditions. It is therefore imperative that samples should be standardized and were grown according to the following protocol to obtain reproducible results. The growth protocol (Figure 3-2) was adapted from earlier work done in the group for the sake of comparison of previously obtained results.

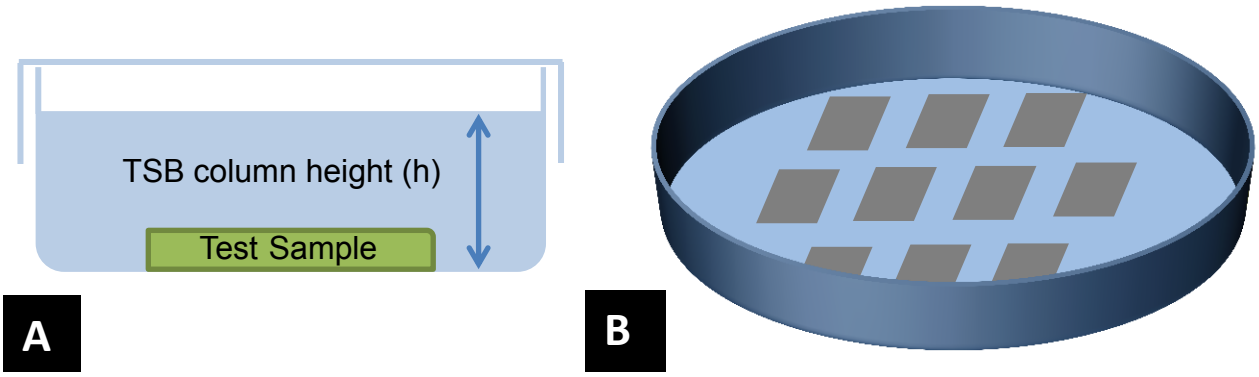


Figure 3-2. Growth protocol (A) petridish growth container with 20ml of TSB (B) sample arrangement within chamber to simulate near identical conditions for the different topographies

The samples (fabricated 1.1cm by 1.1cm silicone elastomer samples) were initially prepared for sterilization by immersing each of the samples for 10 seconds in absolute alcohol and allowing them to dry while in contact with a petri dish. Following this the

samples were dried in vacuum (-25 in Hg).The dried samples were then ethylene oxide sterilized. The samples were always inoculated with 20ml with tryptic soy broth (TSB) containing the bacterium species of interest. The inoculum optical density (OD @ 600nm) was measured and verified to be within 0.2 and 0.4, representing early log phase culture. The culture medium was changed every 24 hours for the length of entire growth period. Before aspiration of the media, the petri dishes were placed on an orbital shaker for 1 minute at 40 RPM. Each time while aspirating the old media, the top pellicle layer was aspirated first followed by the rest of the media. The same growth protocol was used for both *p. aeruginosa* (PAO1) and *s. aureus* (SH1000).

**Confocal Laser Scanning Microscopy (CLSM)**

This method was chosen to study the distribution bacteria on the substrates via fluorescence staining by Syto 9® followed by multiple images obtained for obtaining semi quantitative information.

This method allows for observation of bacteria in a hydrated state as opposed to the SEM imaging method. The microscope slides were stained with SYTO9 by either covering the slide in the petri dish or by placing the slide (biofilm side down) on top of 1 ml of stain. Following which it was incubated for 30 minutes at room temperature in the dark. It was then rinsed with sterile water and dried in the dark. Post drying, 30 µl of sterile water was added and a cover slip placed on the sample. The slide was mounted (coverslip down) on to the microscope and focused using the 100x oil objective with an Argon laser to excite the stain. Ten to fifteen random fields were taken per slide as images for the purpose of quantification.

**Plate Counts**

Plate counts were performed as follows (Figure 3-3). Following the final rinses according to the growth protocol, 8mm punch-outs were obtained using the same biopsy punch for the same patterns across the different conditions. Before moving from one pattern to the next, the punch and the tweezers were dipped in absolute alcohol, burnt off in an open flame to remove any contamination, and allowed to cool between punches. Each punch-out was aseptically transferred to sterile 15 ml tubes (NUNC) with 5 ml 1X phosphate buffer saline (PBS, pH 7.4) with 5 ppm Polysorbate-80. The samples were vortexed for 30 seconds each and then placed on a rack and sonicated 5 times in a sonicating water bath for 1.5 minutes with 1 minute rest intervals per cycle. Each bacterial suspension was ten-fold serially diluted with PBS (100 µl / 900 µl) to a dilution factor of 106 in triplicate.

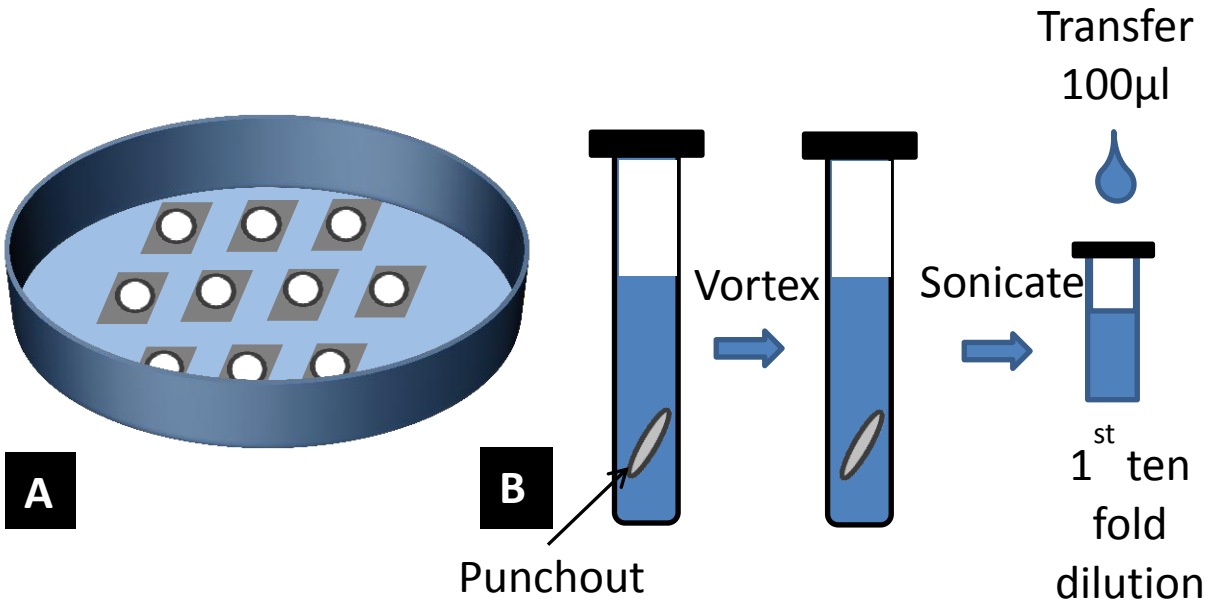


Figure 3-3. Plate count protocol (A) petridish from which 8mm diameter circular pieces are punched out (B) punchouts are then placed in 5ml PBS with polysorbate-80, then vortexed and then serially diluted for plating.

The last four dilutions were plated and incubated at 37°C overnight, following which the number of colony forming units was counted.

**Bio-Timer Assay (BTA)**

The bio-timer phenol red (BT-PR) medium was made by mixing 21 g of Mueller-Hinton (MH) broth, 10 g of glucose and 25 mg of phenol red in 1000 ml of water. The media was sterilized by autoclaving at 121°C and 15 psi for 20 minutes(*154*). Microcentrifuge tubes were also autoclaved at the same conditions and 680 µl of BT-PR medium was transferred into each tube by means of a sterile pipette tip.

Following the final rinses according to the growth protocol, 8 mm punch-outs were obtained using the same biopsy punch for the same patterns across the different conditions. Before moving from one pattern to the next, the biopsy punch and the tweezers were dipped in absolute alcohol, burnt off in an open flame to remove any contamination, and allowed to cool between punches. Each punch-out was carefully immersed in 680µl of BT-PR medium. The lids of the microcentrifuge tubes were then pierced with a sterile 18.5 gauge needle in order to allow for air flow. The samples were incubated at 37°C until the maximal colour change developed in all samples and photographs were taken at 15 minute intervals.

**Calibration curve**

The calibration curve was prepared corresponding to the activity of the bacteria in the volume of BT-PR medium corresponding to the volume to be used for sample testing. The colour change times that were obtained were for the same volume used for sample testing. The CFU/ml determined to be present in an original overnight culture by plate count assessment was used to estimate the number of CFUs/ml contained in the

sample dilutions for the BT-PR colour change assay. A graph of CFUs/ml versus colour change times was plotted to generate a standard reference curve.

**Image analysis**

After the images from the BT-PR colour change assays were obtained, they were analyzed using a matlab code to accurately determine the colour change based on the literature standard. The images were scaled between 0 and 255 for the primary colours (red, green and blue) and a pixel id list was created to map the pixels with the various colour scales. A standard image from the literature was used to obtain the colour change point, and all images were analyzed to determine the colour change point. This was done for the calibration curve images as well as the corresponding mean planktonic equivalent (PE) colony forming units was obtained for all the different surfaces.

**Antibiotic Susceptibility**

This is an indicator of the phenotypic state of the bacteria. If the chosen antibiotic kills more bacteria grown for the same time period on patterned topographies versus smooth control surface it can be concluded that patterned topographies are effective in biofilm growth control.

The antibiotic susceptibility test was carried out for 24 hours following the 7 day growth period. At the beginning of the eighth day, the 24 hours old nutrient medium was aspirated and 20 ml of TSB containing 120 µg / ml oxacillin for s. aureus and 20 µg / ml gentamicin for PA. The concentrations needed for s. aureus were based on earlier work (*208*). The concentration used in that study was close to 10000 times the MIC for the strain ATCC 35556 (0.125µg/ml) and resulted in 100 % kill and might have been over the MBEC. The strain used in this study was wild type strain SH1000 with an MIC of 1.25µg/ml. Thus, a concentration of close to 100 times MIC was used so as to identify

differences in the extent of biofilm differentiation while killing planktonic bacteria assuredly. Following the oxacillin susceptibility protocol, the bio-timer protocol was employed to assess the differences between the various surfaces with respect to its effect on biofilm growth.

For the wild type PA strain PAO1 (MIC of 2 µg/ml gentamicin), 20µg/ml of gentamicin was used to determine the extent of biofilm phenotype differentiation based on gentamicin susceptibility. The plate count protocol was followed with the modification that only ten-fold serial dilutions to a dilution factor of $10^3$ were made, and all dilutions were plated and incubated at 37°C overnight, following which the number of colony forming units was counted.

Following the final rinses according to the growth protocol, with or without antibiotic treatment, 8 mm punch-outs were obtained using the same biopsy punch for the same patterns across the different conditions. Before moving from one pattern to the next, the biopsy punch and the tweezers were dipped in absolute alcohol, burnt off in an open flame to remove any contamination, and allowed to cool between punches. Each punch-out was aseptically transferred to sterile 24-well microplates for BTA analysis. .

After exposing the SA and PA biofilms to the antibiotics for 24 hours, the old antibiotic nutrient mix was aspirated and rinsed 3 times each in 1 X PBS and doubly de-ionized water. Following this, the BTA protocol was employed for SA biofilms and plate count protocol was employed PA biofilms to detect differences between the various surfaces.

**Quantitative Polymerase Chain Reaction (qPCR) sample preparation**

Following the final rinses according to the growth protocol, four 5 mm punch-outs were obtained from each sample and transferred into sterile 2 ml microcentrifuge tubes

with 1 ml of sterile 1X PBS. The samples were then vortexed for 1 minute at maximum speed, sonicated 5 times for 1.5 minutes with 1 minute rest intervals per cycle. The lids were then punctured using a sterile 18.5 gauge needle. Following this they were boiled for 10 minutes at 95°C to lyse the bacterial cells, nature proteins, and inactivating DNase, thus freeing genomic DNA. The tubes were then sealed with paraffin wax and the lysates were stored at -20°C for later use.

**Standard curve**

The qPCR standard curve samples was prepared by extracting genomic DNA from planktonic bacteria, according to the following protocol, and ten-fold serial dilutions were made and ran along with the test samples for quantitative real time PCR analysis.

**For extracting the genomic DNA:** Nuclease free 100% and 70% molecular biology grade ethanol were prepared in RNase & Dnase free 50 ml conical tubes and were chilled at -20°C. Overnight SH1000 cell cultures were prepared and 1 ml of cells was pelleted by centrifuging at 14000 RPM for 5 minutes. Cells were resuspended in 200 µl of 1X PBS.

350 µl of Solution A (Qiagen DNA extraction kit) was added to the cell suspension and was vortexed at 1 second intervals until solution became clear. Then the samples were incubated at 65°C for 10 minutes. 150 µl of Solution B (Qiagen DNA extraction kit) was added and vortexed vigorously until the precipitate moved freely in the tube, and the sample reached uniform viscosity (10 seconds to 1 minute).

**For isolating the DNA:** 50 µl of chloroform was added and vortexed until the viscosity decreased and the mixture became homogenous (10 seconds to 1 minute). The samples were then centrifuged at 14000 RPM for 10-20 minutes at 4°C to separate phases and the upper aqueous phase was transferred into a fresh microcentrifuge tube.

**For DNA Precipitation:** 1 ml of nearly anhydrous ethanol (received 100% anhydrous) (at -20°C) was added to the samples and vortexed briefly, and then incubated at -20°C overnight. The following day the samples were thawed and centrifuged at 14000 RPM for 10-15 minutes at 4°C. The ethanol was then removed from the pellet with a drawn-out Pasteur pipette. The DNA pellet was washed to remove residual salts by adding 500µl of 70% ethanol (-20°C) and inverting the tube 5 times. The samples were then centrifuge at 1400 RPM for 3 to 5 minutes at 4°C. The majority of the ethanol was then removed with a drawn Pasteur pipette and the pellet was retained. The samples were then centrifuged at 14000 RPM for 2 to 3 minutes at 4°C and the residual ethanol was removed with a pipetor. The DNA pellets were then air dried. The pellet was resuspended in 100 µl standard Tris-EDTA (TE) buffer (pH 8.0) and 2 µl of freshly thawed *E. coli* RNaseH (2 U/µl, superscript III first-strand synthesis kit, Invitrogen, Life Technologies, Carlsbad, US) was added to the sample to digest contaminating RNA. The samples were then incubated at 37°C for 30 minutes. The 10-fold serial dilutions standards were made and the concentrations of DNA were measured using a Nanodrop™ spectrometer.

Table 3-2. Constituents and corresponding volumes for qPCR

| Reactants | Volume per reaction (µl) |
|---|---|
| SYBR Green PCR master mix (Applied Biosystems) | 12.5 |
| Genomic DNA* | 1 |
| Forward-Reverse 16s rRNA Primers Mix (10 µM) | 0.5 |
| Nuclease free water (Ambion) | 6 |

* Sample cell lysate or extracted DNA standards

**Quantitative real time PCR (qPCR) plate preparation**

The concentrations of DNA in the various samples were determined by using a quantitative real-time polymerase chain reaction. All sample reactions were performed

in a 96-well PCR plate with a 20 µl total reaction volume per sample with the recipe given in Table 3-2.

The PCR reaction plate was kept on ice during reaction sample preparation until it was load onto a Bio-Rad icycler PCR machine under standard PCR cycle parameters recommended by the manufacturer (SYBR Green PCR master mix, Applied Biosystems).

**Quantitative Reverse Transcriptase PCR (RT-qPCR) sample preparation**

Detection of phenotypic state was performed with mRNA based reverse transcription followed by quantification to confirm the antibiotic susceptibility assay. For accurate quantification of total bacteria present DNA based quantification was used.

Following the final rinses according to the growth protocol, one 8 mm punch-out and two 3 mm punch-outs were obtained from 9 individual test samples in order isolate enough RNA for testing. The samples were then transferred to 2 ml RNase/DNase free microcentrifuge tubes with 500 µl of RNA Protect$^{TM}$ (Qiagen) (used to stabilize the RNA within the bacterial cells), vortexed for 5 seconds and incubated at room temperature for 5 minutes. They were then centrifuged for 10 minutes at 14000 RPM.

All centrifugation was done at 14000 RPM. Only nuclease free molecular biology grade ethanol was used in the process steps. RNase Away$^{TM}$ (Molecular BioProducts, ThermoFisher Scientific) was used to wipe down the work area, containers, and gloves during RNA Experiments. Gloves were discarded between each major step. These directions were followed strictly to prevent RNase contamination.

**For RNA extraction:** 100µl of lysozyme solution was added to the samples and were incubated at room temperature with vortexing for 10 minutes. Following this 350 µl of RLT buffer with β-mercaptoethanol (Qiagen RNeasy Mini kit) was added to the

samples and vortexed at maximum speed for 1 minute. The samples were then stored at -80°C to facilitate complete lysis of the bacterial cells for better RNA recovery.

The samples were thawed and 250 µl 100% molecular grade ethanol was added to each and mixed by pipetting. 700µl of the lysates was transferred to respective RNeasy extract columns (selectively binds nucleic acids) and centrifuged for 15 seconds (flow through discarded). 700 µl of buffer RW1 was added, after processing the 9 lysates, to the columns and centrifuged for 15 seconds (flow through discarded). After this, 500 µl of buffer RPE was added and centrifuged for 15s (flow through discarded). Then, 500µl of buffer RPE was added and centrifuged for 2 minutes (flow through discarded). The collection tube was then changed and the columns were centrifuged again for 1 minute. The old sample collection tubes were swapped for new nuclease free 1.5 ml collection tubes and 50 µl RNase free water was added to each of the columns twice with 1 minute incubation before centrifuging to elute the RNA (total 100 µl elution volume).

**DNase digestion:** DNase treatment was carried out on all RNA extraction samples to eliminate contaminating genomic DNA interference in subsequent RT-qPCR assays. To the RNA extract, TURBO DNase buffer (made up to 1X from 10X stock concentration) was added followed by addition of 1 µl of TURBO DNase (Ambion) (1U/1µg of DNA). Samples were incubated at 37°C for 30 minutes.

**For phenol-chloroform extraction:** The samples were cooled to room temperature and the RNA was extracted with Phenol-chloroform to remove contaminating proteins (i.e., RNases). After final volumes of each sample were brought to 100 µl using nuclease free water (if necessary), 100 µl of acid-phenol-chloroform with

isoamyl-alcohol (125:24:1, pH 4.5; Ambion) was added. They were then centrifuged for 10 minutes at room temperature. The aqueous phase was then transferred to a fresh nuclease-free microcentrifuge tube.

**Ethanol precipitation:** Ethanol precipitation, to remove residual phenol-chloroform or to concentrate nucleic acids, was carried out by adding 0.5 µl of glycogen, 0.1 by volume of 3M sodium acetate (pH 5.5), and 2.5 by volume of ice cold 100% ethanol. The samples were then incubated at -20°C overnight, following which they were brought to room temperature and were centrifuged for 30 minutes at 4°C. The pellets were carefully washed by pipetting with 300 µl of ice cold 70% ethanol (care should be taken in this step as pellet may get dislodged and drawn with the pipette tip). The ethanol was then removed and the pellets were allowed to air dry.

## Methods Used for the Wetting Approach

### Fabrication of Undercut Topographical Surfaces for the Wetting Approach

The fabrication process (Figure 3-4) starts with the deposition of 300nm thick hexagonal silica ($SiO_2$) layer on silicon. Following this, pillars with various aspect ratios were fabricated in a periodic hexagonal pattern using an adaptation of a procedure, previously reported in the literature (*37*).

A $SiO_2$ layer was first deposited onto bare silicon over which positive resist (S1813) was spin coated. This was then exposed to a 400nm wavelength in standard G-line photolithography with the required mask. After the exposed resist was developed off, the wafer subject to a $CHF_3/O_2$ reactive ion etch to etch down to the bare silicon in the exposed regions. The wafer was then subject to the Bosch process in a deep reactive ion etch with $SF_6\&O_2/C_4F_8$ etch chemistries to yield etching in between and under the silica tops.

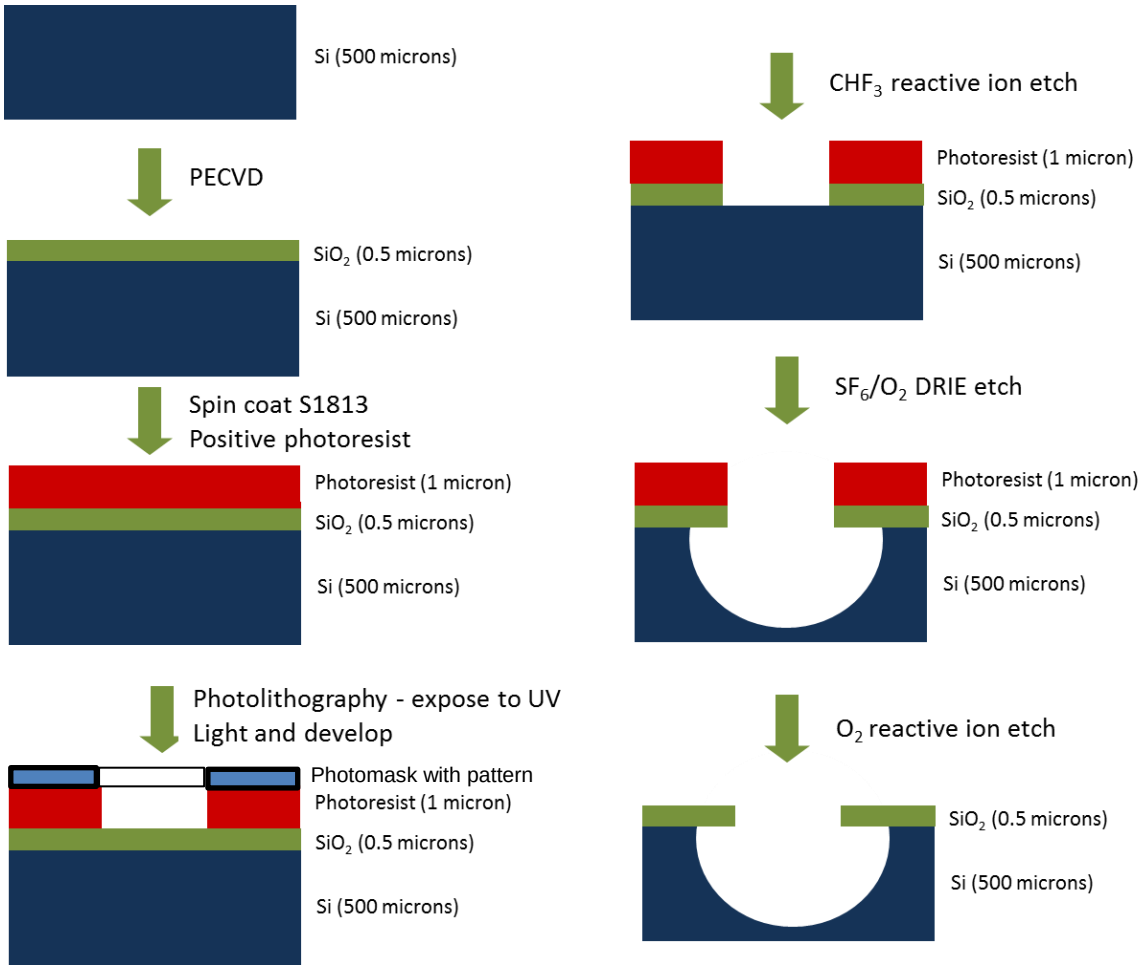


Figure 3-4. Fabrication process schematic for topographies for water wetting studies

A final coat of $C_4F_8$ (part of the STS deep reactive ion etching process) was given to hydrophobize the surface.

**Breakthrough Pressure Measurement**

The breakthrough pressure measurement was conducted by immersing the patterned topography in a 1 cm column of water in a pressure tight sealed container as shown in Figure 3-5. When non-wetting patterned topography is immersed in water, it has a definite shimmer due to the vapour trapped at the surface. The first observable point where the shimmer disappears was recorded as the initial breakthrough point. The

disappearance of the last observable shimmer was recorded as the final breakthrough point.

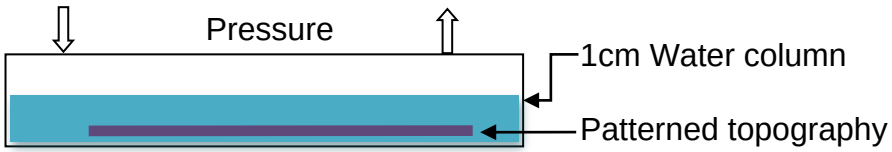


Figure 3-5. Schematic view of the breakthrough pressure apparatus

Some measure of error is expected due to the fact that the initial disappearance and the corresponding final disappearance points were judged by human visual observation.

**Imaging and Measurement of Static and Dynamic Water Contact Angles**

Fresh 18MΩ nanopure water was used for all contact angle measurements. Contact angles were imaged using a Rame-Hart contact angle goniometer (model 190 CA, Rame-Hart Instrument Co.). In order to ensure reproducibility of results, the following precautions were taken: droplet volume and the manner in which the needle is inserted into the droplet were standardized.

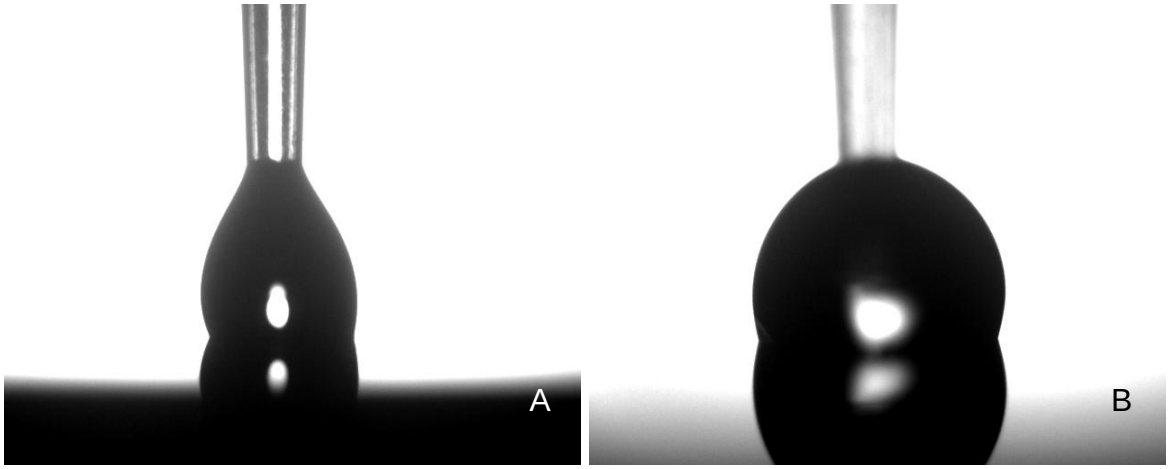


Figure 3-6. Receding contact angle measurements (A) erroneous (B) correct method

The starting volume for advancing contact angle measurements was 20µl. The starting volume for receding contact angle measurements was 30-35µl. In order to obtain adequate reflection during imaging, bare silicon was use as the reflective material adjoining the test specimen sample. The increment/decrement volume of droplet was 0.2 µl. Between measurement sets, the samples were dried at 60 degrees Celsius for 5 minutes in a conventional oven. For sessile drop measurements a standard droplet volume of 25µl was used.

The lowest angle reached immediately before the droplet moves and comes to rest is defined as the receding contact angle. While performing this operation it was observed that the shape of receding droplet can become distorted due to the presence of the syringe (Figure 3-6). It is important to carry out the procedure so that the contact angle is measured free of such distortions. Contact angles were measured using the drop snake B-spline method in Big Drop Analysis (*209*). The external energy was set to 75/25 gradient/region and the region method to Gaussian. Each image was analyzed twice and averaged to reduce inconsistencies generated from vertex placement.

## Statistical Methods

Bacterial numbers were reported as mean colony forming units per ml except in the PCR results. For, qPCR the data was represented as the mean starting quantity of DNA and for RT-qPCR it was expressed as a ratio of 16S rRNA to arcA gene expression.

All pairwise comparisons were performed using the student's t-test at a 95% confidence level (Microsoft Excel 2010). One way ANOVA was performed to determine statistically significant differences followed by Tukey's test for multiple comparisons at a 95% confidence interval. Principal component analysis was performed to determine the

contribution of the different material properties to the variability in the results. All statistical analyses were performed in Minitab (version 15, Minitab Inc, State College, PA) statistical analysis software.

CHAPTER 4
RESULTS AND DISCUSSION

## The Confinement Approach

### Characteristics of the Test Topography

Test samples were analyzed for defects using SEM and optical microscopy. Replication quality was manually checked using an optical microscope for defects over the entire 1.15 by 1.15 $cm^2$ at 10X magnification. Only samples without defects were used for bacterial testing. Samples with excellent replication quality were then prepared for bacterial tests.

Table 4-1. Dimensions of topography used for bacterial testing

| Pattern | Edge to Edge (E-E) (µm) | Spacing (S) (µm) | Beam Length ($B_L$) (µm) | Feature Height/Depth (H/D) (µm) |
|---|---|---|---|---|
| 2µm Pits | 2.12 | 5.82 | - | 3.03 |
| 7µm Pits | 7.46 | 5.00 | - | 3.13 |
| 17µm Pits | 17.45 | 4.93 | - | 3.15 |
| 5µm Pillars | 5.06 | 3.23 | - | 2.35 |
| 11µm Pillars | 10.84 | 2.16 | - | 2.39 |
| 21µm Pillars | 20.58 | 2.09 | - | 2.54 |
| 2µm Cross | 3.01 | 1.72 | 9.22 | 4 |
| Sharklet™ | 2 | 2.00 | 4 - 16 | 3 |
| 5µm Cross | 5.26 | 4.86 | 22.9 | 21.22 |

The topographies tested with bacteria are presented in Figures 4-1, Figure 4-2 and Figure 4-3. 2µm, 7µm and 17µm hexagonal pits, 5µm, 11µm and 21µm hexagonal pillars and the 2µm cross topography, all at 3µm feature heights were tested with *s. aureus* and *p. aeruginosa.*

*E. cloacae* tests were conducted with 2µm cross, 5µm cross, 10µm hexagonal pits, 10µm hexagonal pillars and Sharklet™ topographies. Detailed feature dimensions from SEM image based characterization are given in Table 4-1.

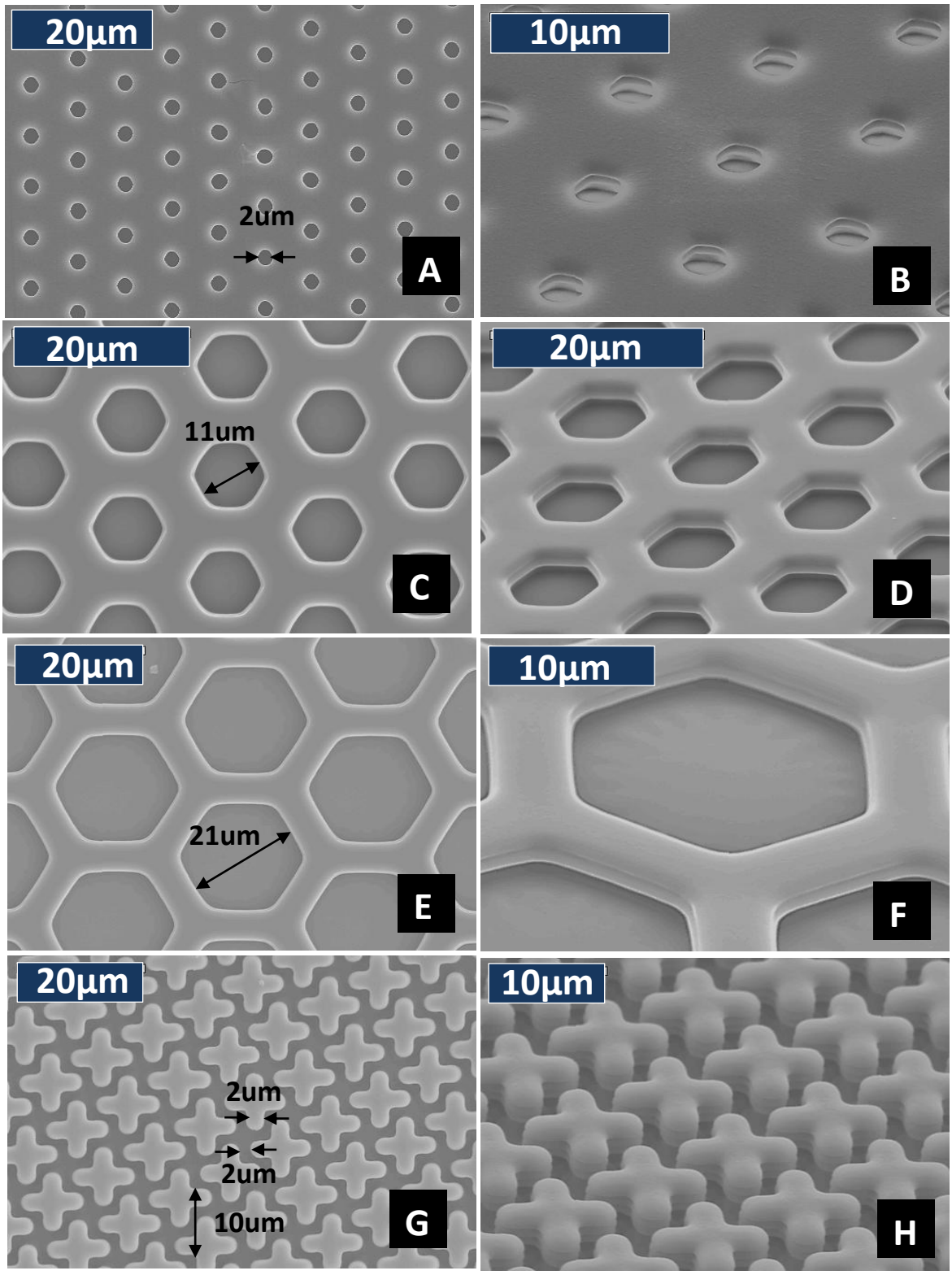


Figure 4-1. SEM images of the test topography on PDMSe. Representation: A&B - 2µm, C&D - 7µm E&F - 17µm hexagonal pits and G&H 2 micron cross, top and perspective views.

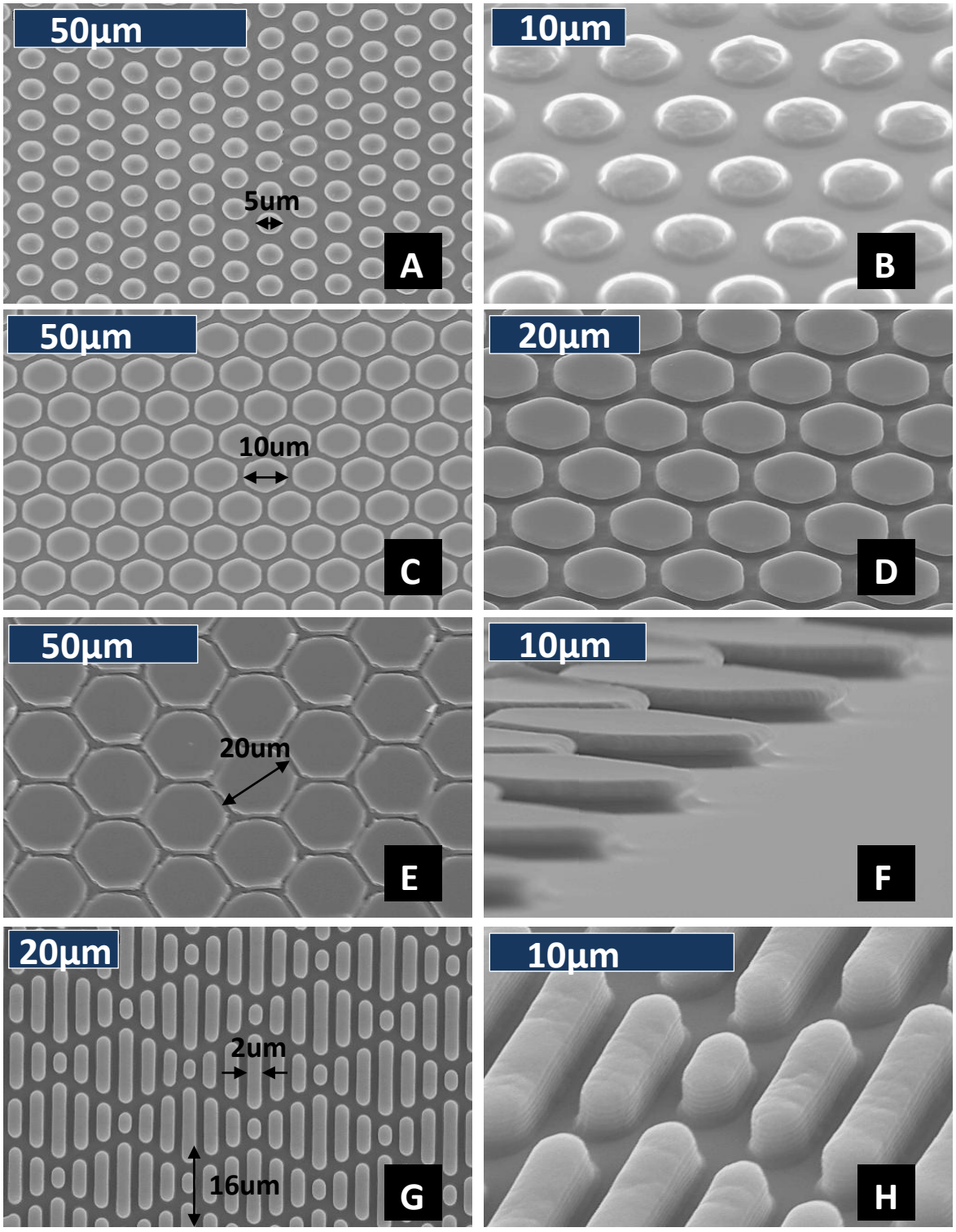


Figure 4-2. SEM images of the test topography on PDMSe. Representation: A&B - 5µm, C&D - 11µm E&F - 21µm hexagonal pillars and G&H Sharklet$^{TM}$, top and perspective views.

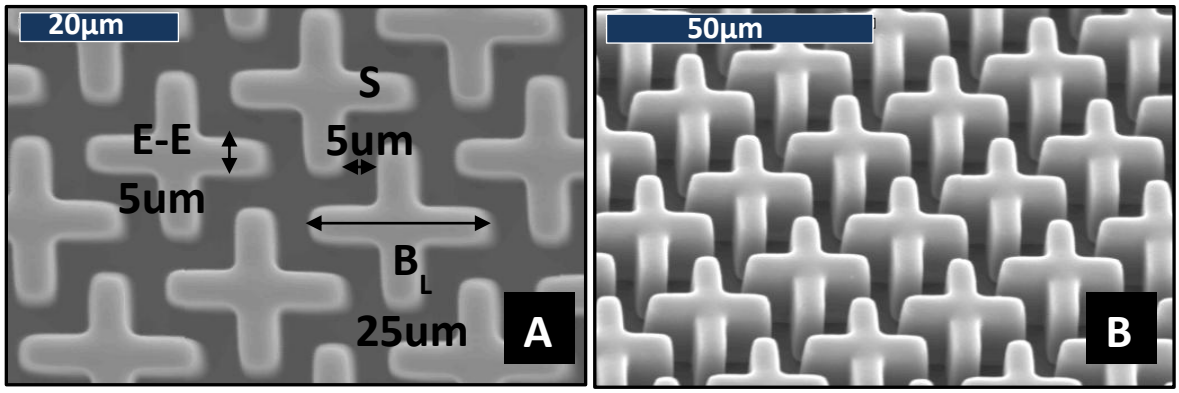


Figure 4-3. 5 micron cross topography (A) Top down view of the 5µm wide, 25µm long intersecting beams spaced by 5µm S – spacing, E-E – edge to edge thickness and $B_L$ – beam length(B) Perspective view of the same topography (height of the features is 20 microns)

Figure 4-4 lists the biofilm characterizations roadmap for which results are presented and discussed below.

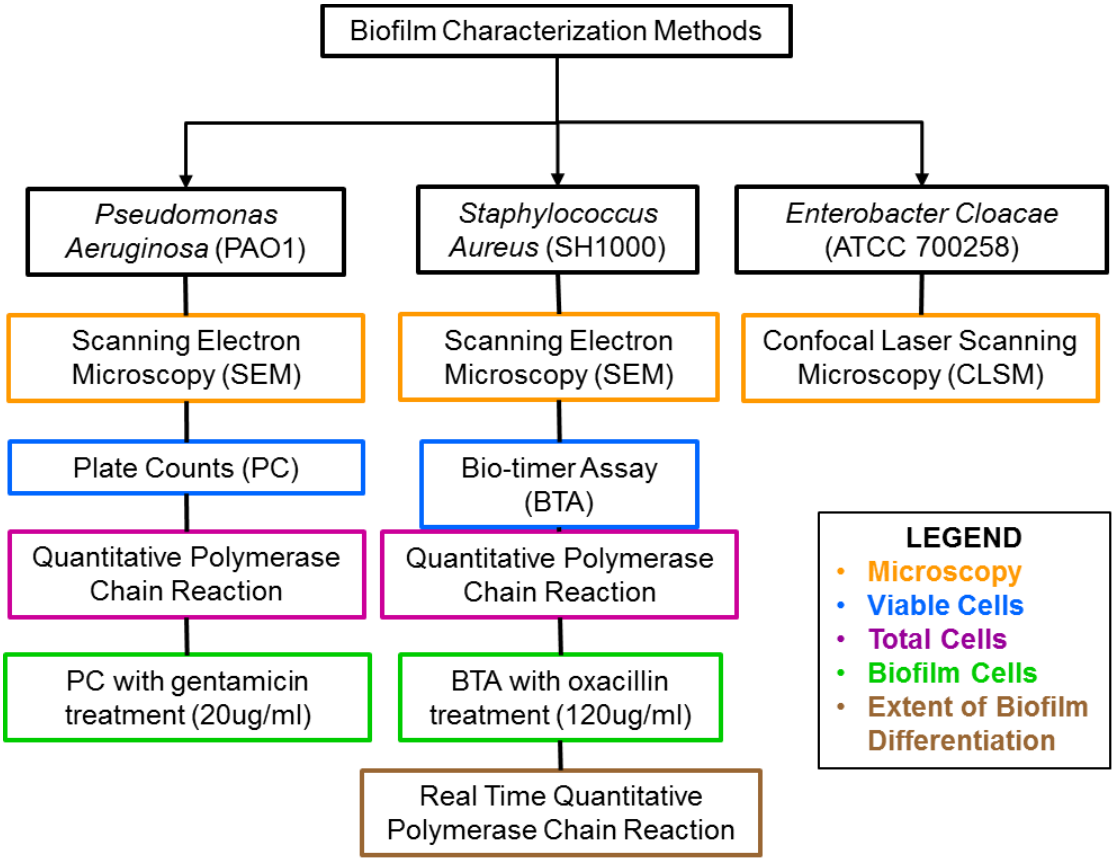


Figure 4-4. Biofilm characterization methods used for topographies testing the confinement approach to inhibit biofilm formation

These reference measurements were used in calculating following pattern characteristics and are in Table 4-2:

- Sessile drop contact angle
- Solid area fraction of the top portions of the topographies ($\phi_S$)
- Wenzel roughness factor (r)
- Engineered roughness index II ($ER_{II}$)

Initially, both confinement and wetting approaches were intended to be tested for their efficacy of inhibition of biofilm formation. This effort was completed for the confinement approach for which the results are presented below. Only fabrication and characterization has been performed for the wetting approach.

Table 4-2. Material characteristics for the samples prepared for biofilm tests

| Pattern | θ* | ϕS | fD | Recessed Volume (cu. microns) | r |
|---|---|---|---|---|---|
| 2µm Pits | 112.48 (±2.25) | 0.92 | 0.08 | 12.74 | 1.41 |
| 7µm Pits | 124.42 (±2.10) | 0.65 | 0.35 | 146.43 | 1.58 |
| 17µm Pits | 132.99 (±3.14) | 0.41 | 0.59 | 802.94 | 1.42 |
| 5µm Pillars | 130.26 (±2.70) | 0.36 | 0.64 | 89.26 | 1.85 |
| 11µm Pillars | 139.83 (±5.82) | 0.63 | 0.37 | 128.50 | 2.51 |
| 21µm Pillars | 127.22 (±2.56) | 0.80 | 0.20 | 220.83 | 3.04 |
| 2µm Cross | 131.47 (±3.73) | 0.59 | 0.41 | 130.15 | 2.67 |
| Sharklet™ | 150.74 (±0.54) | 0.48 | 0.52 | 138.00 | 2.50 |
| 5µm Cross | 147.69 (±2.78) | 0.47 | 0.53 | 5099.50 | 5.29 |
| Smooth PDMSe | 112.83 (±3.12) | 1.00 | N/A | N/A | 1.00 |

### *Pseudomonas Aeruginosa* Biofilm Formation

#### Morphology of biofilms on patterned topography

The morphology of *p. aeruginosa* on test surfaces was **assessed by SEM imaging**. SEM images of *p. aeruginosa* biofilm formation are shown in Figure 4-7 through Figure 4-15 and are discussed in the same order. The smooth PDMSe surface has sporadic colony type growth with clumps of bacteria but in the majority of the sites of bacterial cluster attachment are well separated, indicating even distribution of

colonizing bacterial cells during initial attachment after inoculation. In the case of the 2 µm pits, most of the settlement appears to be in the raised area in between the pits and occasionally within. The 7 and 17 µm features appear to have a more evenly distributed settlement. In the 5 µm and 11 µm pillars, most of the settlement appears to be in the recessed area in between the pits and occasionally on top of the pillars.

SEM images indicate that there may have been more biofilm formation on the 21µm pillar type structures as there is a definite remnant of EPS. The attached bacteria definitely appear to have lost their flagella and are non-motile.

### Quantitative and phenotypic evaluation of patterned topography on biofilm formation

*P. aeruginosa* biofilm formation on test surfaces was **assessed by plate counts, antibiotic susceptibility**. Figure 4-5 represents a global comparison of plate count based (CFU/ml) on all the samples tested for PA biofilm formation following the growth protocol for 7 days. Data analysis shows no statistically significant difference (ANOVA, α=0.05, p=0.842, 6 replicates) between the various patterns nor between the patterned and smooth surfaces.

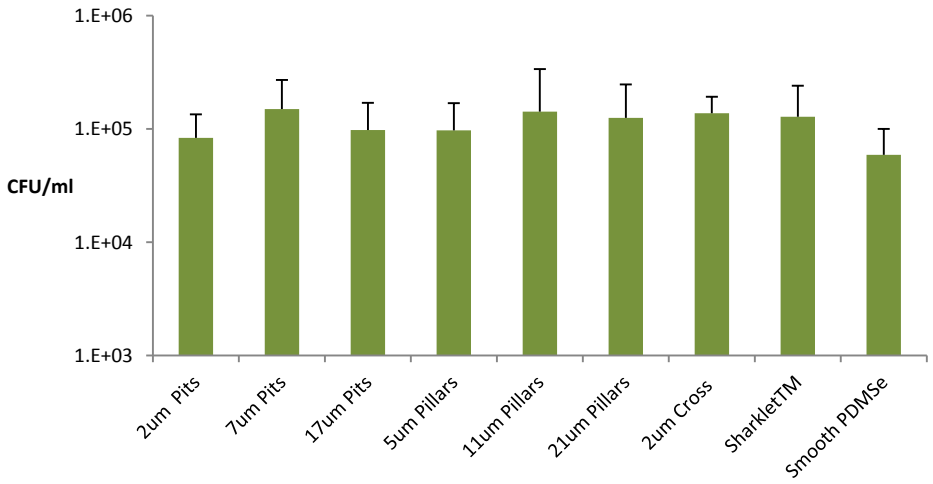


Figure 4-5. Plate count numbers following 7 day PAO1 biofilm growth on topography and smooth PDMSe surface. Error bars represent one standard deviation.

Table 4-2 lists Wenzel roughness(*192*) data for the all the tested surfaces. Given the apparent variation in patterning, there seems to be no detectable positive or negative trend in relation to biofilm growth. **Thus, it can be deduced that patterning on PDMSe doesn't have an effect on *p. aeruginosa* biofilm formation, at the end of 7 days, in terms of the number of viable cells.** (Appendix B: plate count results on the PA Rochester strain). Antibiotic susceptibility tests were carried out at 20 µg/ml and 200 µg/ml of gentamicin for PAO1 for 24 hours. No observable colony forming units were obtained after performing plate counts, indicating a hundred percent kill.

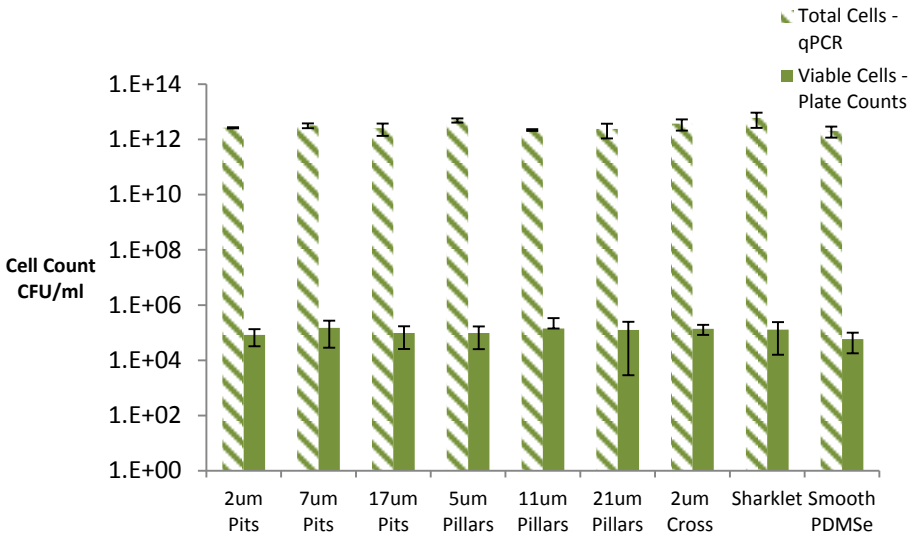


Figure 4-6. Plot of total number of cells calculated from qPCR (hatched bars) and viable cells as plate counts CFU/ml (solid bars) for PAO1 on the various patterned topography and smooth PDMSe

The mean start DNA quantity (Appendix D) is a function of the amount of DNA from the total number of cells which results from the total number of cells present in the test sample/situation. So, by calculation, the total number of cells was deduced from these numbers. Results for the total number of PAO1 cells attached to surfaces, shown in Figure 4-6, indicate an average of about $10^{12}$ to $10^{13}$ cells on all the patterns.

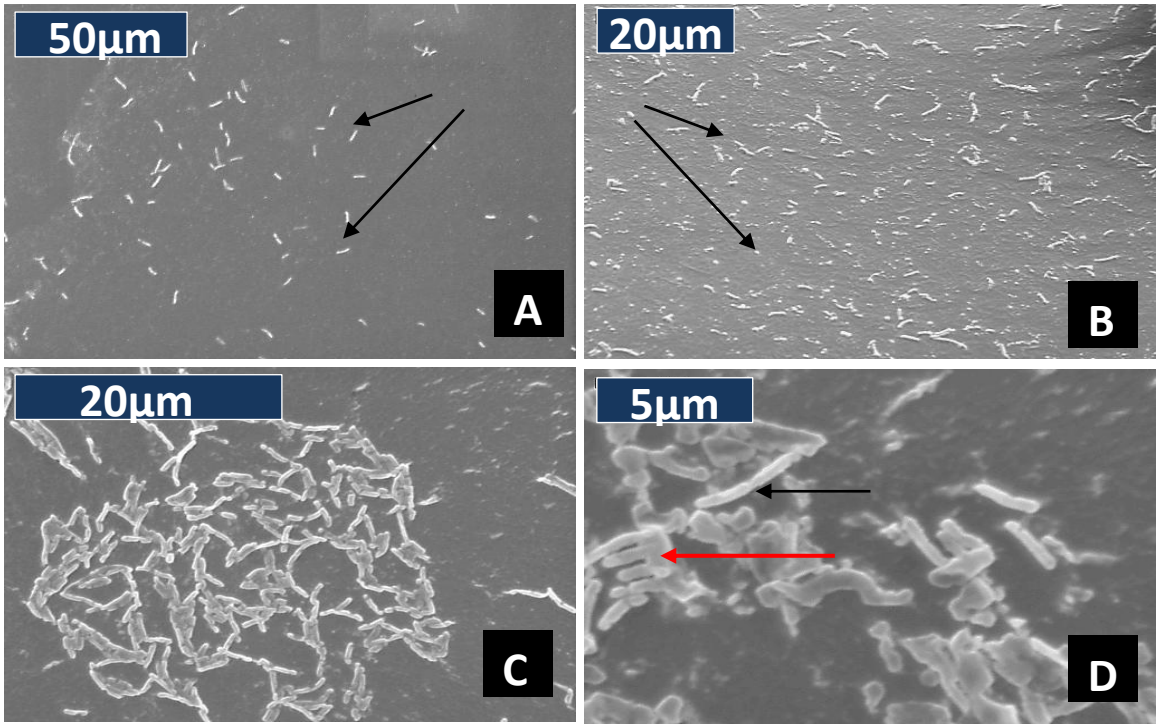


Figure 4-7. *P. aeruginosa* bacterial morphology on smooth PDMSe after 7 days. (A) & (B) black arrow - dispersed cells (C) & (D) denser coverage (D) Black arrow- end to end connection & red arrow- parallel aggregates

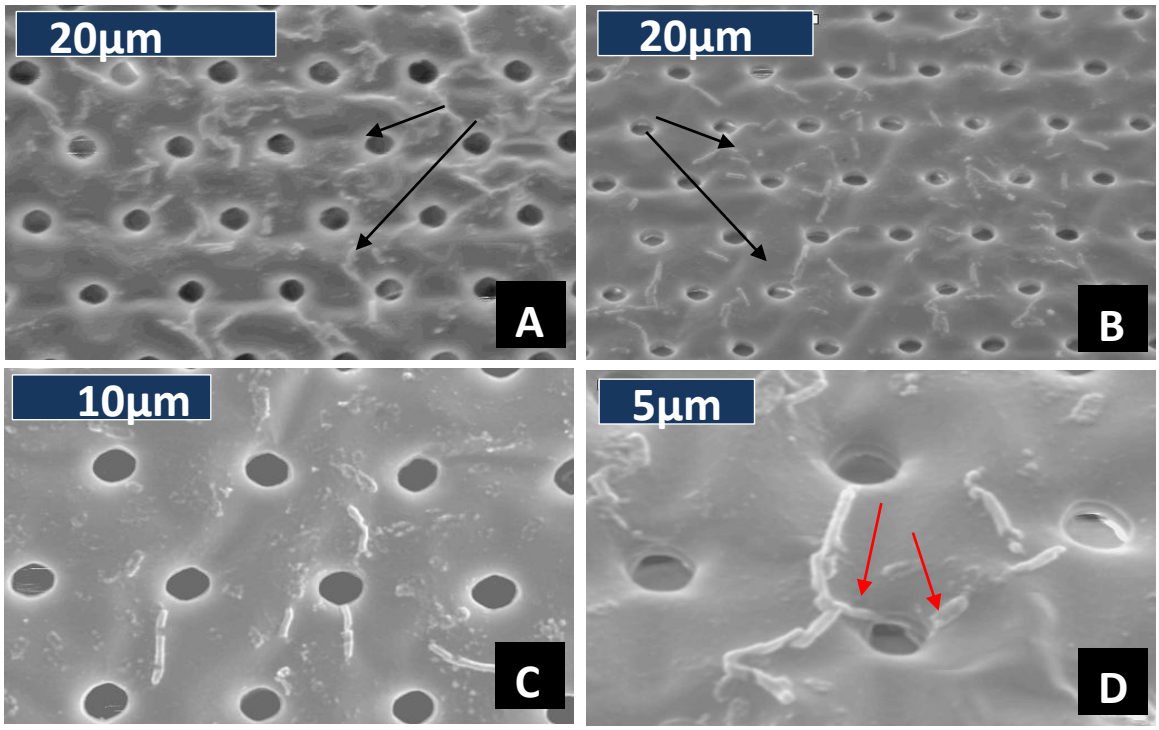


Figure 4-8. *P. aeruginosa* bacterial morphology on 2µm pit topography after 7 days. (A) & (B) dispersed cells (black arrow) (C) & (D) disperse coverage (D) red arrow- cell present over a gradual curvature of the topography

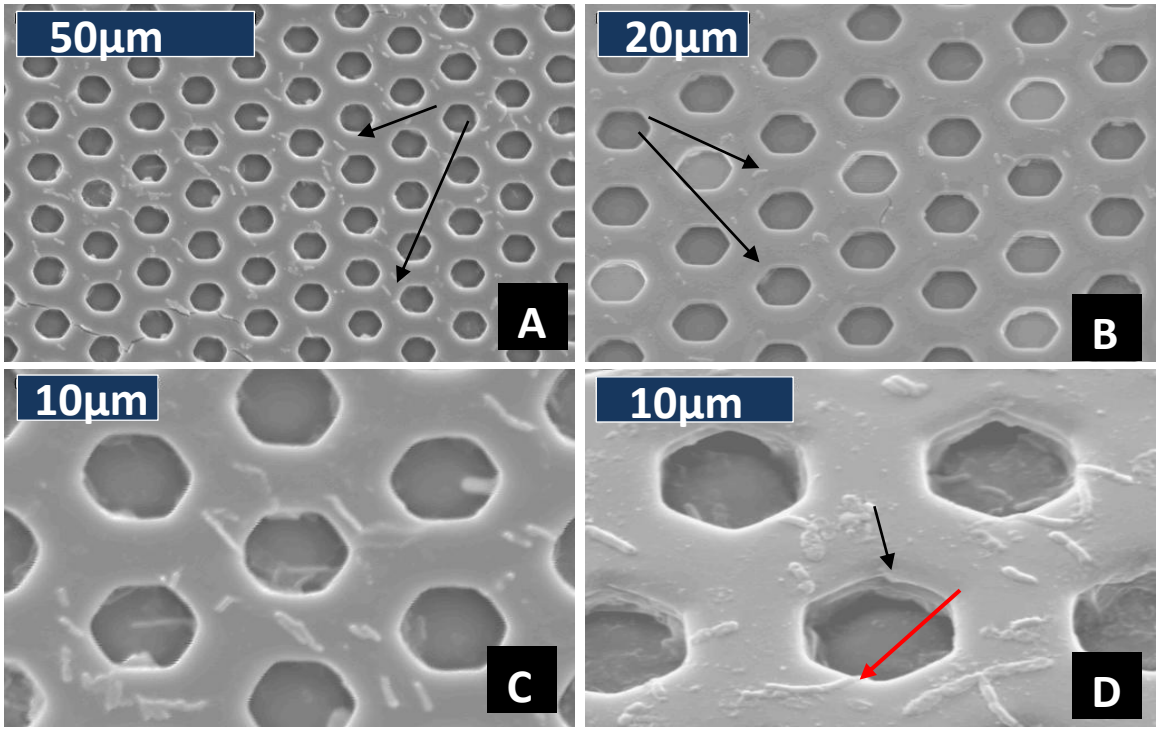


Figure 4-9. *P. aeruginosa* bacterial morphology on the 7µm pit topography after 7 days (A) & (B) dispersed cells (black arrow) (C) & (D) black arrow – gradual change in curvature; red arrow- cell curving over curvature of the topography

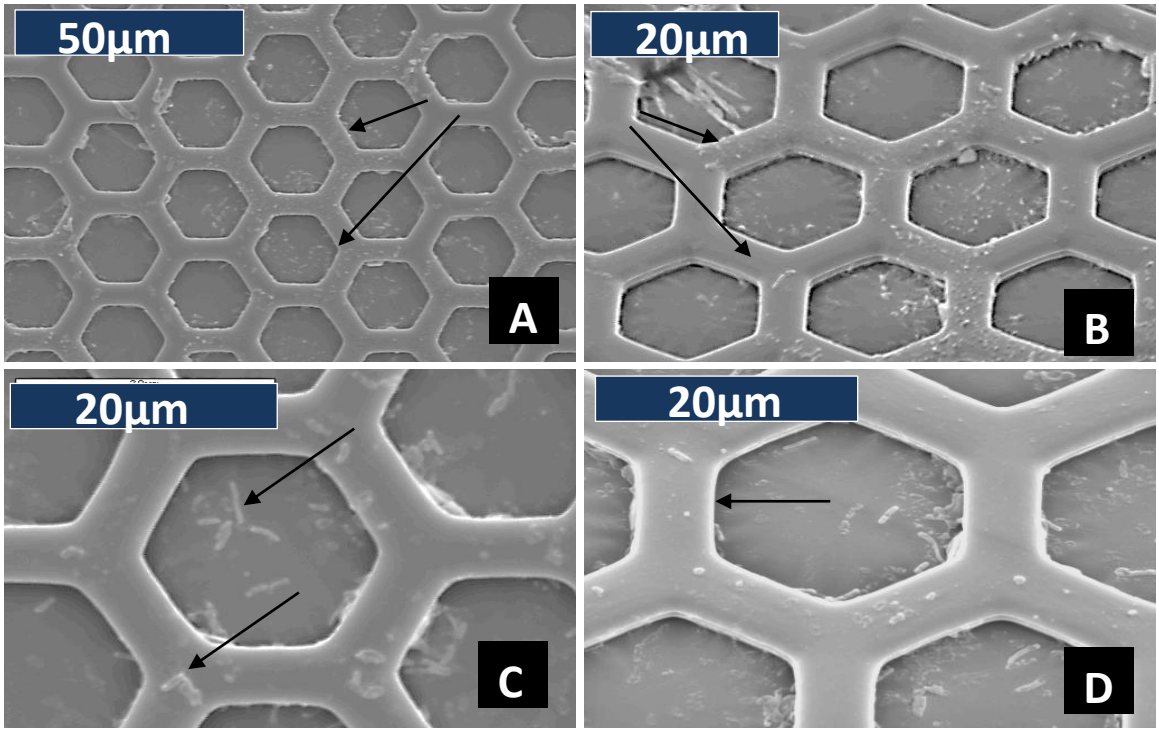


Figure 4-10. *P. aeruginosa* bacterial morphology on the 17µm pit topography after 7 days (A), (B) & (C) dispersed cells (black arrow) (D) black arrow – gradual change in curvature

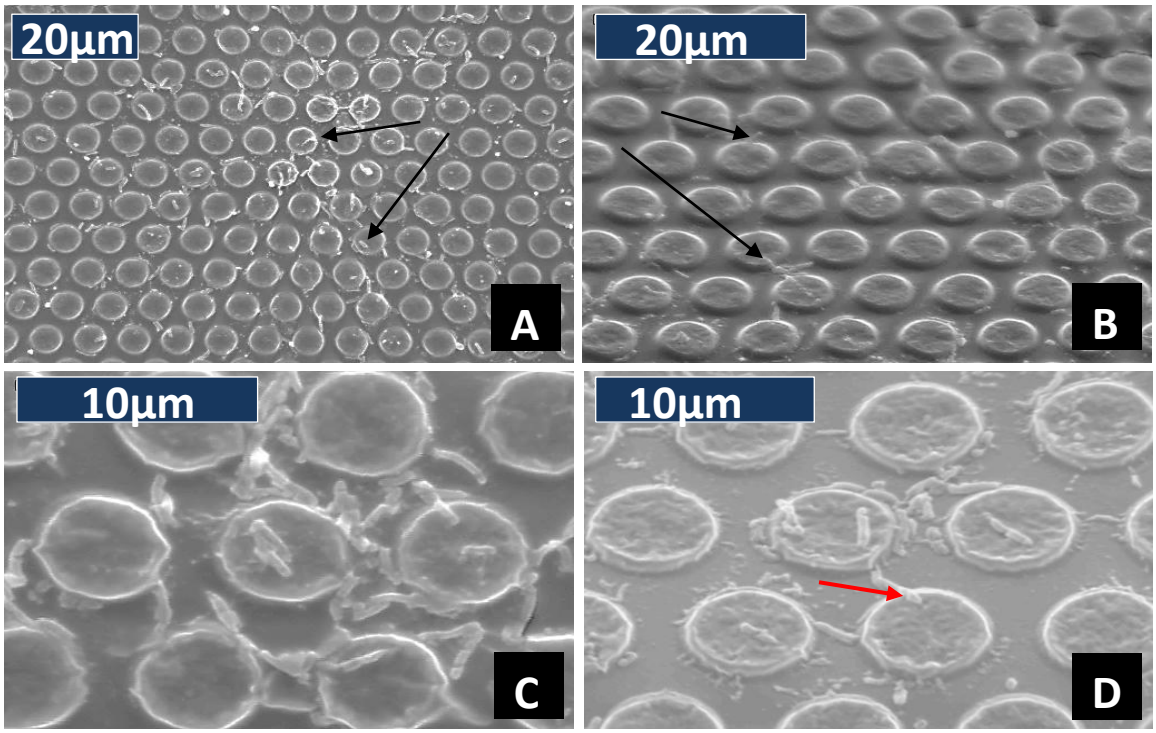


Figure 4-11. *P. aeruginosa* bacterial morphology on the 5µm pillar topography after 7 days (A), (B) & (C) dispersed cells (black arrow) (D) black arrow – gradual change in curvature

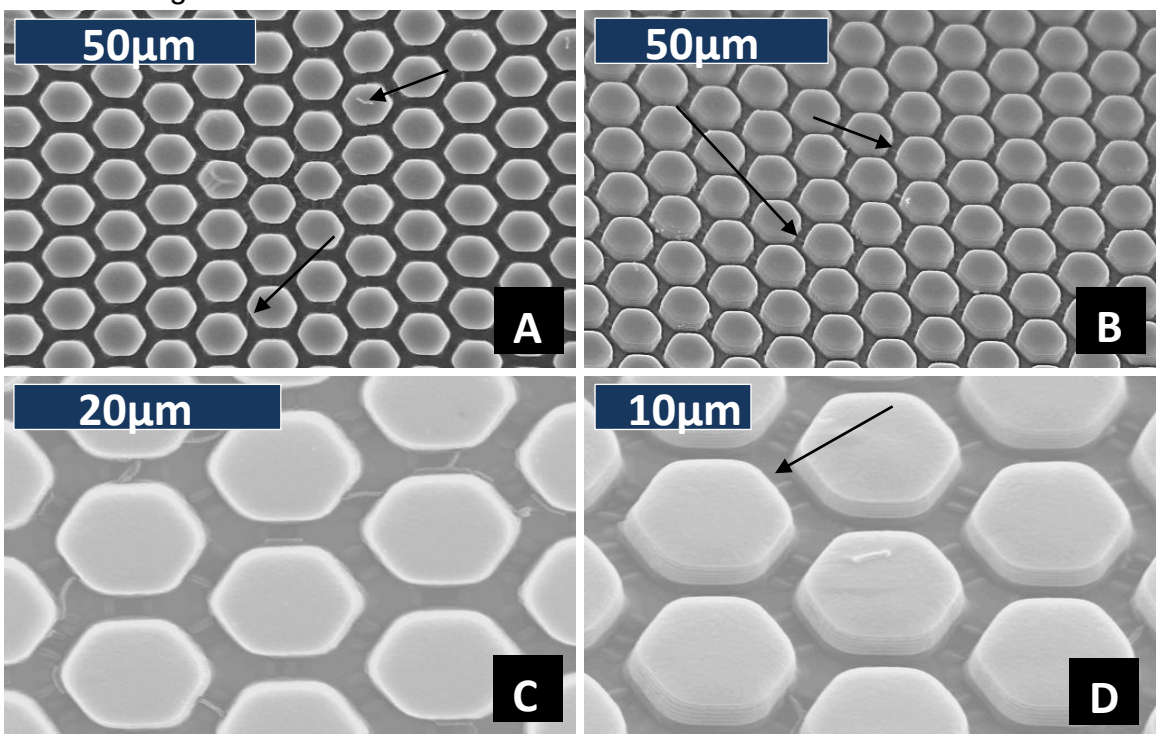


Figure 4-12. *P. aeruginosa* bacterial morphology on the 11µm pillar topography after 7 days (A), (B) & (C) dispersed cells (black arrow) (D) black arrow – gradual change in curvature

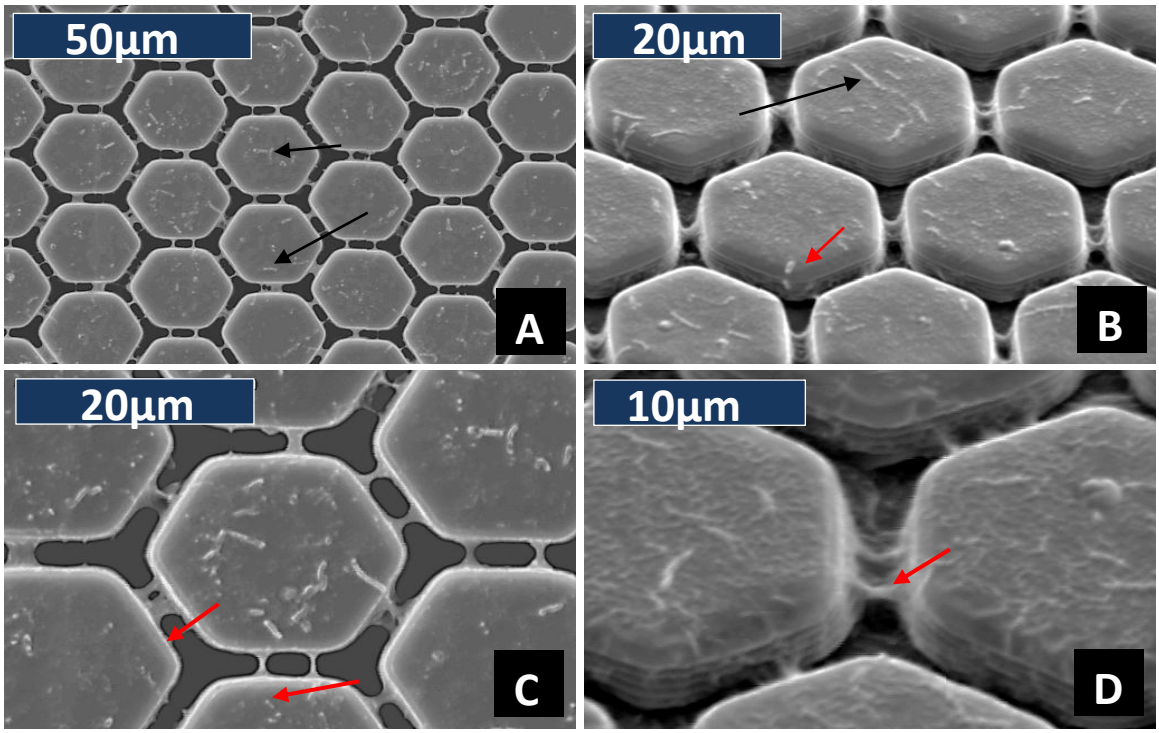


Figure 4-13. *P. aeruginosa* bacterial morphology on the 21µm pillar topography after 7 days (A), (B) black arrow - dispersed cells; red arrow - cell curving over curvature of the topography (C) & (D) red arrow – EPS remnant

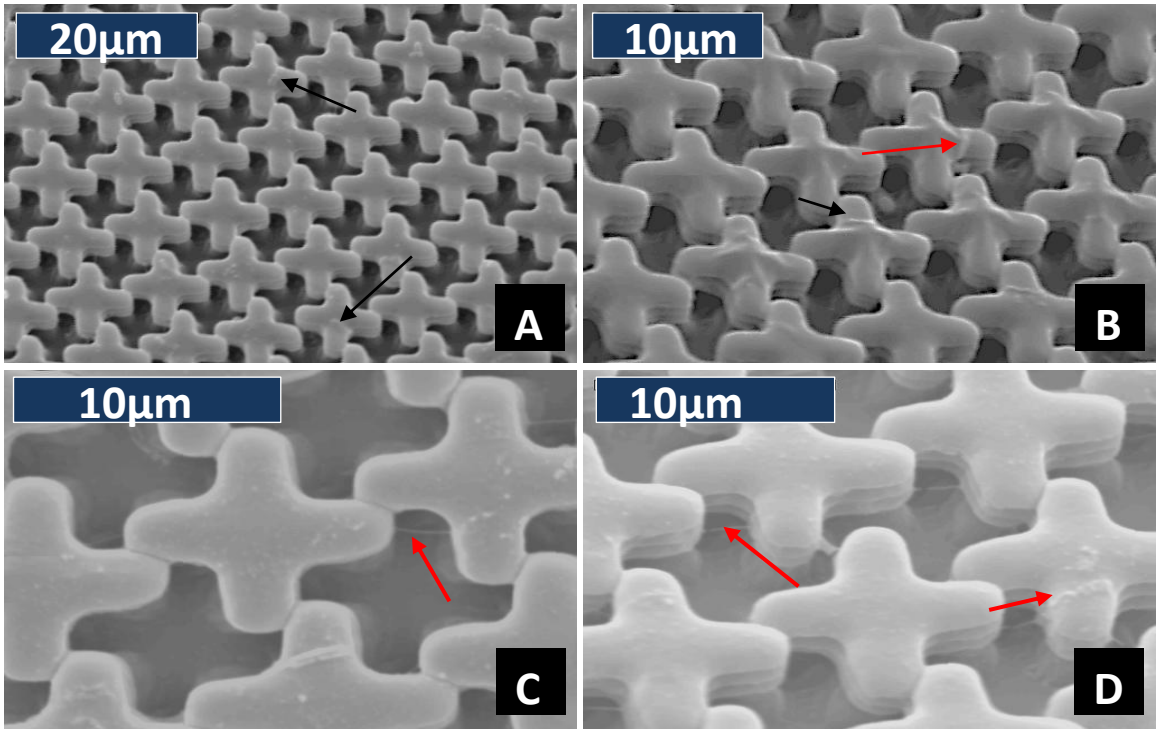


Figure 4-14. *P. aeruginosa* bacterial morphology on the 2µm cross topography after 7 days (A) & (B) black arrow - dispersed cells; red arrow - cell curving over curvature of the topography (C) & (D) red arrow – EPS remnant

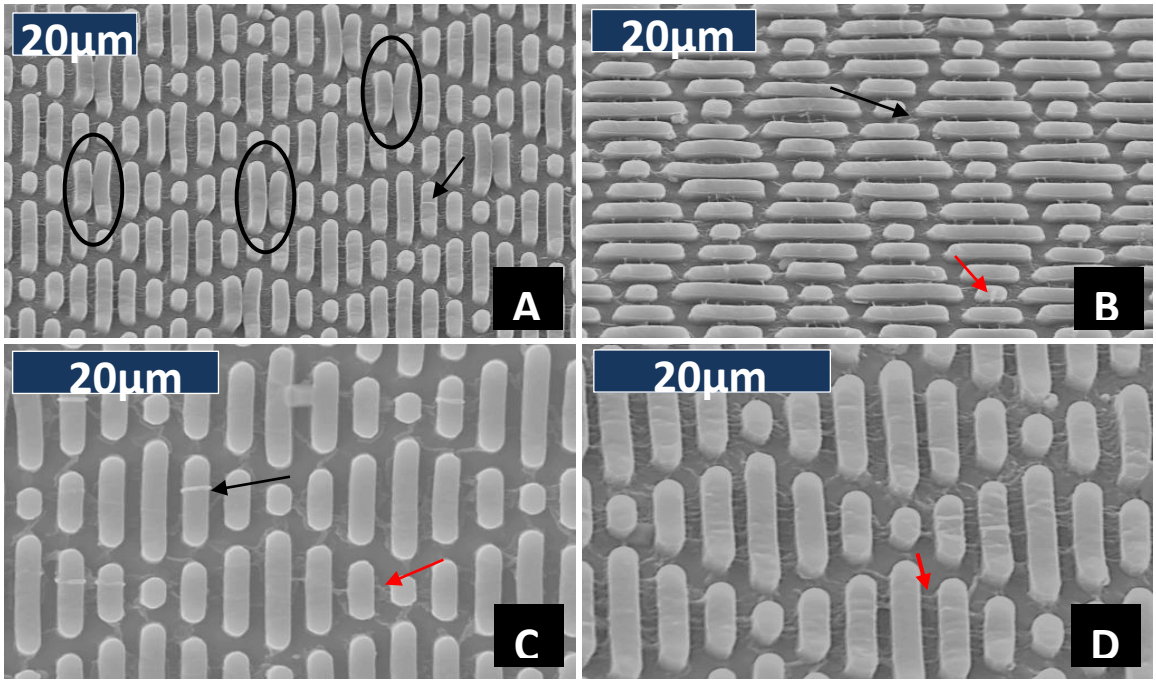


Figure 4-15. *P. aeruginosa* bacterial morphology on the Sharklet™ topography after 7 days (A) black arrow - dispersed cells; black circles – bending and attached features due SEM sample preparation method, not observed prior to start of bacterial assay (B) black arrow - dispersed cells; red arrow - cell curving over curvature of the topography (C) & (D) red arrow – EPS remnant

There are some overall statistically significant differences (ANOVA, α=0.05, p=0.045, 3 replicates) although Tukey's multiple comparison yielded p values above 0.05 for all the patterns indicating no significant differences between samples.Thus, there is a large gap between the number of cells counted as alive using plate counts and counted on the basis of DNA extract and qPCR because of accumulation of dead cells over the 7 day period.

***Staphylococcus Aureus* Biofilm Formation**

**Morphology of biofilms on patterned topography**

**SEM images** of *s. aureus* biofilm formation are shown in Figure 4-16 through Figure 4-24 and are discussed in the same order. The smooth PDMSe surface had significant clumping in some regions whereas smaller microcolonies are observed in other areas.

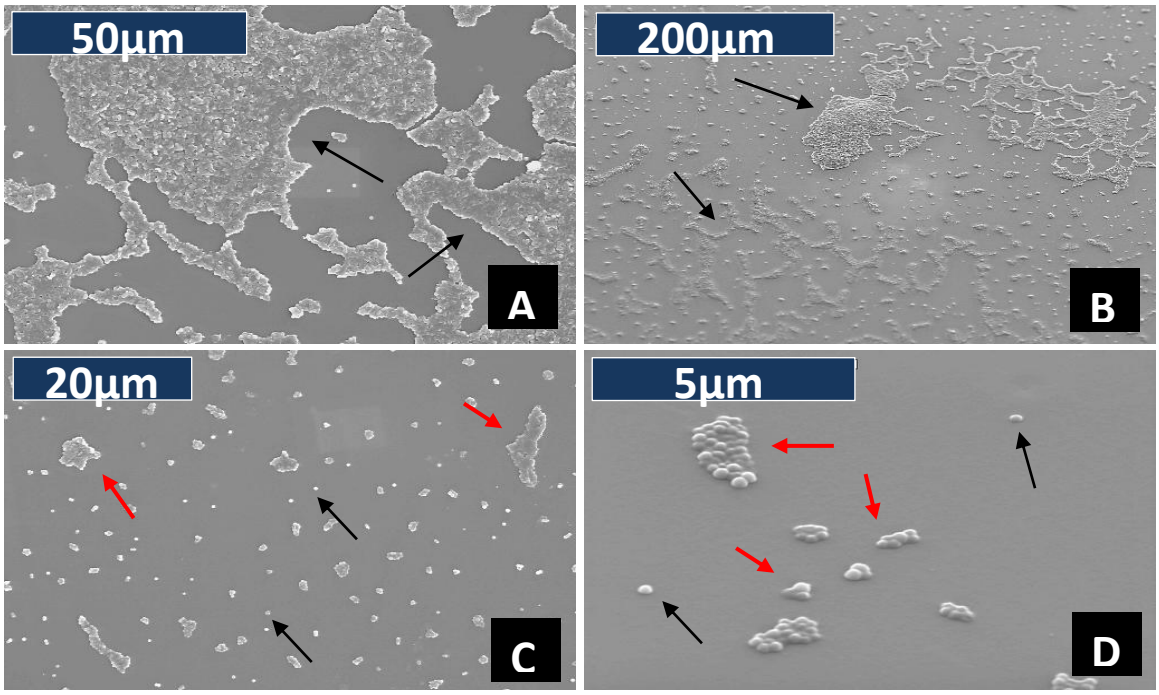


Figure 4-16. *S. aureus* bacterial morphology on smooth PDMSe after 7 days (A) & (B) black arrow – dense coverage; red arrow – cells curving over curvature of the topography (C) & (D) black arrows - isolated cells; red arrow- small clusters

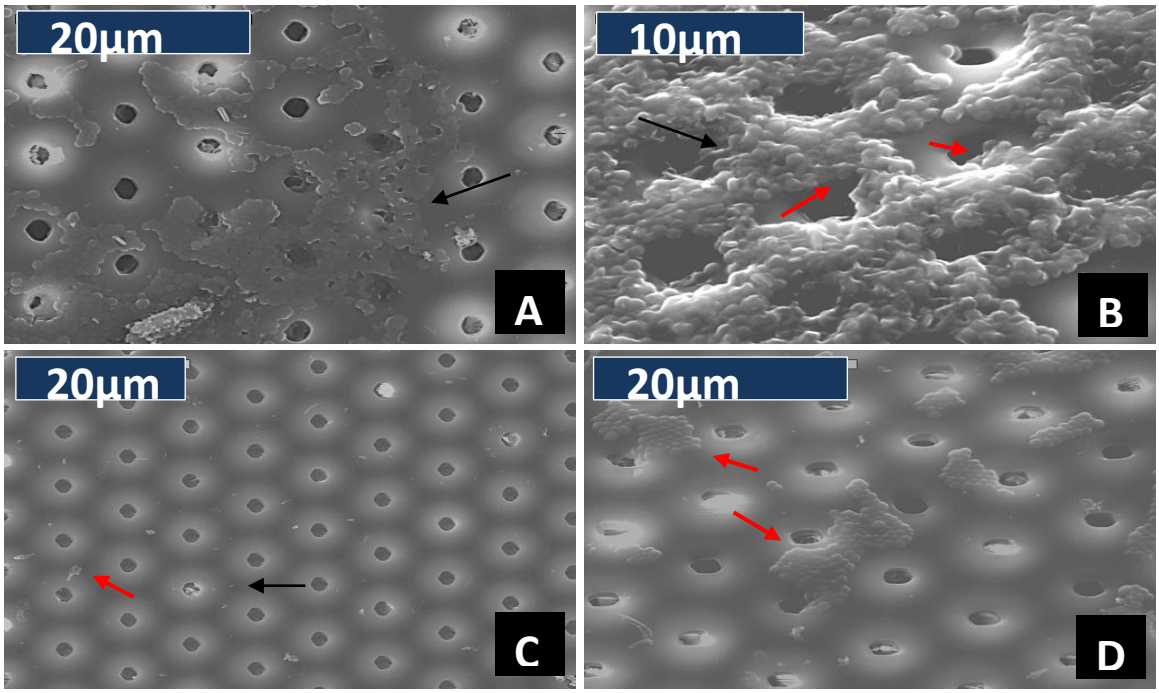


Figure 4-17. *S. aureus* bacterial morphology on the 2µm pit topography after 7 days (A) & (B) black arrow – dense coverage (C) & (D) black arrow - isolated cells; red arrow - small clusters

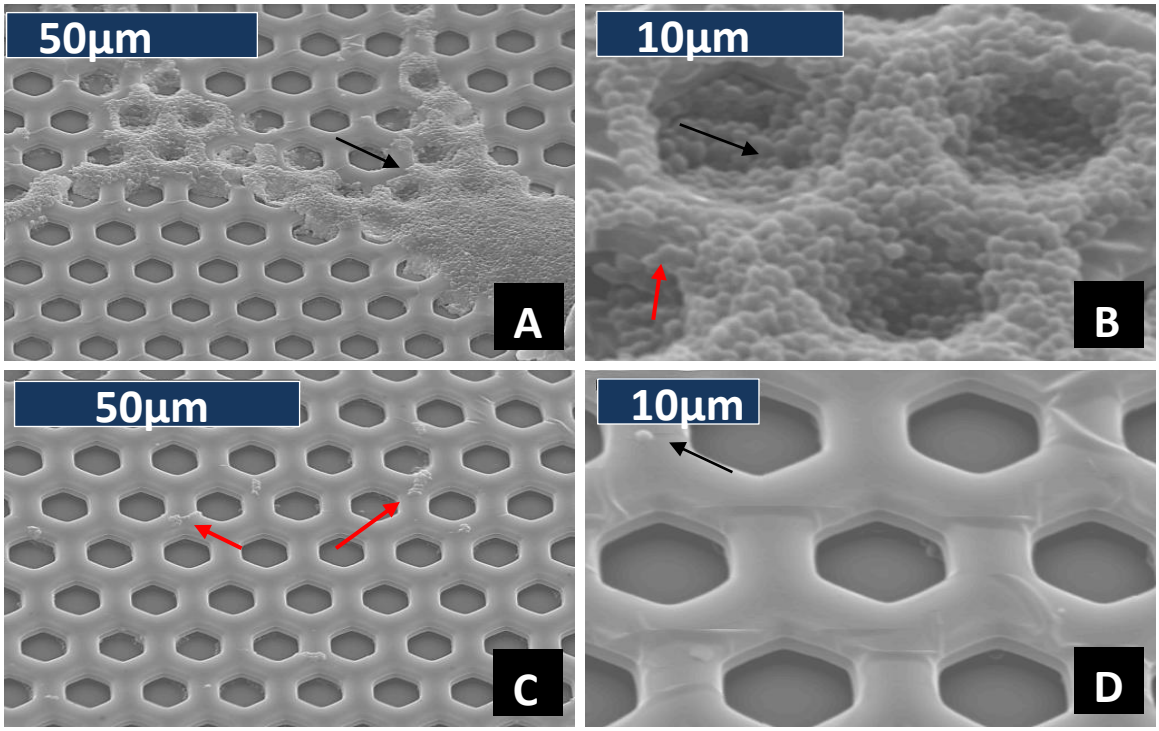


Figure 4-18. *S. aureus* bacterial morphology on the 7µm pit topography after 7 days (A) & (B) black arrow – dense coverage; red arrow – cells curving over curvature of the topography (C) & (D) black arrow - isolated cells; red arrow- small clusters

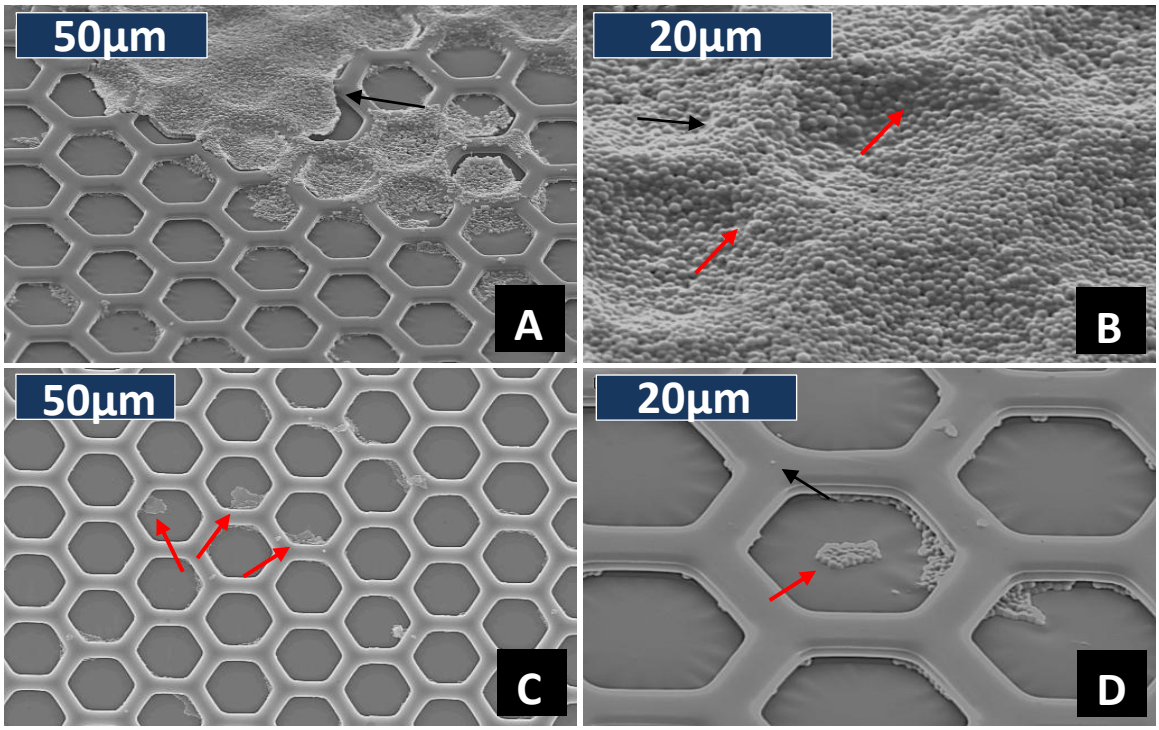


Figure 4-19. *S. aureus* bacterial morphology on the 17µm pit topography after 7 days (A) & (B) black arrow – dense coverage; red arrow – cells curving over curvature of the topography (C) & (D) black arrow - isolated cells; red arrow- small clusters

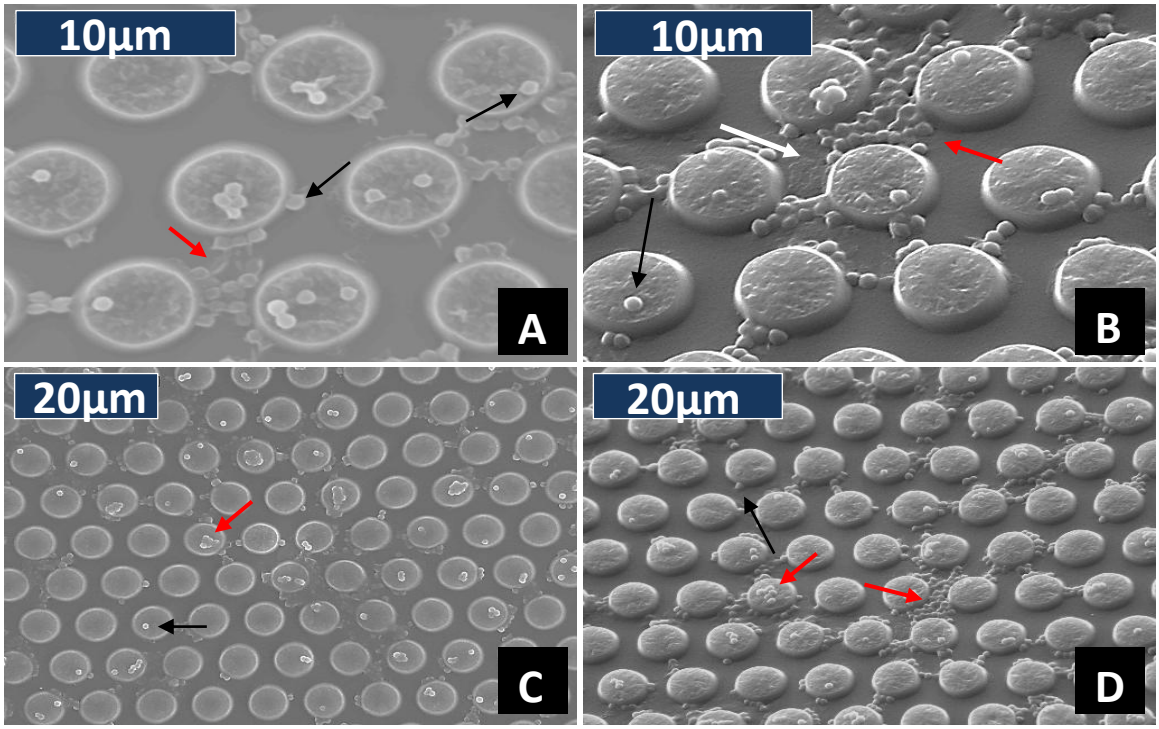


Figure 4-20. *S. aureus* bacterial morphology on the 5µm pillar topography after 7 days (A), (B), (C) & (D) black arrow – isolated cells; red arrow – small cluster of cells; white arrow – eps remnant; No dense coverage observed over the entire surface

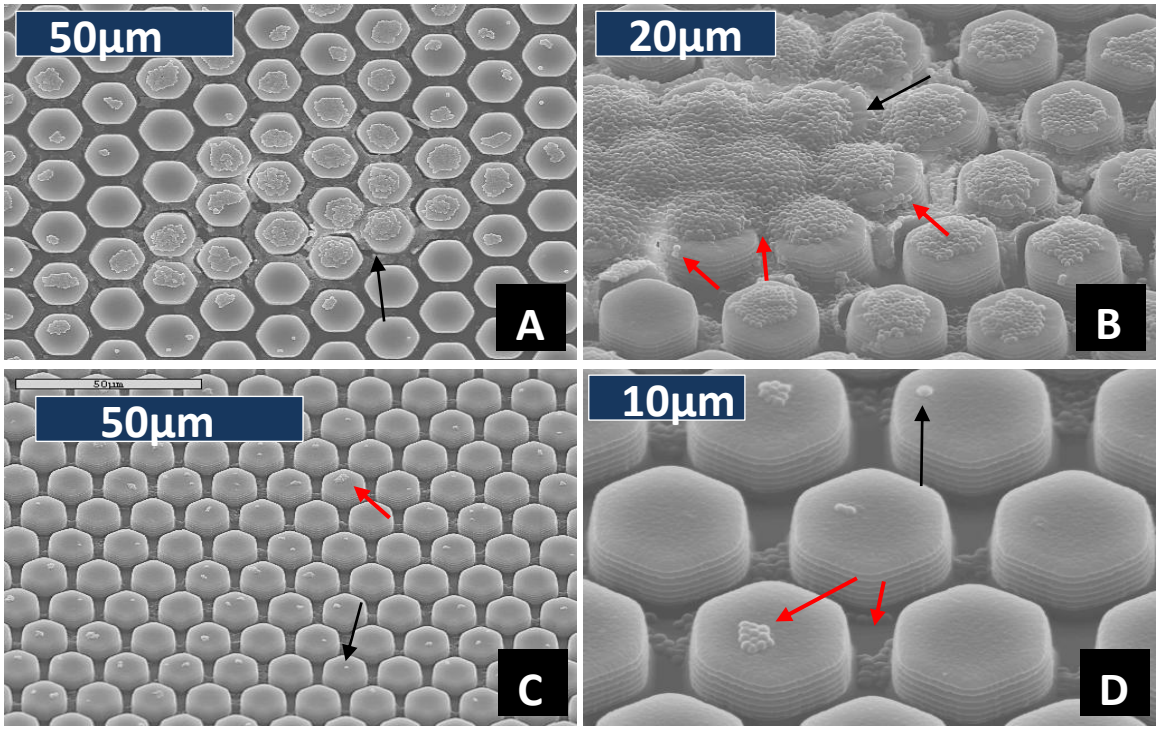


Figure 4-21. *S. aureus* bacterial morphology on the 11µm pillar topography after 7 days (A) & (B) black arrow – dense coverage; red arrow – cells curving over curvature of the topography (C) & (D) black arrow - isolated cells; red arrow- small clusters

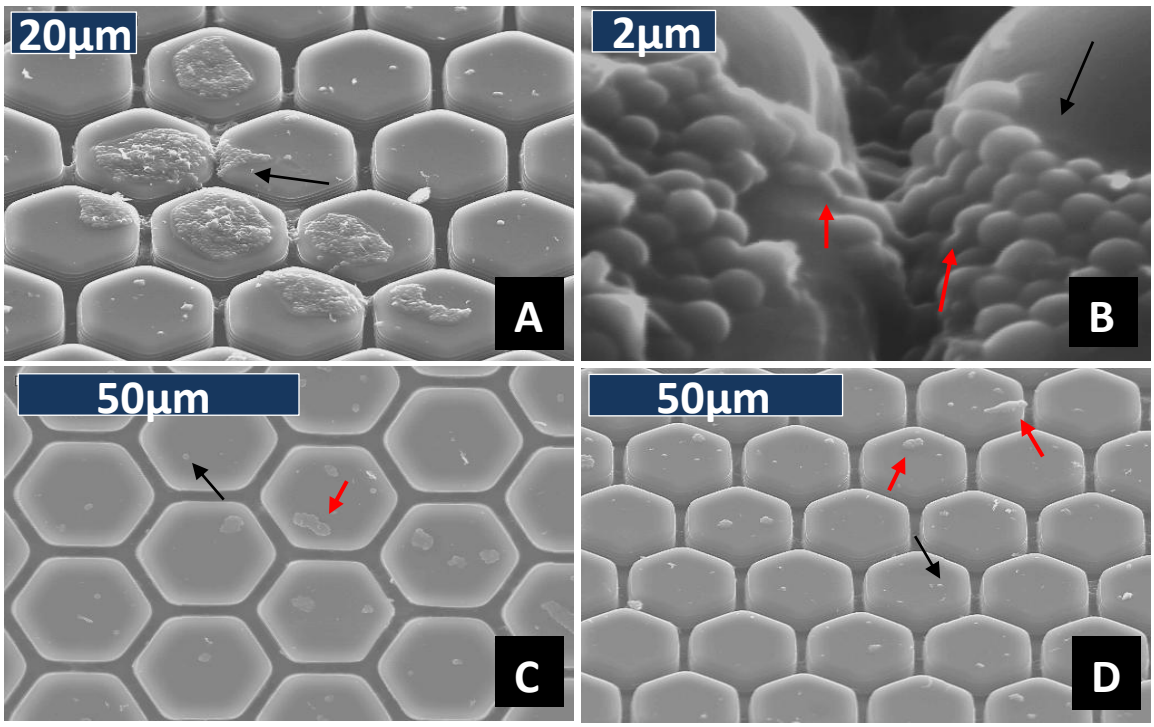


Figure 4-22. *S. aureus* bacterial morphology on the 21µm pillar topography after 7 days (A) & (B) black arrow – dense coverage; red arrow – cells curving over curvature of the topography (C) & (D) black arrow - isolated cells; red arrow- small clusters

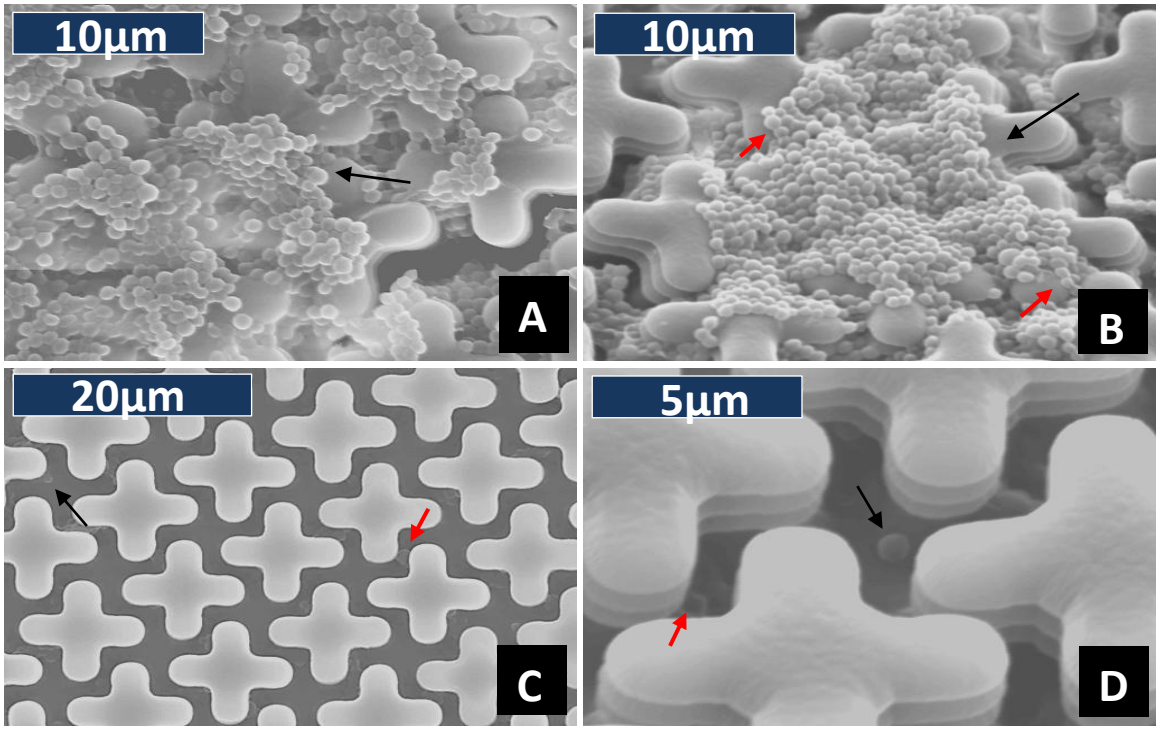


Figure 4-23. *S. aureus* bacterial morphology on the 2µm cross topography after 7 days (A) & (B) black arrow – dense coverage; red arrow – cells curving over curvature of the topography (C) & (D) black arrow - isolated cells; red arrow- small clusters

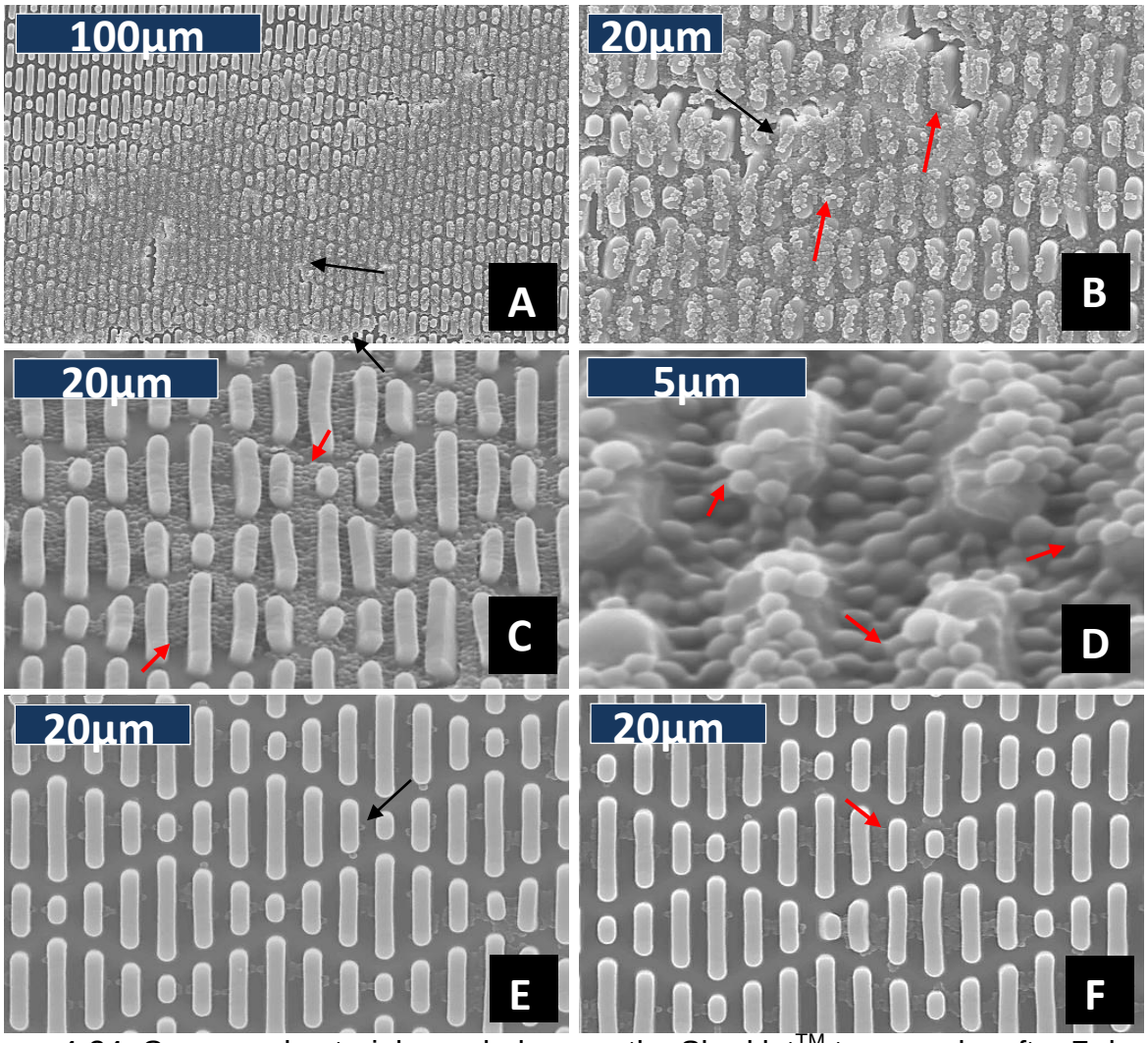


Figure 4-24. *S. aureus* bacterial morphology on the Sharklet™ topography after 7 days (A) & (B) black arrow – dense coverage; red arrow – cells on the top of the features (C) red arrow – cells in the recessed regions, both in the parallel channels and also in between features & (D) red arrow – cells connected continuously over the curvature of the topography (E) & (F) black arrow - isolated cells; red arrow- small clusters; temporally varied growth

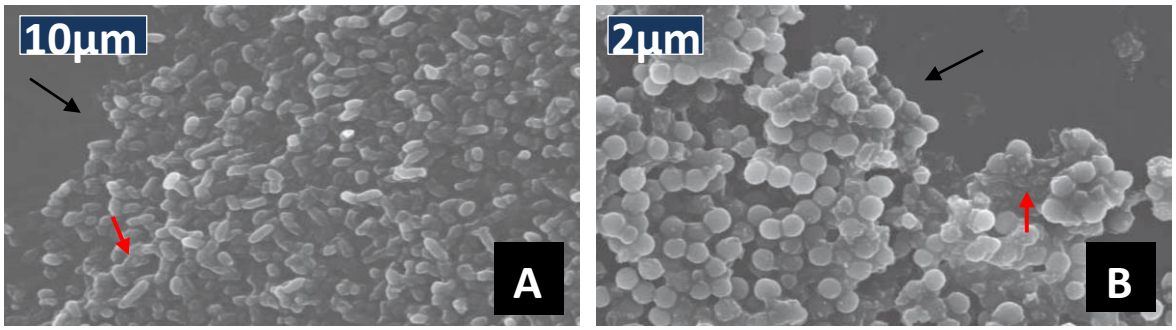


Figure 4-25. Example biofilm images on PDMSe tympanostomy tubes (A) *p. aeruginosa* biofilm and (B) *s. aureus* biofilm. Black arrow – dense coverage with several layers of cells; red arrow – bacteria embedded in an EPS matrix (*139*)

There is some separation of attached bacterial clusters as well, suggesting random attachment overall followed by growth or clumping. For the pit type topographies, morphology appears to be random. On 11 µm, 21 µm pillars and Sharklet$^{TM}$ topographies, most of the settlement appears to be within the recessed area in between the pits and occasionally on top of the pillars, with both types showing, instances covering tens of unit cells. Only on the 5 µm pillars was there no continued colony formation.

**Quantitative and phenotypic evaluation of patterned topography on biofilm formation**

*S. aureus* biofilm formation was evaluated using the **Bio-timer analysis (BTA), quantitive polymerase chain reaction (qPCR), antibiotic susceptibility, reverse transciptase, quantitative polymerase chain reaction (RT-qPCR)**. Figure 4-26 and Figure 4-27 show the results for the BTA test following the 7 day growth protocol. There are some overall statistically significant differences [7 day colour change: (Based on colour change times: ANOVA, $\alpha$=0.05, p= 0.002, 4 replicates; based on mean PE CFU/ml: ANOVA, $\alpha$=0.05, p= 0.01, 4 replicates); 24 hour oxacllin treatment: (Based on colour change times: ANOVA, $\alpha$=0.05, p= 0.000, 3 replicates; based on mean PE CFU/ml: ANOVA, $\alpha$=0.05, p= 0.001, 3 replicates)].

Tukey's multiple comparison for the colour change times and the mean PE CFU/ml before and after oxacillin treatment yielded p values as follows (respectively): 5 µm pillars [(0.0012, 0.004);(0.0012,0.0227)], Sharklet$^{TM}$ [(0.0172,>0.05);(>0.05,0.455)], smooth PDMSe [(>0.05,0.0283);(>0.05,>0.05)], 7 µm pits (>0.05,>0.05);(0.0075,>0.05)], and above 0.05 for all other patterns for both measurements.

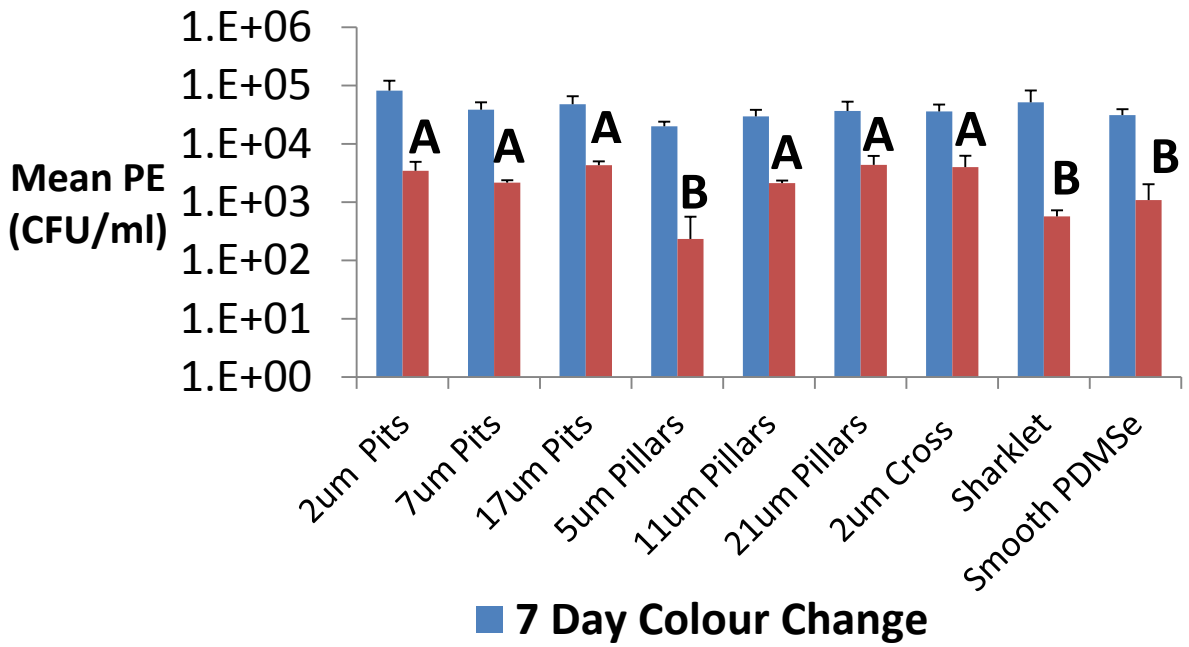


Figure 4-26. Biotimer assay results post 7 days of *s. aureus* SH1000 growth protocol in terms of mean PE CFU/ml. Error bars represent one standard deviation.

Despite finding statistically significant differences for the 5 µm pillar topography based on the 7 day colour change based on the number of metabolically active *s. aureus* cells, any variation within samples is within one order of magnitude (<1 log).

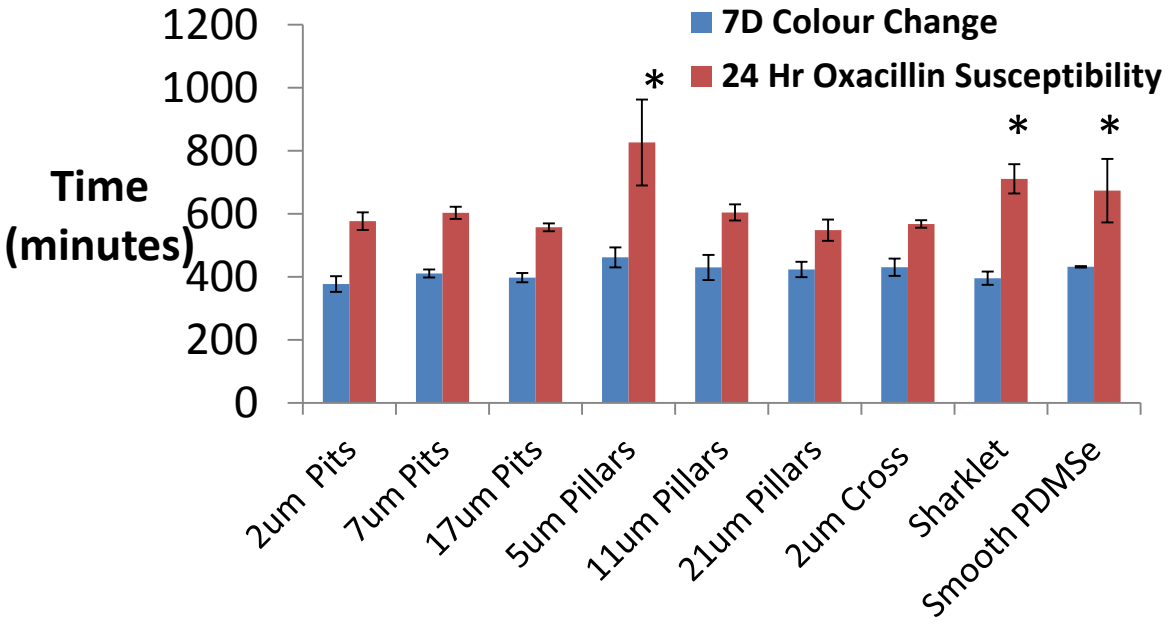


Figure 4-27. Biotimer assay results post 7 days of *s. aureus* SH1000 growth protocol in terms of colour change time. Error bars represent one standard deviation.

Considering the fact that bacteria grow and multiply at a high rate, the perceived differences may not be significant in terms of real world application, even though some of the results may be statistically significantly different under these growth conditions. The use of the calibration curves (Figure 4-28) for back calculating the mean planktonic equivalent CFU/ml is justified from the excellent correlation coefficients.

**Antibiotic susceptibility:** The amount of log reduction was calculated and is summarized in Table 4-3. Since over a period of 24 hours antibiotics kill nearly all the planktonic bacteria (*1*), a 3 to 5 orders of magnitude of reduction in the number of bacteria is expected to be planktonic or immature biofilm kill (given a 5 log original presence). Samples with less than 2 orders of magnitude or lesser kill are taken to indicate the presence of a “functional” mature biofilm.

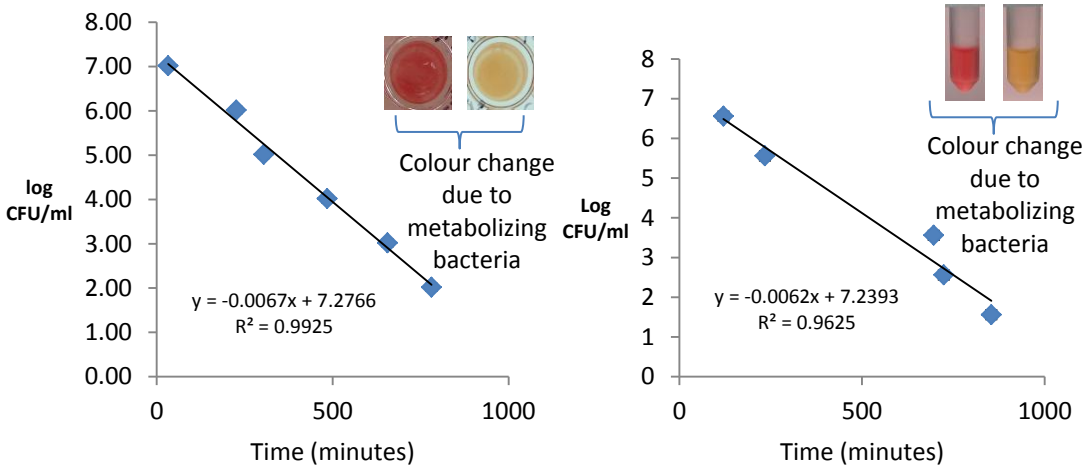


Figure 4-28. The correlations of log CFU/ml versus time required for color switch from red to yellow for planktonic s. aureus cultures used as calibration curves in BTA assays. Graphs on the left and right are two test configurations used

Based on this, all pit samples, the 11 µm pillars, 21 µm pillars, and the cross pattern appear to have mature *s. aureus* biofilm growth. The 5 µm and Sharklet$^{TM}$ topographies on PDMSe appear to have little or no mature *s. aureus* biofilm formation.

The smooth PDMSe response is a special case that shows 2 to 3 orders of magnitude kill which suggests that some regions do have mature biofilm growth and some don't.

**Correlating susceptibility to material characteristics:** Scatter plots of CFU/ml versus apparent contact angle and recessed area fraction ($f_D$) are shown in Figure 4-33 and Figure 4-34. The recessed area fraction relates to the stability of air pockets in submerged patterned substrates (a more detailed discussion is conducted in Chapter 4 under the breakthrough pressure section). For mean PE CFU/ml versus recessed area fraction, there appears to be a slight trend of decreasing mean PE CFU/ml with increasing recessed area fraction. An outlier in this trend is the 20 µm pit ($f_D$ = 0.59) which has a recessed fraction but shows presence of biofilm. In cases where there is more than 3 log reduction from a maximum of 5 log number of bacterial cells, there are two possible reasons that work in tandem for explaining the low number of *s. aureus* cells contributing to colour change in the end.

Table 4-3. Log reduction data from antibiotic susceptibility experiment along with corresponding inference for SH1000 biofilm formation

| Pattern | Log Reduction | Inference |
|---|---|---|
| 2µm Pits | <2.0 | Indicates presence of biofilm |
| 7µm Pits | <1.5 | Indicates presence of biofilm |
| 17µm Pits | 1.0 | Indicates presence of biofilm |
| 5µm Pillars | 3.0 | Little or no biofilm<br>Persister cells may be present(*210*) |
| 11µm Pillars | <1.5 | Indicates presence of biofilm |
| 21µm Pillars | 1.0 | Indicates presence of biofilm |
| 2µm Cross | <1.5 | Indicates presence of biofilm |
| Sharklet™ | 3.0 | Little or no biofilm<br>Persister cells may be present |
| Smooth PDMSe | 2.0-3.0 | Some areas may have biofilm while others have no biofilm<br>Persister cells may be present |

**Total cell count:** based on DNA concentration for *s. aureus* was calculated by performing qPCR. The results are shown in Figure 4-29. All of the topographies tested

appear to have the same quantity of total start DNA which indicates the same number of *s. aureus* cells is present on each surface sample. The total quantity of DNA includes both the live and dead cells present on the surfaces. Through the 7 day period during which the test is conducted, there are several different processes leading to the number of cells on the surface. These are 1) settlement of planktonic cells from suspension, 2) growth of previously attached cells on the surface, 3) locomotion of cells on the surface, 4) release planktonic cells from the surface colonies in to suspension and dead cells attached from all these processes. The total cell count data calculated from qPCR analysis corresponds to the sum of both live and dead bacteria. It indicates an average of about $10^{10}$ to $10^{11}$ cells on all the patterns. There are some overall statistically significant differences (ANOVA, $\alpha$=0.05, p=0.000, 3 replicates). The ratio of in the total number of cells to the number of viable is of the order of $10^{5}$.

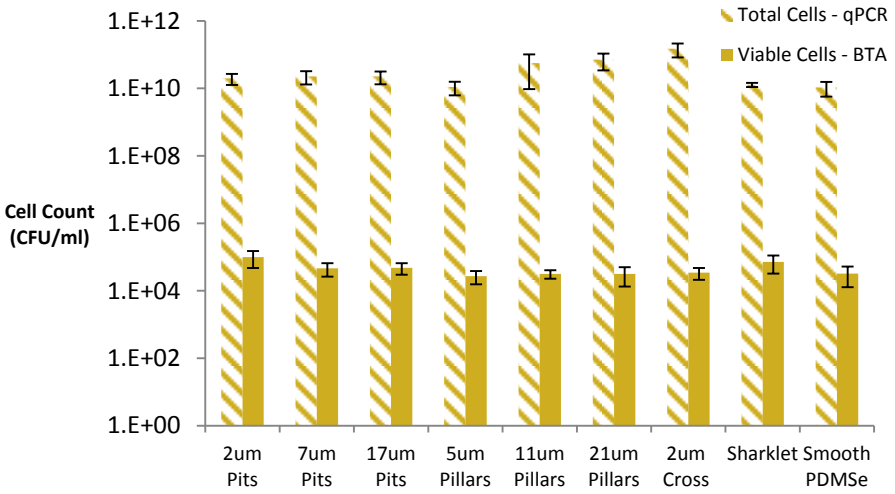


Figure 4-29. Plot of total number of cells calculated from qPCR (hatched bars) and viable cells as mean PE CFU/ml (solid bars) for *Staphylococcus aureus* SH1000 on the various patterned topography and smooth PDMSe.

Based on the data obtained from the antibiotic susceptibility test of *s. aureus* with oxacillin treatment and BTA assessment it appears that there is *s. aureus* biofilm

formation on most of the samples, but as to whether this response is due to sessile dormant (metabolically inactive) biofilm bacteria or just a reduced number of viable cells on the surface leading to this response was not apparent with this assay.

**Gene expression results:** To shed more light on this, a direct approach was applied to determine the phenotype based on biofilm type gene expression levels using RT-qPCR. Global *s. aureus* gene expression patterns have been identified previously, and it was found that the arcA expression was upregulated, relative to constitutively expressing 16S rRNA, as the bacterium differentiated into biofilm phenotype (*207*). Based on the results of that study, RT-qPCR was performed for each sample using custom designed primers to arcA and 16S rRNA to determine the phenotypic characteristics of the bacteria on each test sample in this study.

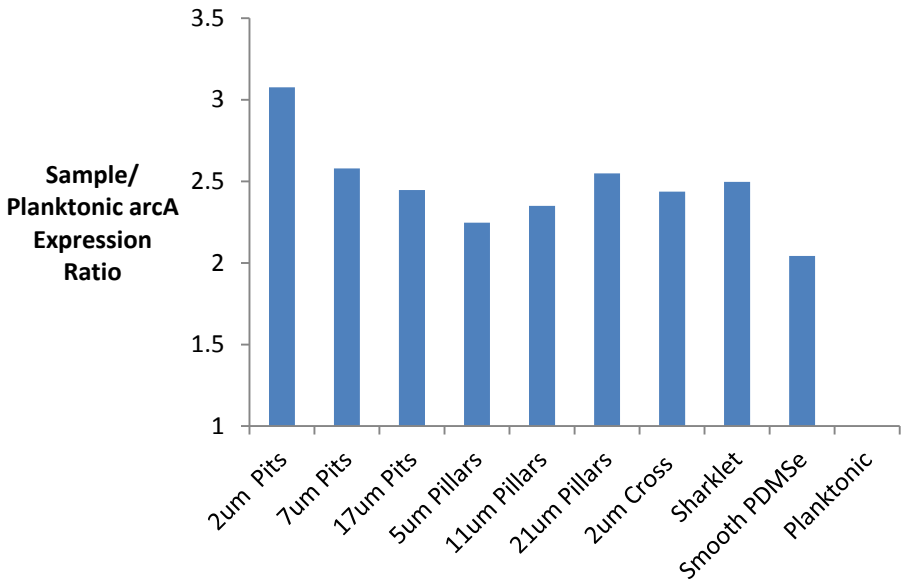


Figure 4-30. Relative arcA gene expression levels on patterned topography and smooth PDMSe (normalized with 16S rRNA expression) represented as a ratio of arcA expression in early log phase planktonic bacteria. **Data lacks error bars** because it is obtained from 9 replicates combined in one run, representing an average. Compared with the planktonic phenotype, arcA expression is upregulated, confirming presence of biofilm phenotype in all the samples.

Since RNA was extracted from a combination of 9 replicates per pattern for this test, the data from this sample set may be considered quantitative. The relative acrA expression level was calculated by determining the Ct ratios of arcA to 16s rRNA amplification (internal normalizing control) within each sample. The relative arcA expression level was then plotted as a ratio of sample to early log phase planktonic *s. aureus* arcA expression level.

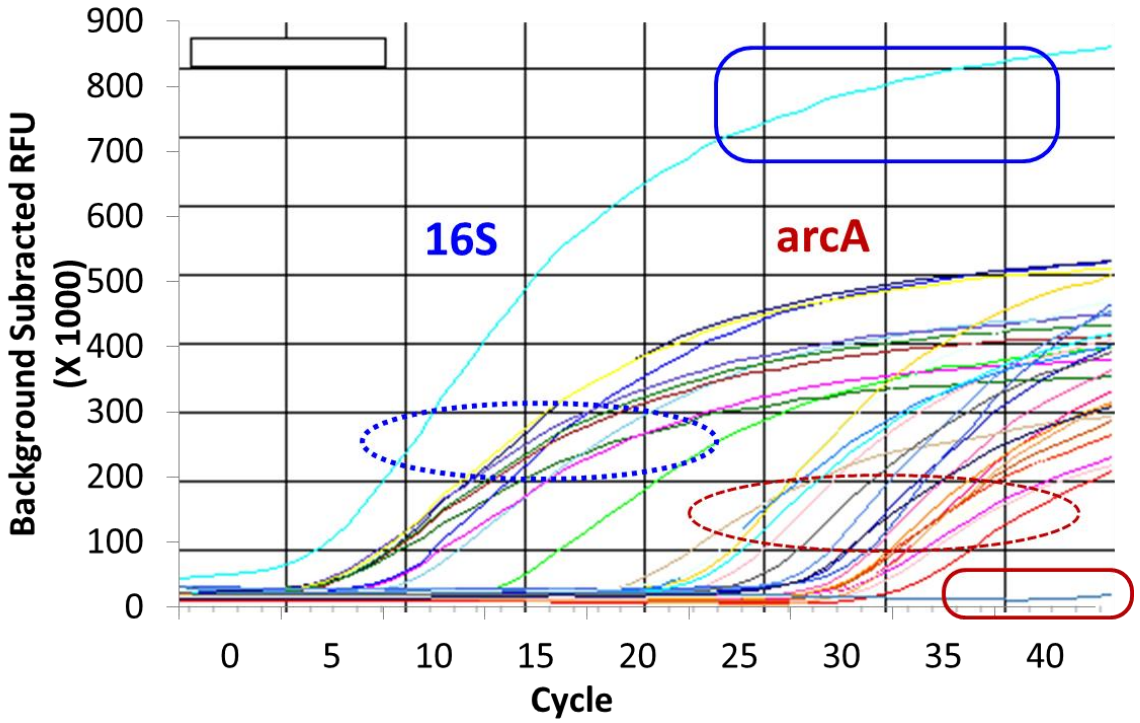


Figure 4.31. Real-time PCR fluorescence intensity amplification chart – SH1000 qPCR. Top red box indicates fluorescence intensity of 16s planktonic expression which confirms presence of SH1000 planktonic species. Bottom blue box indicates the nearly zero planktonic arcA expression indicating absence of biofilm phenotype. All other curves show positive expression for the arcA gene expression from test topography suggesting presence of biofilm phenotype.

A ratio of 1 corresponds to no difference in expression compared to planktonic bacteria. The smaller the ratio, the greater the proportion of planktonic like phenotype cells present on the samples. The results are shown in Figure 4-30. The arcA

expression level for *s. aureus* on the 2 µm pit topography sample is the highest and the pit topographies seem to follow the trend for BTA with oxacillin susceptibility.

Planktonic mRNA was harvested from an overnight culture and checked for 16S and arcA gene expression (Figure 4-31). In order to confirm that the lack of arcA expression in the planktonic case was not due to poor extraction efficiency or a systemic error or due to lack of reagent, 16S expression from mRNA extract was also tested simultaneously. In the planktonic as well as other sample cases there was a very strong signal for all 16S expression and this was used as basis to compare the arc expression levels.

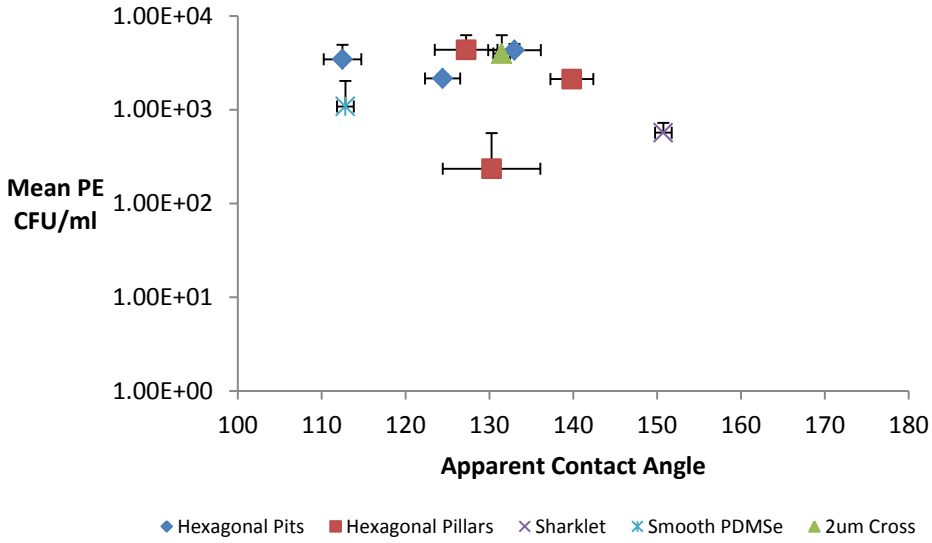


Figure 4-32. Oxacillin susceptibility results in terms of mean PE CFU/ml versus apparent contact angle. Displays no significant trend.

Apparent contact angle did not appear to influence biofilm formation as measured by oxacillin susceptibility tests in terms of mean PE CFU/ml (Figure 4-32). Oxacillin susceptibility results (Figure 4-33), expressed as mean PE CFU/ml plotted against recessed area fraction, for hexagonal pit and cross topographies did not show any statistically significant differences, confirming equal “functional biofilm” presence.

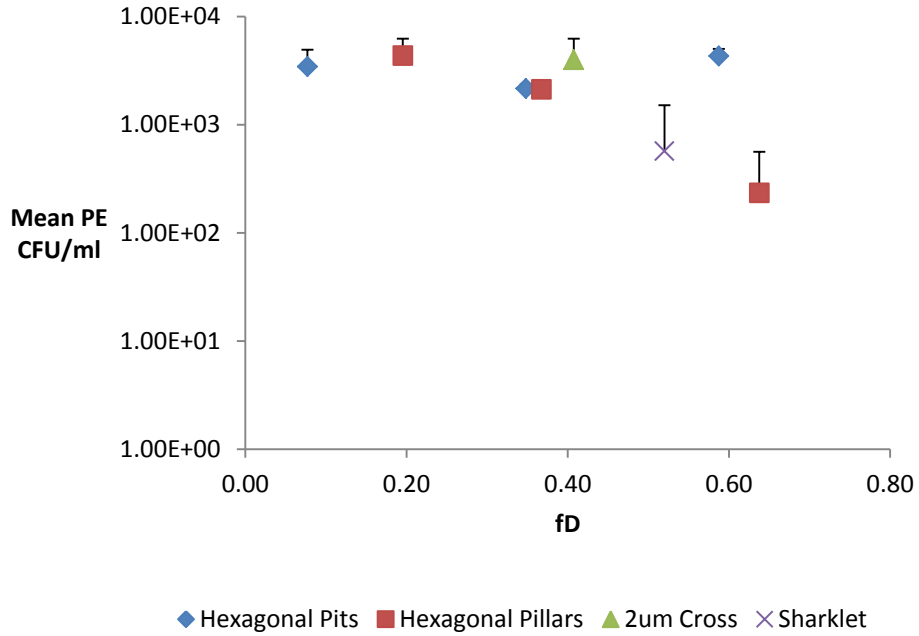


Figure 4-33. Oxacillin susceptibility results in terms of mean PE CFU/ml versus recessed area fraction. Only in the case of hexagonal pillars there decrease in mean PE CFU/ml with increasing recessed area fraction.

However, hexagonal pillar topography indicated a decreasing trend (with increasing recessed area fraction (The Confinement Approach Chapter 4: Discussion).

### ***Enterobacter Cloacae* Biofilm Morphology**

Confocal microscopy images of representative planes are shown in Figure 4-34 through Figure 4-37. Anecdotally, similar distribution of bacteria was observed on all planes. The smooth surface (Figure 4-34 (A)) was almost completely covered by *e. cloacae* (ATCC 700258), whereas there was significantly lesser coverage on the other topographies. The 7µm hexagonal pit type topography (Figure 4-34 (B)) has bacteria mainly in recessed regions and within it the arrangement is along the walls of the pits. In some cases the inverse configuration of 7µm hexagonal pit, the 11µm hexagonal pillar had settlement on both the tops and in the recessed regions between the features (Figure 4-37 (A) & (B)).

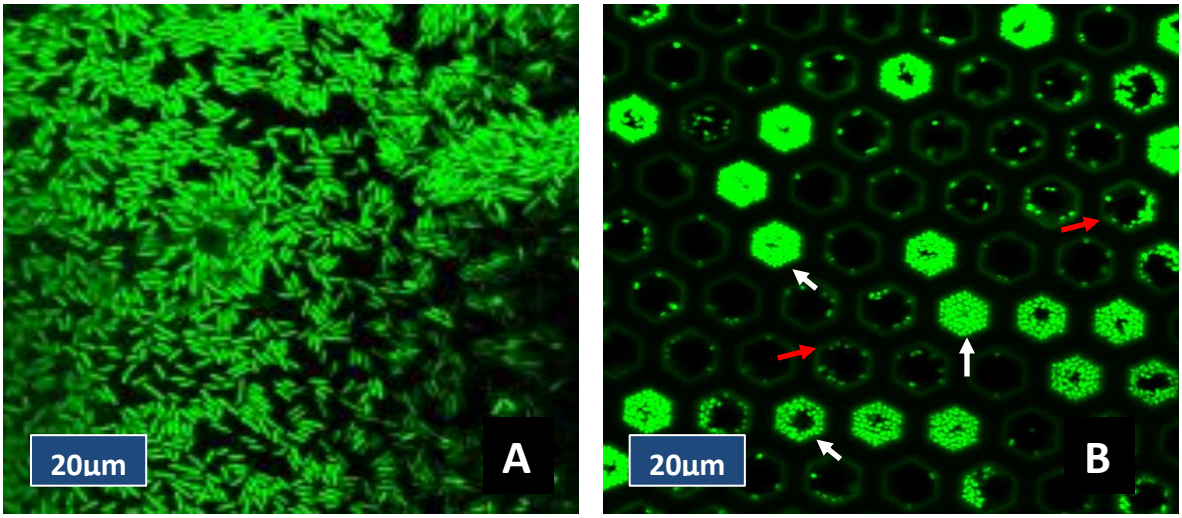


Figure 4-34. Confocal images of *e. cloacae* growth on silicone elastomer (courtesy: Megan Merritt, ERDC, MS) A: Smooth surface, dense coverage; B: 7µm hexagonal pits, white arrow – pits with clusters; red arrow – isolated cells attached to pit walls

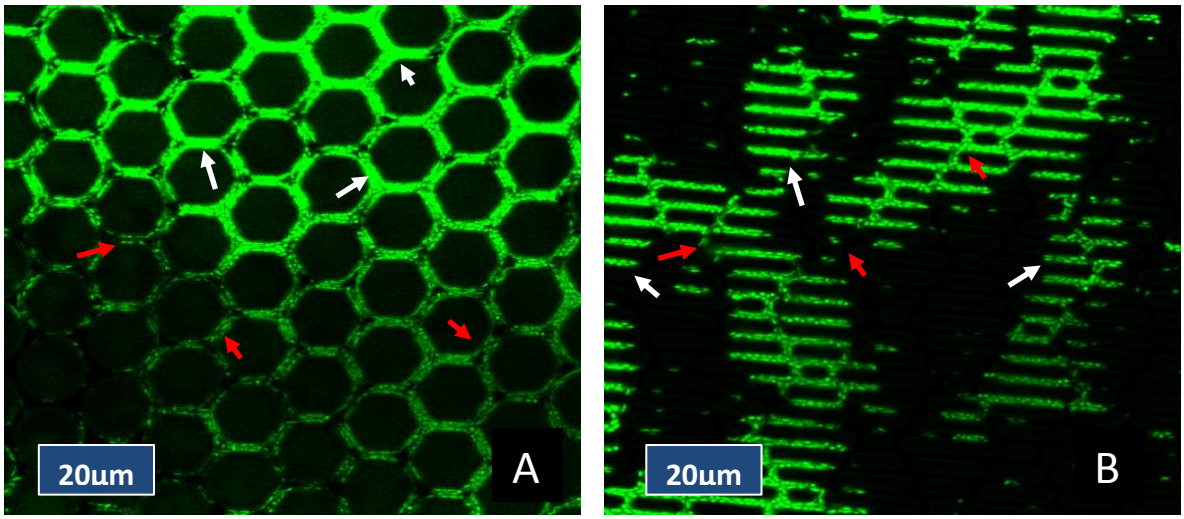


Figure 4-35. Confocal images *enterobacter cloacae* growth silicone elastomer over a 48 hour period (courtesy: Megan Merritt, ERDC, MS) A: 11µm hexagonal pillars, white arrow – depressed regions with clusters; red arrow – isolated cells and clusters in between ridges; B: Sharklet™ 2µm spacing and 3µm height, white arrow – depressed regions with clusters; red arrow – isolated cells and clusters in between ridges

The Sharklet™ pattern displayed bacteria mainly in the recessed regions (Figure 4-35 (B)). They were observed mostly in the uninterrupted valleys but as indicated by the white arrows, settlement/growth was also observed in between adjacent ridges.

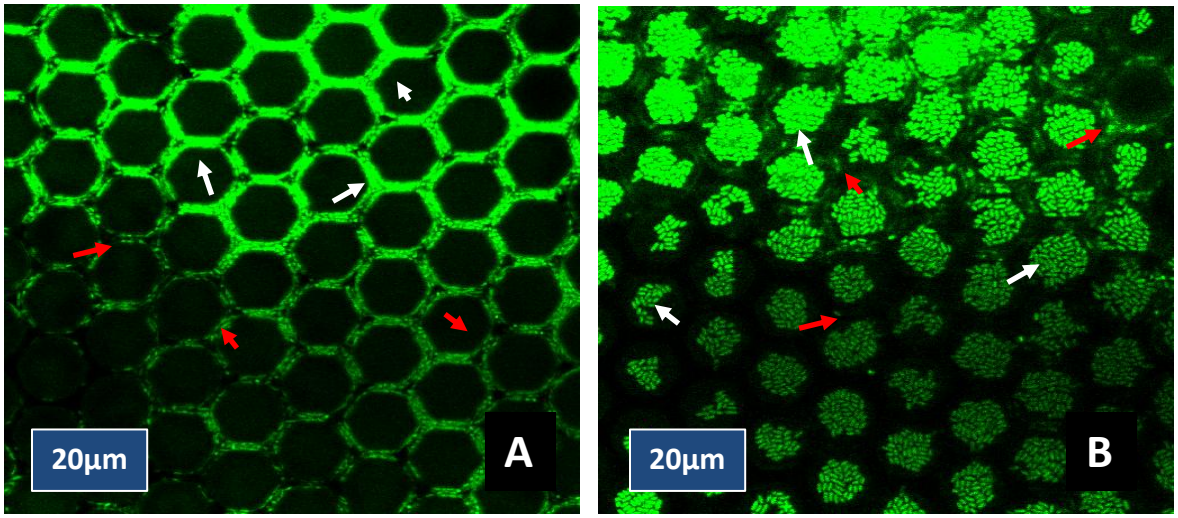


Figure 4-36. Confocal images *enterobacter cloacae* growth silicone elastomer over a 48 hour period (courtesy: Megan Merritt, ERDC, MS) A: 11µm hexagonal pillars, white arrow – depressed regions with clusters; red arrow – isolated cells attached to depressed regions; B: 11µm hexagonal pillars, white arrow – feature tops with cell clusters; red arrow – isolated cells in depressed regions

It appears that the amount coverage is the same in the parallel channels versus the intermittent regions of the topography. The 2µm cross pattern (Figure 4-37 A) showed bacteria only in the recessed regions.

The lowest coverage was observed on the 5µm cross pattern (Figure 4-37 B). Since the depth of the features on this topography 20µm compared to the 3µm depth on the other topographies, on the other samples the observed effect could be due to either 1) the non-wetted state of the topography resulting in lesser area for colonization or 2) lack of image results on all the 1µm plane stacks other than the plane in which the observation was made. Since it was anecdotally observed that the all planes had similar areal coverage, the total number of bacteria on the 5µm cross topography will add up due to its height. Hence, there is a definite need for additional images before conclusive statements can be made. However, from the sparseness of coverage observed, it maybe speculated that the total number of bacteria on the same topography maybe

lesser then that observed on the other topographies. Thus, most of the bacterial settlement/growth was observed to be in the valleys with the exception of 11µm pillar topography (Figure 4-35 (A) and Figure 4-36 (A) & (B)). As settlement is observed in both the recessed regions as well as the tops, this may be taken as evidence for being completely wetted.

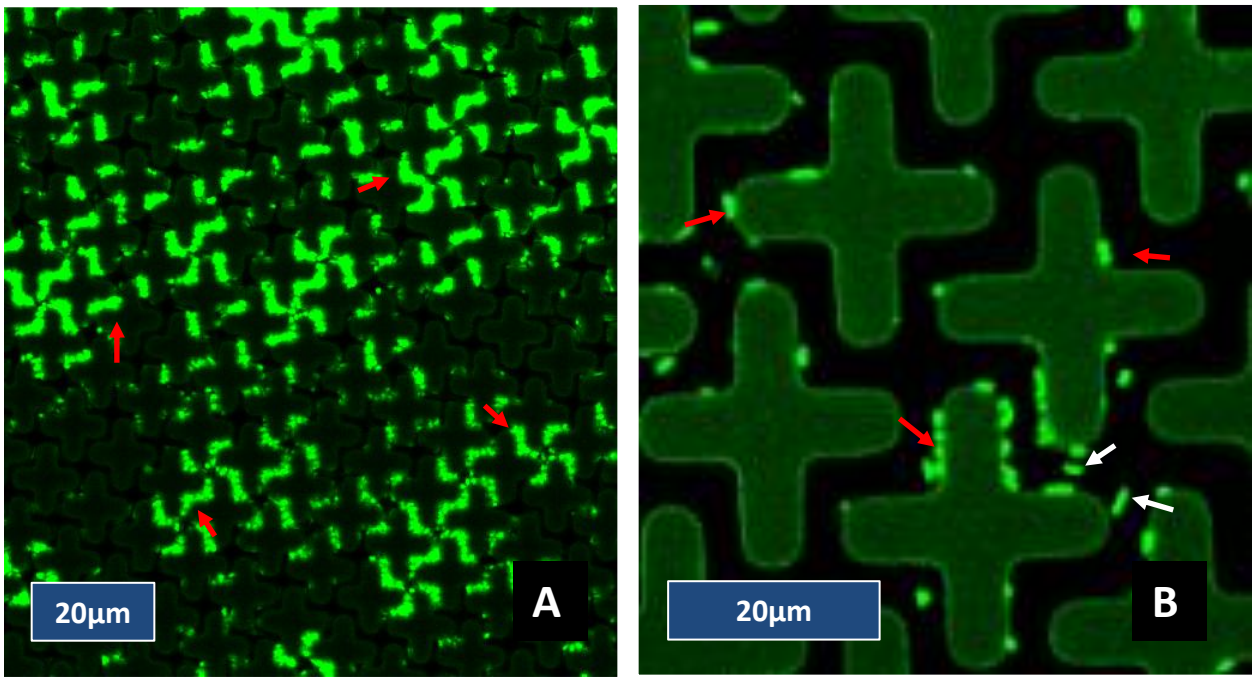


Figure 4-37. Confocal images *enterobacter cloacae* growth silicone elastomer over a 48 hour period (courtesy: Megan Merritt, ERDC, MS) A: 2µm cross pattern, red arrow –cells attached to walls within depressed regions; B: 5µm cross pattern, white arrow –isolated cells within depressed regions, not attached to walls; red arrow – isolated cells in depressed regions, attached to walls

**The Wetting Approach**

The wetting approach consists of attempts to make novel, robust, micropatterned surfaces with the biofilm inhibition application for the CAUTI problem in mind. In this study novel undercut surfaces were designed, fabricated and characterized for this purpose. Future efforts could use the recommendations provided here to test biofilm inhibition efficacy of these designs.

**Characteristics of Test Topography**

Example **SEM images** of the undercut topography used in this study are shown in Figures 4-38 (A) and (B) represent 10µm hexagonal undercut pillars, spaced by 5µm and 20µm hexagonal undercut hexagonal pillars spaced by 26µm respectively. The variation of height and extent of the undercut used in the previous account (*184*), from which the process was adapted, was not independent of each other due to the nature of the method used. In order to independently change the height and extent of the undercut, two sequentially anisotropic and isotropic etching steps were incorporated into the protocol for fabrication of undercut topography.

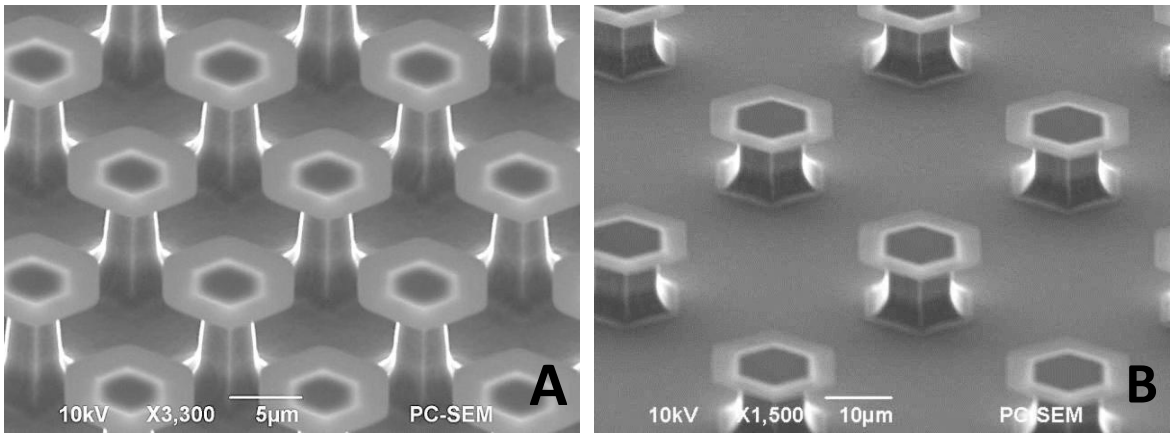


Figure 4-38. Example image: 10µm wide hexagonal array spaced by 3µm

The surfaces were named based upon the extent of the undercut or height. Short, normal, and tall indicate height of test samples with short and tall having half or twice the anisotropic processing time of the normal respectively, but with the same isotropic processing time as the normal. The isotropic etch times of the normal sample was set to be halfway in between ‘less undercut’ and ‘more undercut’ samples. Although exact measurements vary across the different samples, the undercut on the normal sample was 3µm and the height was 5.89µm. This classification is explained in Figure 4-39

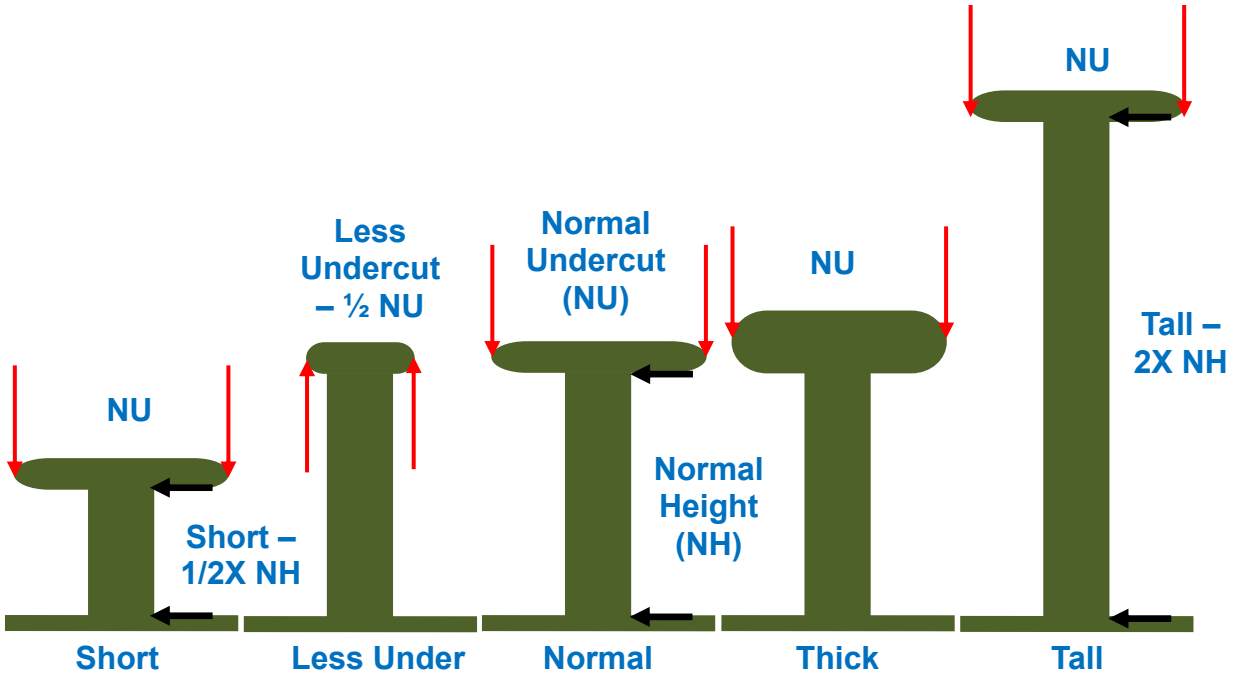


Figure 4-39. Classification of samples based on extent of under and height of features

**Breakthrough Pressure Analysis**

Breakthrough pressure data (Figure 4-40) was plotted against the various patterns as averages for the start and finish of breakthrough. These points were defined on the subjective basis of shimmer that starts to disappear at the beginning of breakthrough (0-5%) and completely disappears (95-100%) at the end. They provide an empirical basis to compare the underwater performance of super-hydrophobic patterns. The data was replotted in sets for the sake of clarity.

Figure 4-41 compares averaged 30-100µm breakthrough pressures among various etch conditions. The data indicate significant differences between no undercut ($p=0.0134$) and normal ($p=0.00$) but not between the other etch conditions taken pairwise. Figure 4-42 compares the averaged 20µm spaced by 6, 12 and 24µm breakthrough pressures among various etch conditions.

Tall (p=0.000) and thick etch (p=0.002) feature breakthrough pressures are significantly different from no undercut (0.0178). The short, less undercut and normal conditions form a second set significantly different from the tall.

This measurement is very relevant to some applications such inhibition of biofilm formation, where patterned topography is used in a completely submerged state and it may be necessary to know to which pressure the designed surface will remain non-wetting. The results in this study indicate that the presence of any undercut and the height of the features have a significant effect on the stability of non-wetted state.

**Triple Phase Contact Line Analysis**

Contact angle results are shown in Figure 4-44 and Figure 4-45 that correspond to the original design dimensions of 10 µm through 100 µm and 20 µm samples spaced 3 µm through 96 µm apart and were plotted as a function of feature size and spacing respectively.

Even though there was a spread of 5° to 10°, a major portion of the sample contact angle measurements overlapped. This implies that as long as the droplets in the ‘Cassie’ state, undercut or height do not have a very significant effect as there was a lot of overlap between the patterns.

Only the normal and tall advancing and sessile curves cause the observed spread, suggesting this may be more due to height of the features. As a result, comparisons of measured and predicted dynamic contact angles reported in this study were limited to the normal sample, normal surface here refers to the mid-point of the height and extent of undercut planned during the fabrication process (Figure 4-39)

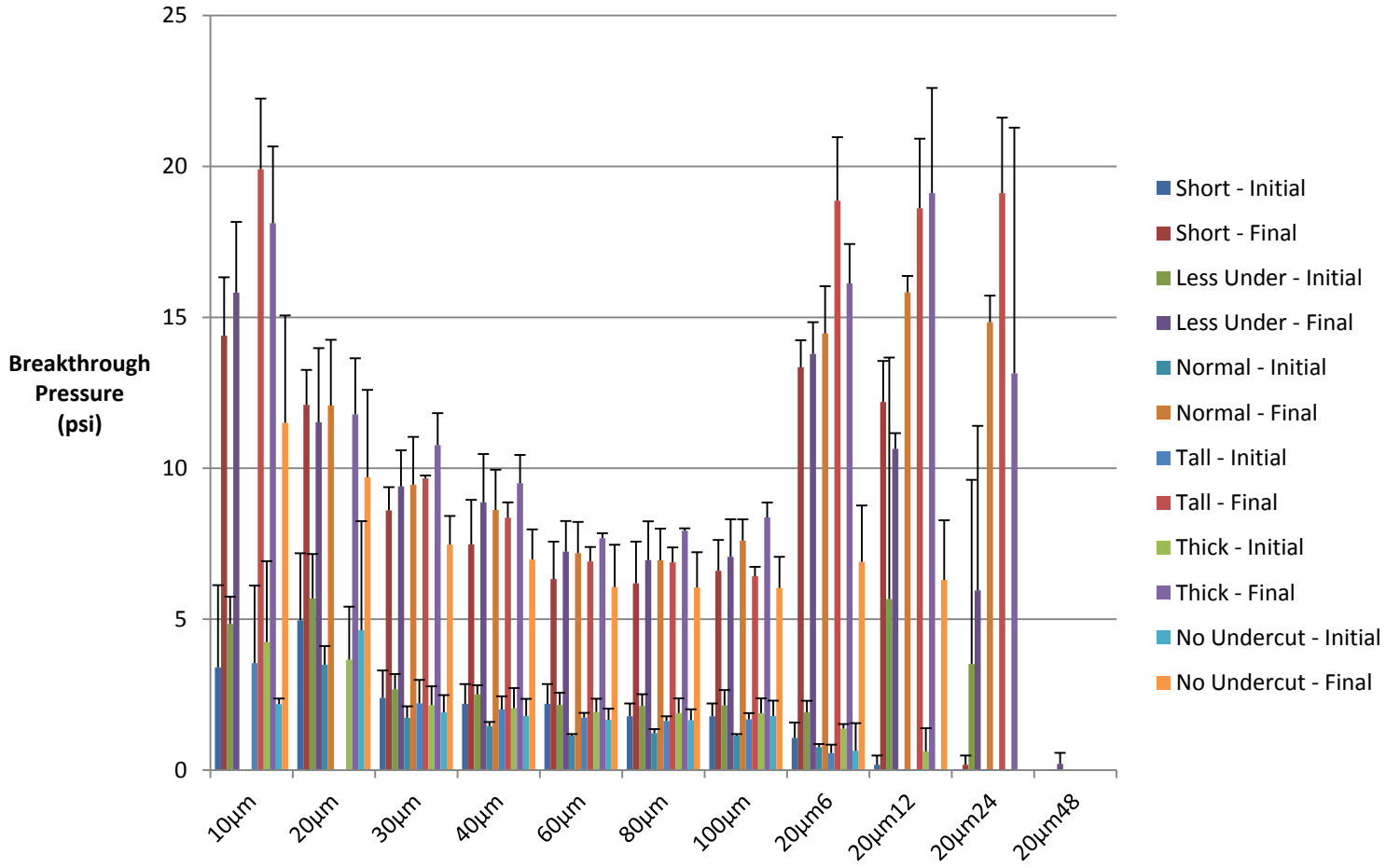


Figure 4-40. Collected view of the breakthrough pressure data on all the undercut patterned topography tested. Statistically significant differences are not shown here because of large number of data points. For the sake of clarity, these comparisons are presented in the following graphs.

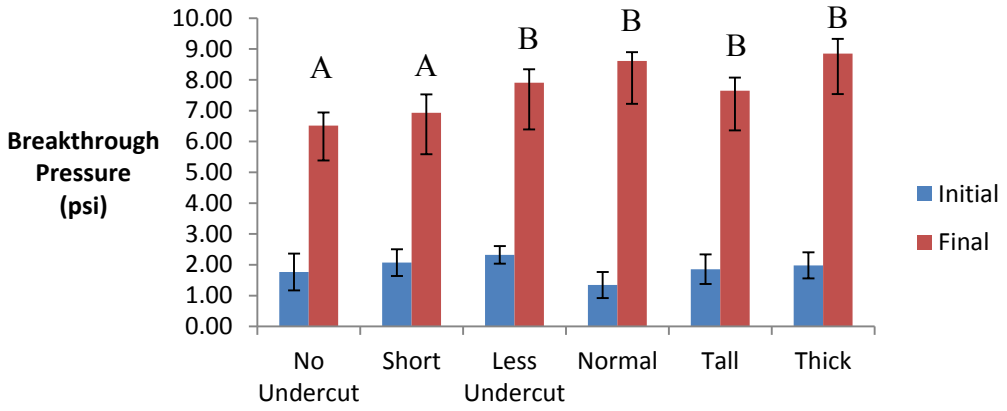


Figure 4-41. Average (30µm through 100µm) breakthrough pressure versus etch type; A and B represent statistically significantly different groups.

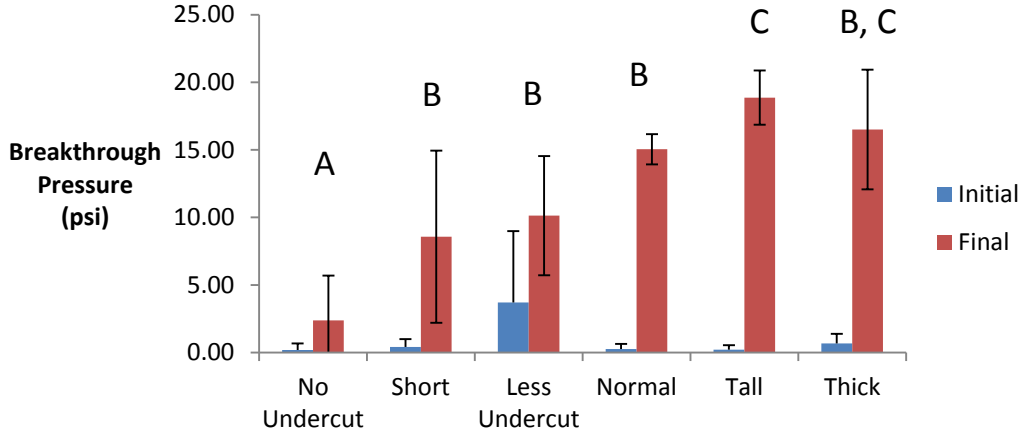


Figure 4-42. Average (20µm by 6µm-24µm) breakthrough pressure versus etch type; A, B and C represent statistically significantly different groups.

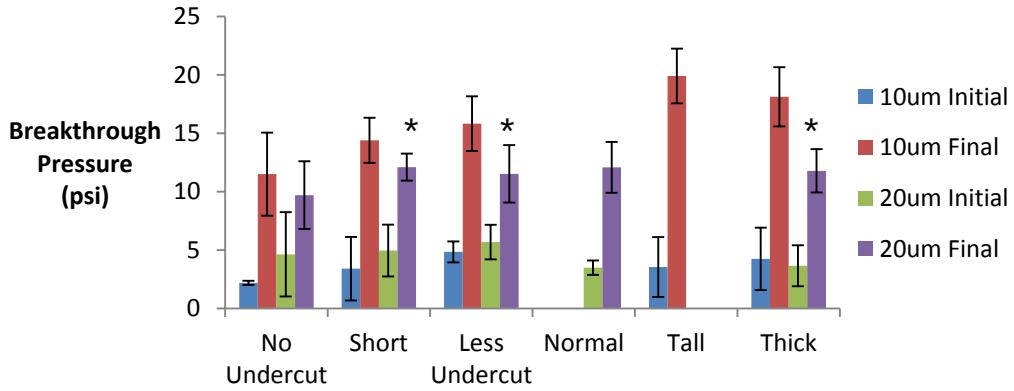


Figure 4-43. Comparison of breakthrough pressure on 10&20µm samples versus etch condition; Asterisk represents statistically significant difference between the 10µm and 20µm final breakthrough pressures on respective samples

Advancing contact angles were found to be consistently in the 160° range whereas, both predictions based on linear and areal fractions were much lower and were monotonically decreasing with increasing areal fraction (Figure 4-47).

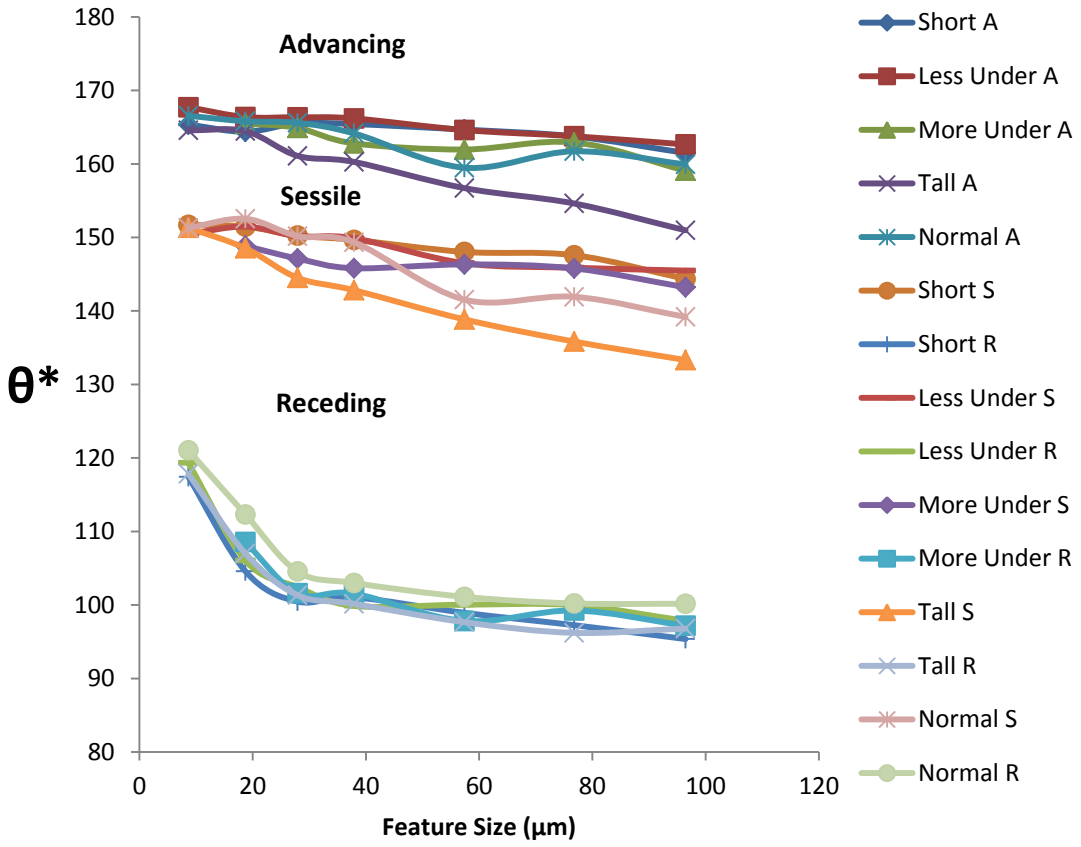


Figure 4-44. Advancing and receding water contact angles on 10µm through 100µm wide surfaces spaced apart by 3µm. Error on all data points is within 2 degrees.

On surfaces with undercut structures (ψ≤90°), the pinning effect should lead to a contact angle of 180° at a microscopic level(*39*). Errors are present when contact angle measurements are considered at a macroscopic level. Vibrational damping, focusing, and measurement errors are some errors that lead to the observed high (not 180°) and rather uniform contact angle across the variation in spacing and size. Measured receding contact angles also decreased monotonically with increasing areal fraction, or

more appropriately, with increasing linear fraction approaching the smooth surface near which the difference between the models and measurements diminished (Figure 4-48).

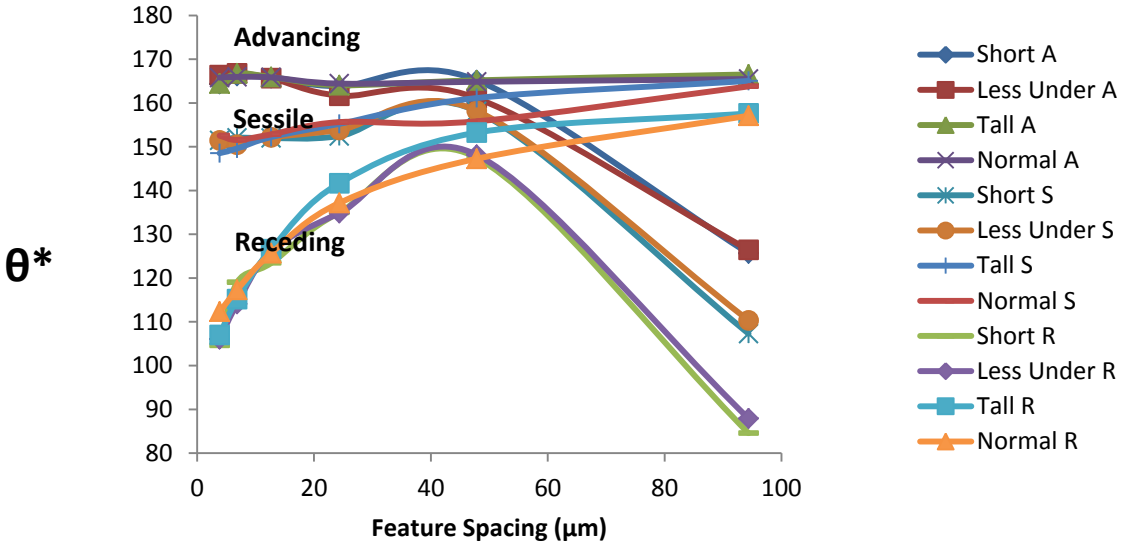


Figure 4-45. Advancing and receding water contact angles on 20µm wide surfaces spaced apart by 3µm through 96µm. Error on all data points is within 2 degrees.

The measurements made were predicted more accurately using linear fractions ($R^2$=0.999, p=$10^{-5}$) than using areal fractions as dictated by the Cassie-Baxter model ($R^2$=0.996, p=$10^{-4}$). This is a change in the linear fraction as the spacing is varied.

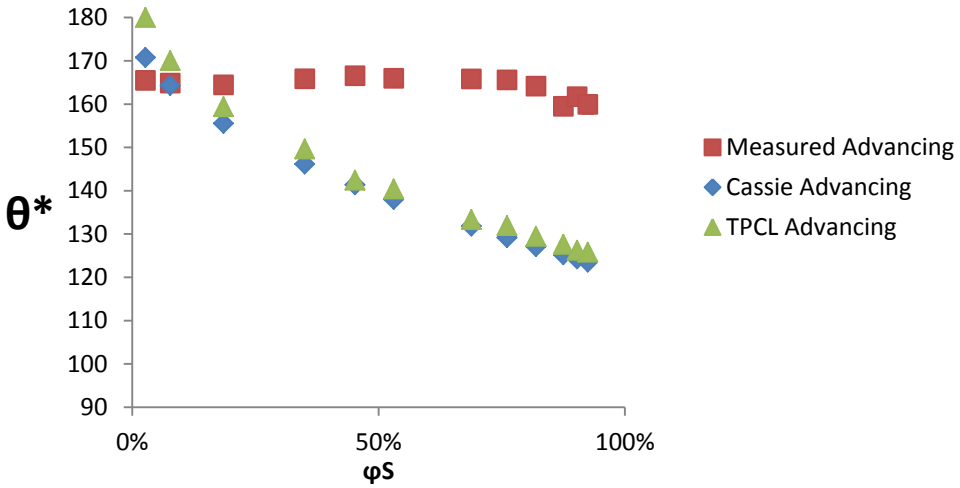


Figure 4-46. Advancing water contact angles versus solid wetted area fraction on the normal wafer, with theoretical predictions for 20µm spaced apart samples. Error on all data points is within 2 degrees.

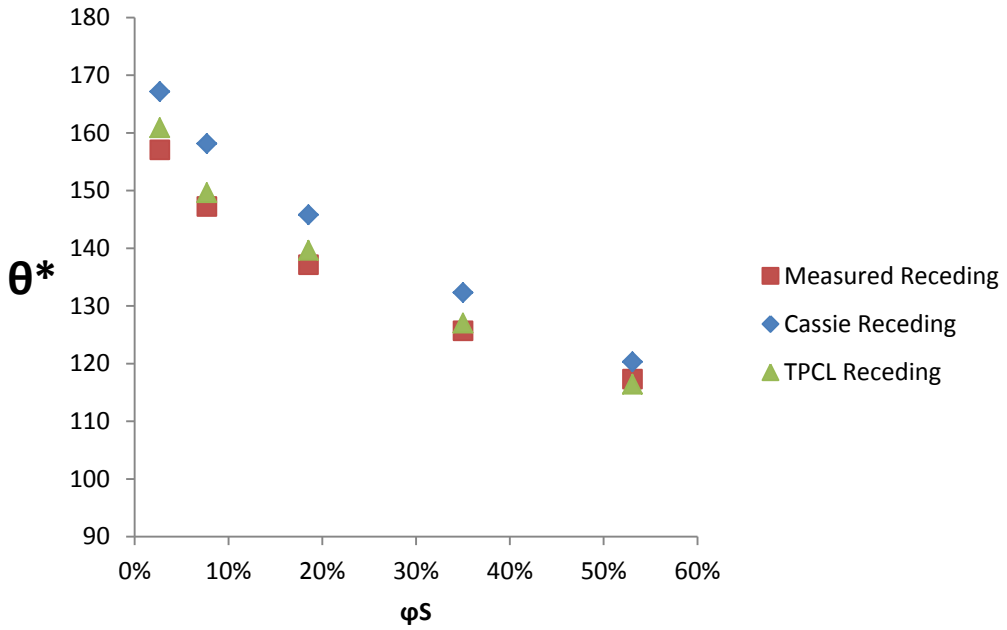


Figure 4-47. Advancing water contact angles versus solid wetted area fraction on the normal wafer, with theoretical predictions for 20µm spaced apart samples. Error on all data points is within 2 degrees.

## Discussion

### The Confinement Approach

Based on the definition of antibiotic susceptibility, it may be understood that *p. aeruginosa* (PAO1) cells attached to the surfaces did not differentiate into biofilm phenotype that could tolerate gentamicin exposure at the concentration and exposure time used. Since, *p. aeruginosa* (PAO1) was unable to form "functional" biofilms on PDMSe based on the susceptibility argument, direct gene expression level determination of the phenotype was not carried out in this study. A key difference from previous work with *p. aeruginosa* (PAO1) biofilm growth on PDMSe(*139*) was that a much smaller volume of nutrient and therefore **nutritional exhaustion** may have forced *p. aeruginosa* (PAO1) to switch to a more tolerant biofilm phenotype, (Figure 4-24(A): example image of mature *p. aeruginosa* (PAO1) biofilm). In this study, a 20ml nutrient volume was used; therefore an **excess availability of nutrients** may have caused the

surface attached bacteria PAO1 cells to switch to planktonic mode again, resulting in no “functional biofilm” formation. Another study cultivated *p. aeruginosa* biofilms using both a flow based and starvation based approach(*147*).

**Quorum sensing and phenotypic effects:** A remarkable study showed that by grouping bacteria at close quarter within micron sized traps revealed that even small populations of bacteria (as little as 8 PAO1 cells) can exhibit significantly increased antibiotic tolerance (thus “functional” biofilm phenotype) (*157*). The understanding that bacteria do not grow as single cell layer lawns, rather as architecturally structured microcolonies based on chemical signaling, is reiterated by the results in this study. On all topographical and the smooth PDMSe surfaces, there are areas where colonies are observed in widespread/connected communities. This indicates that in a period of 7 days, in the case *s. aureus* (SH1000) biofilms, there are certainly regions that can tolerate antibiotic action through transition to the biofilm phenotype. However, BTA suggests that there is similar quantity of bacteria based on bacterial metabolism across the different topographies and the smooth surfaces. When these two results are taken together, it may be supposed that confinement can lead to differentiation to biofilm phenotype. Thus, smaller colonies in between the topographies are also capable of differentiating in to the biofilm phenotype. The BTA observations are based only on numbers obtained from the colour change images and calibration curve analysis. The cells that survive when most of the other cells die are likely to be of persister type (*210*) after having withstood the oxacillin treatment at 120µg/ml concentration, a 100 times the minimum inhibitory concentration for 24 hours. It was shown through earlier antibiotic susceptibility tests that biofilm formation in the sense of definite presence of EPS is not

essential for decreases in antibiotic susceptibility in adherent bacteria and that slower growth rates might partially account for decreased susceptibility. Also, there is a potential connection between small colony variants, which are “slow-growing subpopulation of bacteria with distinctive phenotypic and pathogenic traits” (*211*), which display an increase biofilm forming capacity and retain resistance even in the planktonic state (*212*), and antibiotic susceptibility (*144*).

In previous work (Figure 4-48) it was suggested that slow metabolism due to the presence of bioifilm may be the cause of delayed colour change on smooth PDMSe surfaces (*134*). On the surfaces investigated in this study, the 5 µm pillar has smaller sized widely distributed microcolonies and yet it shows longer times for maximal colour change. Based on this, it maybe reasoned the using the mean PE CFU/ml readings as equivalent plate count readings may be justified.

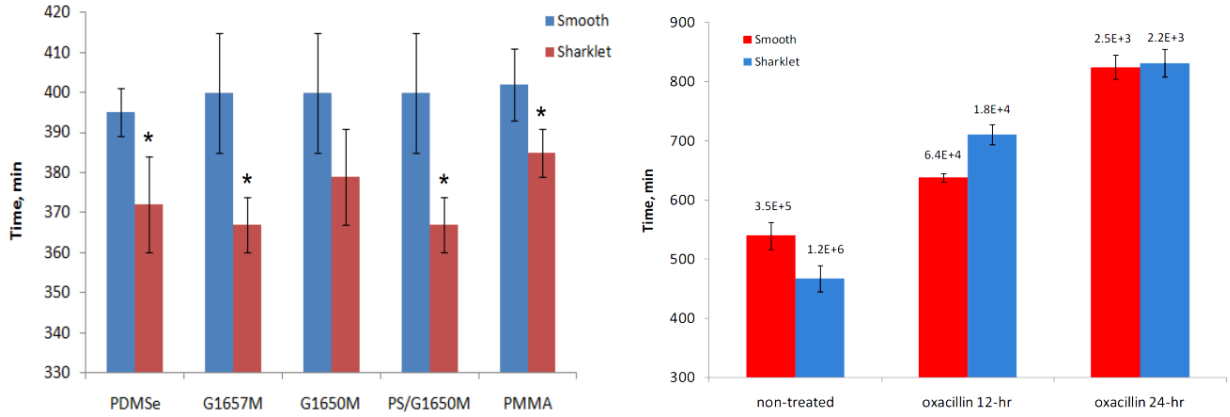


Figure 4-49. Previous study biotimer assay results post 7 days of SA growth protocol. Error bars represent one standard deviations (*134*)

In earlier work, with *s. aureus* (ATCC 35556) grown in TSB growth medium for 7 days on test surfaces, it was suggested that there was more planktonic like activity on topographies , on five different polymers versus, their smooth counterparts assessed by BTA for quantifying differences between Sharklet$^{TM}$ and smooth PDMSe (Figure 4-25).

There are three possible reasons why the data in this study differ from earlier work, they are:

- Firstly, the bacterial strain used here is different from the earlier work, it is restated to emphasize that it was necessary to choose a strain that closely matched the available NCBI genetic sequence (*206*).
- A second factor that may have contributed to the observed difference from earlier results is using a matlab program (Appendix C) to analyze BTA images for colour chage times. This was an important advance because it eliminated subjective error in making the decision of colour change based on the observer.
- The third reason could be the increased percent area of the samples tested in this study, (8 mm punches out 1.15 sq.cm wafers) representing about 39% of the total sample area versus 31% (four 8 mm punches of a nearly 1 sq. inch of sample).

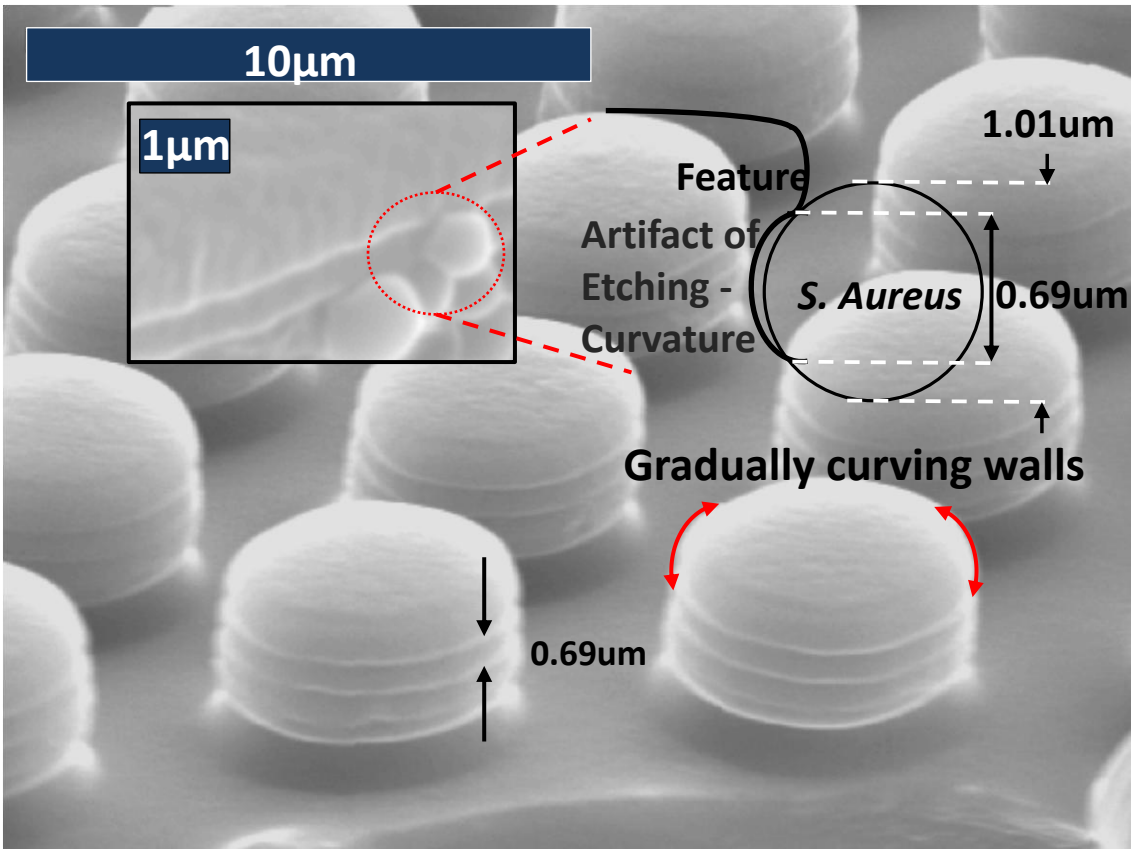


Figure 4-49. 5µm hexagonal pillar perspective view, black dimension arrow – indicates artifact of etching, about 0.69µm in diameter, slightly larger than radius of curvature of the bacterium. The inset shows an *s. aureus* (SH1000) bacterium attached to the curvature of the artifact. The red curving arrows indicate gradually change in curvature at the edge of the feature.

**Curvature effects:** Curvatures of the lesser than 100µm was shown to have an effect on the orientation of chick heart fibroblasts because greater curvatures are slight in comparison with the dimensions of the chick heart fibroblasts. It was also found the frequency of crossover of cells over a feature decreased with an increase in angle of features from 8° onwards (*44*). The flexibility of the exoskeleton of eukaryotic cells varies to a large extent and the ability of cells to crossover topographical barriers is proportional to their flexibility (*54*).

Since, bacteria are less flexible compared to cells (*58*), the curvature effects seen for some of the cells which are also less flexible compared to others may be applicable to bacteria as well. Although this may be true, the bacterial cells have been shown in this and a previous study (*17*) to be capable of forming continuous colonies over the edge of the topographical features (Figure 4-22). In the topographies used in this study (Figure 4-49) there is a gradual change in the curvature of topography over the edge of features. Thus, topographies displaying gradual changes in curvature may not be capable of confining biofilm formation.

*E. cloacae* (ATCC 700258) cell clusters and individual cells were primarily observed in the recessed regions of the topography, except for the 11µm hexagonal pillar topography. This suggests that 11µm feature size may be above the threshold value above which the valley and feature top morphology occurs with equal probability. *Escherichia coli* (*e. coli*) morphology based on a 24 hour study with 5µm, 10µm, 20µm, 30µm, 40µm and 100µm square pillars in a square array with 5µm, 10µm and 20 µm revealed a potential threshold between 15µm and 20µm beyond which no significant differences in morphology were observed. Lesser coverage was observed on the 5µm,

10µm and 15µm samples, all data in comparison to the smooth surface (*148*). The proposed threshold is very close to the 11µm threshold observed in this study.

*S. aureus* (SH1000) bacteria are found in clusters in certain areas and are found to be isolated cells in other areas (Figure 4-16 through Figure 4-24 except for Figure 4-20). This distribution appears in all the cases except the 5µm hexagonal pillars. The nature of the distribution can be attributed to the temporal variation in settlement. As indicated by the clusters of cells growing over many lattices of the features, the cells may have grown after attaching or colonized in a cluster from earlier time points. Following the initial settlement, the bacteria spread over the lattices in some regions forming the regions of dense coverage that is seen in the SEM images. On the basis of BTA based quantification all samples including the smooth sample statistically had equal numbers of bacteria. However, the 5µm hexagonal topography shows disperse small clusters, much less dense in coverage and isolated settlements. Given that this topography was exposed for the same amount of time, it was expected to have a denser coverage in certain regions. In order to explain this it is necessary to look at the dimensions involved. *S. aureus* (SH1000) diameter by SEM observation is about 1.01 ± 0.1µm and the depressed area fraction per unit cell (Table 4-1) vary from 0.08 for the 2µm hexagonal pits to 0.64 for the 5µm hexagonal pillar. Thus, the fraction available for settlement and growth within recessed area is higher than all other samples. Therefore, there appears to be lesser dense settlement throughout the sample in the 5µm hexagonal pillar topography. Although, the above arguments explain the morphology of *s. aureus* (SH1000) on the topographies, they don't adequately explain the morphology on the smooth surface, which one would expect to be colonized to a greater extent. In

order to explain this, consider the following argument; a few bacteria, once attached to a surface could provide a secondary (cell to cell) attachment site, along with other chemical cues. So, based on signals from sessile bacteria, and the sense of their surroundings, other bacteria could theoretically remain unattached (in suspension or dividing and shedding from surface attached cells) until they settle upon a suitable spot with maximal surface area (*131*) for attachment. Since patterned topographical offer a lot of such sites, additional surface area to attach to, they are capable of forming such irreversibly attached microcolonies these sites with maximum area of attachment. This may explain why they are more wide spread on the topography compared to the smooth PDMSe surface while the total number remains the same between topography and smooth surface. Also, the fact that a smooth surface has similar quantity of bacteria as that of the topographies (Figure 4-26), this can be taken as evidence that on attaching to topographical surfaces, bacteria grow at a rate similar to that of the smooth surface, despite the presence of topography.

In a related study (*213*), polyethylene terephthalate and polystyrene nanocylinders with a height of 160nm, 110nm in diameter, spaced 220nm apart were tested for biofilm formation with *s. aureus* (ATCC 25923), for a duration of 270 minutes, compared against the smooth surface with a roughness was 1 ± 0.2nm. Based on static culturing, they observed that the nanoscale surfaces did not affect the number of bacteria attached. The dimensions in the nanocylinder topography study are approximately a fifth of the bacterial diameter and since no significant effect was found to occur, this suggests that there may be a lower bound for interaction of the topography. This observation is consistent with earlier studies which suggest a lower limit of 200nm

(*124*). Another recent study tracked the effect of variation of spacing of square arrays 300nm posts from 2.2µm to 700nm apart on the morphology of *p. aeruginosa* (PA14), *bacillus subtilis* (*b. subtilis*) and *e. coli*. The bacteria were found to attach in a similar pattern in all 3 cases to the topography arrays when the spacing approached their length scales. The study was conducted in both stationary and flow modes for up to 48 hours. The author notes that up to 20 hour the spontaneous assembly was identical in both methods, but beyond 20 hours there were differences based on movement modes and nutrient media (*131*).

The SEM images of both *s. aureus* (SH1000) and *p.aeruginosa* (PAO1) and CLSM images of *e. cloacae* (ATCC 700258) on the topographies indicate that a major part of the bacterial attachment/growth occurs in the recessed portions of all patterns, which indicates that patterned topography are probably in the fully wetted state at the end of respective tests. One possible reason for this is that, the artifacts introduced by etching offer submicron features (Figure 4-49) that are only slightly smaller than the bacteria themselves. This probably provides very strong interaction points all along the sides of the topographical features.

From the observations in this study and other relevant studies in the literature, the dimensions of topography that are capable of interacting with bacteria can be narrowed down to 250nm through 10µm. Also, when the topographical features are very close together, although bacteria attach to them in an isolated manner from each other and may seem planktonic, the phenotypic changes brought about by virtue of attachment cannot be discounted. For CAUTI and other medical device applications, longer time periods might induce contiguous colony formation and expansion over the features.

Based on these arguments the original Confinement Hypothesis that **growing bacterial colonies are confined by abrupt changes in topography** is proposed to be modified to, **topography in the range of 250nm to 10µm, influences bacterial adhesion** (Figure 4-50).

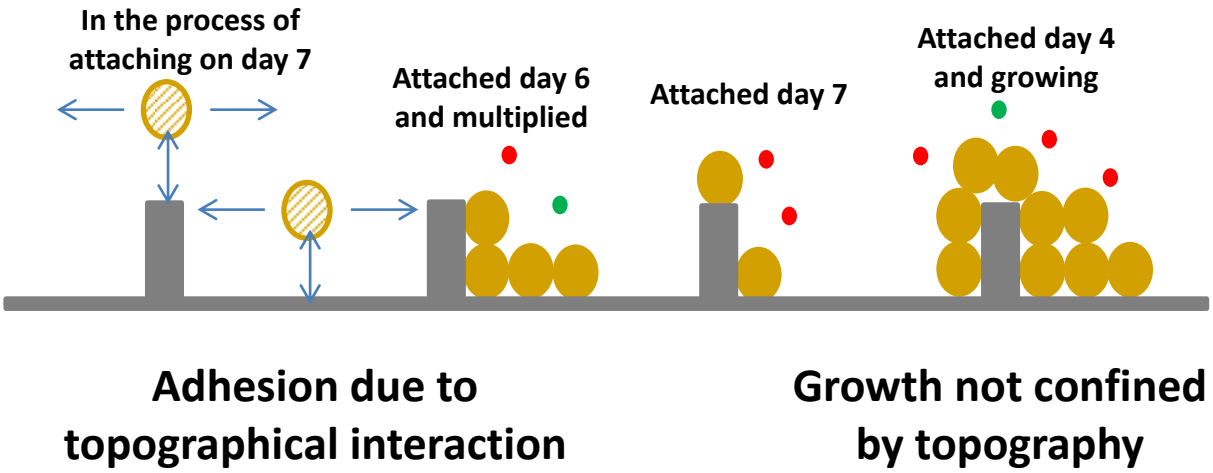


Figure 4-50. Hypothetical snapshot of the biofilm formation process on day 7. Topography influences bacterial adhesion within a certain size scale and does not confine growth.

**The Wetting Approach**

The presence of an undercut contributes to an increase in the breakthrough pressure and the within equally spaced samples there is not much of a variation across due to the extent of undercut or height. Secondly, for the samples spaced apart, feature height appears to have a significant effect on the breakthrough pressure.

These observations may be explained by taking into account bending of the water-air interface between the features due to the action of the pressure (*184*). In order to breakthrough, it may be imagined that the sag needs to reach the bottom between the undercut curves. This sag is much less in the case of the lesser spaced samples. So, they take longer to get to the initial breakthrough point but the interface may be

destroyed earlier due to the curvature caused by the increase in pressure whereas in the larger spaced samples the curvature due increase in bending undergoes a more gradual increase.

The Cassie-Baxter model is very useful, and the error in using it arises from conceptual errors. That the apparent contact angle was a weighted average is valid, provided that linear weighting was used instead of area weighting.

The maximization and minimization of differential area fractions as a droplet advances and recedes was applied to modify the Cassie-Baxter equation (*188*). However, as a droplet moves, it comes in contact with a variety of surface features. Depending on the angle of approach, the TPCL will be pinned to varying degrees by pattern. Based on this idea, the maximum and minimum linear contact fractions were calculated using a matlab code (*198*) on the basis of surface maps generated from SEM measurements in AutoCad®.

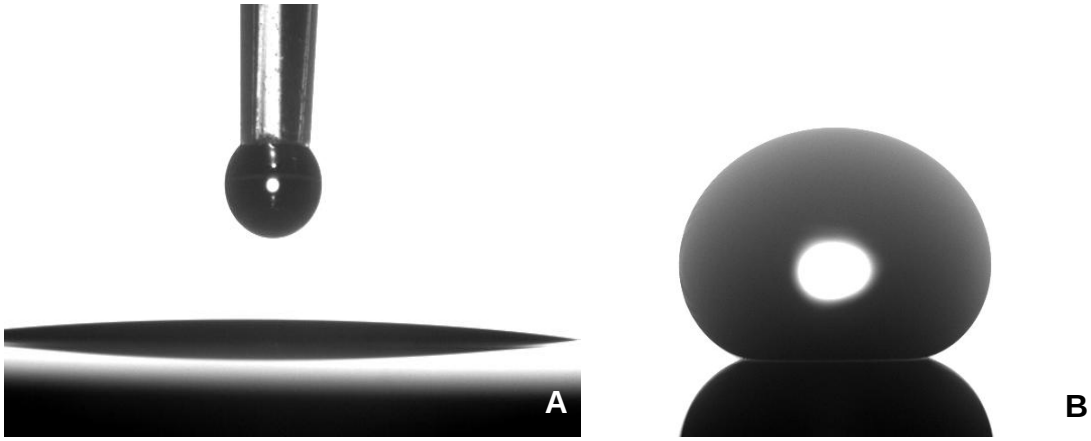


Figure 4-51. Contact angle images for 20µm spaced by 24µm with a $\varphi_S$ of 0.19 (A) 15° on cleaned, dried uncoated where water droplet is in contact with silica tops (B) 144° on surface coated with $C_4F_8$ plasma

The TPCL fractions were then used to predict dynamic contact angles. Incidentally, 300nm undercut silica capped 20 µm hexagons spaced by 24 µm pattern with a $\varphi_S$ of 0.19 were completely wetted by water without coating, and non-wetting with

C4F8 (Figure 4-51). This was different from the expected metastable states indicated on patterns without coating and silicon cap with a $\varphi_S$ of 0.25 displaying a contact angle of 144° (*183, 214*). This may be due to the lower contact angle exhibited by silica versus the contact angle of 74° shown by hydrogen terminated silicon.

Table 4-4. Example tests: material, bacterium, protocol and results

| Test Material | Bacterium | Protocol | Results |
|---|---|---|---|
| Smooth PDMSe Sharklet$^{TM}$ (*215*) | *S. aureus* | 7, 14, 21 days with media change every day | SEM image based results indicate lesser biofilm on patterned topography |
| Smooth PDMSe, PS,PMMA, SEBS Sharklet$^{TM}$ on each (*134*) | *S. aureus* | 7, 14, 21 days with media change every day | SEM and BTA results indicate lesser biofilm on patterned topography |
| Smooth PDMSe PVP coated PDMSe (*139*) | *S.aureus* *P.aeruginosa* | 4 day – every day media change followed by oxacillin treatment | SEM and plate counts indicate presence of mature biofilm |

# CHAPTER 5
# CONCLUSIONS AND SUGGESTIONS FOR FUTURE WORK

## Conclusions

The effects of different types of patterned topography on biofilm formation in the confinement and wetting approaches were studied and the conclusions are summarized as follows:

*P. aeruginosa* biofilm formation was observed on the topography in silicone elastomer and compared with smooth control using microscopic and plate count assessment. Through microscopic analysis it was observed that only sparse attachment was observed under the test conditions used here. **Despite the apparent difference in roughness, even up to 21 days, there seems to be no measurable, statistically significant differences between the surfaces under the growth conditions tested.**

A more objective method for quantification of *s. aureus* biofilm formation based on image analysis to obtain BTA colour change times was developed. Apparently, over a period of 7 days, all the pattern topographical surfaces along with the smooth PDMSe appear to have similar levels of total bacterial metabolism (based on pH change of the growth medium). However, the pillar configurations with larger recessed area but smaller spacings appear to have less ‘functional’ biofilm growth when assessed using oxacillin susceptibility. The overall trend seen with arcA (involved in L-arginine catabolism) gene expression results corroborates the oxacillin susceptibility results. Although indirect, RT-qPCR is more sensitive than BTA in detecting variation in total bacterial metabolism per sample in response to differences in surface topography.

The method for quantifying the total number of bacteria on surfaces using qPCR for *p. aeruginosa* and *s. aureus* was adapted successfully for use with polymeric

patterned topographical substrates. As this is a very sensitive method it can yield useful, reliable, and quantitative information for early time point studies, whereas plate counts and BTA methods may not be sensitive enough.

Even though patterned topography affects orientation and morphology of resulting bacterial colonization, under the test conditions used in this study**, it appears that there are no phenotypic differences between the bacterial cells growing on patterned topography and smooth surfaces.**

Progress was made in measuring and quantifying differences in breakthrough pressure which will serve as design rules for fabricating undercut patterned topography for the inhibition biofilm formation. Breakthrough pressure measurements indicated that smaller spacings between topography are capable of resisting initial breakthrough but have an overall lower final breakthrough pressure. Whereas, larger spaced topography have a lower initial breakthrough but have a higher overall final breakthrough pressure. Breakthrough pressure appears to be most dependent on the height of features.

- A design, such as the novel cross topography, with features capable of remaining undistorted at large feature heights, with an undercut could be a useful candidate in testing the biofilm formation inhibition efficacy.
- **Linear fractions on a TPCL based approach are able to predict receding contact angle data more accurately than an areal solid wetted fraction based approach (Cassie-Baxter model)**

## Suggestions for Future Work

Based on the current work, there are several interesting questions that still need to be answered with regards to the use of patterned topography for biofilm inhibition.

The use of tests based on biofilm formation by expanding from a central bore hole, as used in some models, is suitable only for certain applications. This would probably depend entirely upon wetting; since, bacteria require the presence of water in order

develop a biofilm. This would imply that any surface design capable of impeding the advance of the wetted interface should be capable of inhibiting biofilm formation. Such designs maybe based on the criteria provided from the model devised in the wetting approach on undercut surfaces.

In order to test the hypothesis that recessed area fraction combined with smaller spacing may be important for delaying biofilm formation, it is possible to design an experiment where the spacing can be varied using different patterns, while keeping the recessed area fraction constant. In all cases, increasing the height would directly contribute to the stability of trapped air pockets (breakthrough pressure section in wetting approach). When the height is increased, especially for PDMSe, it was shown that the 2 µm pillars do not remain rigid. Patterns such as the cross, and other hypothetical ones, should be able to maintain rigidity at such small dimensions, with an increase in the height, due to mutual support of the intersecting beam type structure.

Creeping of water in to the capillaries formed by patterned topography over time, and due to bacterial action, also needs to be studied. It has been suggested that undercut features on polymers may enhance inhibitory effect of patterned topography on biofilms. But as observed in the 11µm and 21µm pillar topographies, it may be argued that a static column of liquid may be pinned by undercut structures. However, as bacteria secrete many types of molecules, these features may modify the air water interfaces (surface tension) at capillary sites by coating the solid, and/or may facilitate creep by lowering the surface energy. Thus given time, factoring the creep of water into the capillaries, all such designs may be expected to involve a completely wetted system. From the hypothesis that smaller colonies in between the topographies are also

capable of differentiating into biofilm phenotype, future attempts at using patterned topography to inhibit biofilm formation should investigate topographies designed to prevent any type of contact between bacteria. In order to better understand the effects of topography on presence of persister cells and/or small colony variants, a confocal imaging based surface map with live/dead staining following antibiotic susceptibility will provide a better understanding of nature of bacterial adhesion, advancing topography as a method for biofilm inhibition.

One of the limitations of the current study is the growth protocol. The biofilms were grown in a stagnant column of liquid media. While this applies to situations where there are stagnant pools leading to biofilm growth, other applications such as industrial pipelines, ship hulls, and in some instances even catheters, deal with flow based systems. Also, there are additional stresses which make biofilms, such as starvation, that were not dealt with in this study. Future work should also include assays to determine the effect of patterned topography on biofilm growth under such stresses as flow and nutritional limitation.

The nature of the breakthrough pressure measurement conducted in this study was at best qualitative and needs to be developed further on at least two counts:

- Droplet on surface penetration tests: Generating droplets from a height may be important for characterizing the material.
- Long-term submersion tests: Long-term submersion may be relevant for biofilm formation.

A more objective method needs to be developed to quantify the relationships between breakthrough pressure, undercut and height hinted at in this study. A model needs to be developed so that surfaces can be design on the basis of the model for more robust submersed states. Using this and the roll-off models, it should be possible

to design surfaces that have very similar apparent contact angle and hysteresis, but different geometries on a given material. Another possibility is to design surfaces with very similar apparent contact angle and hysteresis, but different surface properties and geometries. When these surfaces are tested for applications such as biofilm formation, it may be possible to dissociate the effect of geometry on such processes, thus better designs can be made.

One method by which water breakthrough over long term could be tested is to use a low concentration dye solution capable of adsorbing quickly onto a hydrophobic surface, and mapping the dye adsorption on the surface as a function of time.

It is possible to make lithographic molds with undercut at the ends of channels. A simple over etching step at the end of a Bosch process could easily yield a undercut cap in an elastomeric polymer such as silicone elastomer (Figure 4-2 F).

Another possibility is to use silicon on insulator (SOI) type wafers. As a process recipe, the etching should be done until the insulator layer is reach following which any attempts to etch will result in an undercut. This can then be used as a mold to produce undercut topographies on silicone elastomer.

APPENDIX A
SEM IMAGING OF SAMPLE WITH AND WITHOUT MECHANICAL TREATMENT FOR PLATE COUNT PROTOCOL FOR *PSEUDOMONAS AERUGINOSA*

In order to make sure that the plate count protocol completely removes PA biofilm from test specimens, SEM images Figure A-1 (1) & (2) were obtained before and after the plate count protocol. These images clearly indicate complete removal of PA biofilm from the surface of the wafers. These images are from 7 day biofilm tests.

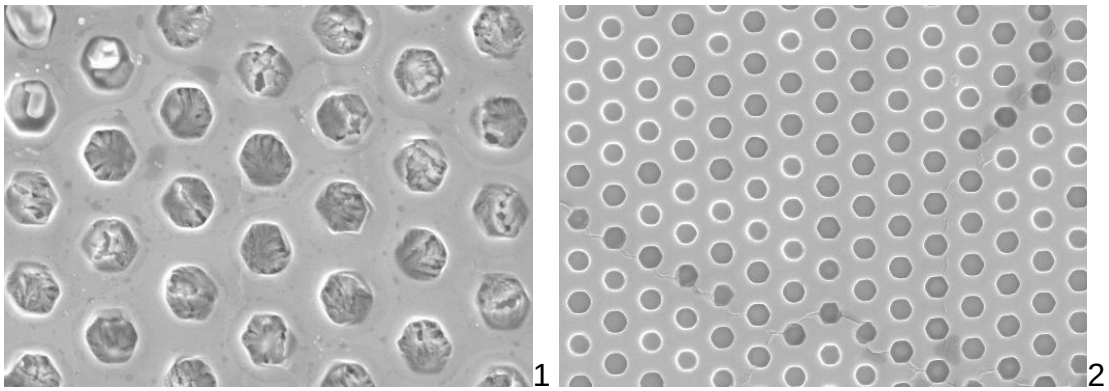

1 2

Figure A-1. Sample areas on the 10µm honeycomb pattern: 1) with sonication and vortexing; 2) without sonication and vortexing

The process of sonication and vortexing removes most of the material attached to the surface and thus can be used in the plate count procedure.

APPENDIX B

*PSUEDOMONAS AERUGINOSA* ROCHESTER STRAIN BIOFILM FORMATION

Figure B-1 represents plate count based CFU/ml measurements obtained from the samples tested for PA Rochester biofilm formation, following the growth protocol for 21 days. PA Rochester is a clinical isolate which was previously characterized as being able to form biofilm like growth on smooth PDMSe surfaces based on EPS coated colonies observed by SEM analysis, following a 14 day growth protocol. 200µg/ml of gentamicin, used to elucidate differences based on gentamicin susceptibility, was chosen as the upper concentration limit based on previous work in which PAO1 biofilm formation was studied on a porcine skin model (*74*). As stated earlier, considering bacterial growth rates, the differences may not be significant even though

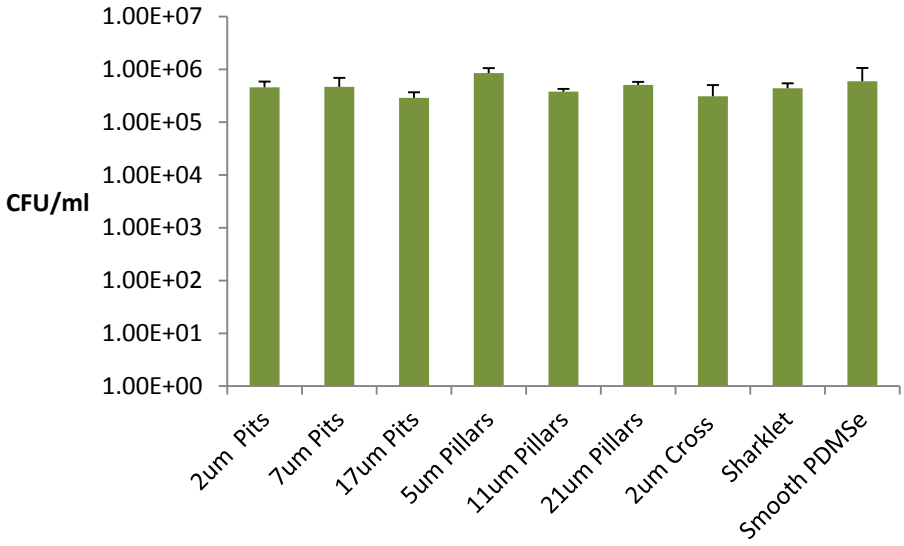


Figure B-1. Number of colony forming units following 21 day biofilm growth on hexagonal pit, pillar, cross pattern, Sharklet™, and smooth PDMSe surface.

Data analysis indicates that there was no statistically significant difference between the various patterns, nor between the patterned and smooth surfaces.

# APPENDIX C
## MATLAB CODE FOR ANALYZING BTA IMAGES FOR COLOR CHANGE

```
function intensity = AnSH1000E27DOXCCD

prefix='DSCSH1000E27DOXCCD(';

suffix=').JPG';

pic=[1:121];

for t=1:numel(pic)

    img=[prefix,num2str(pic(t)),suffix];

    im  = imread(img);

    imagesc(im);

    pos=floor(ginput(2));

    im=im(pos(3):pos(4),pos(1):pos(2),:);

    a   = double(im);

    r   = a(:,:,1)/255;

    g   = a(:,:,2)/255;

    b   = a(:,:,3)/255;

    mask = r-b >0.2;

    mask = bwareaopen(mask,6000,4);

    stats = regionprops(mask,'PixelIdxList');

    len = length(stats);

    for obj=1:len %for loop with obj counting up from 1 to the length of the variable
stats to obtain the mean green index value of various objects within a binary image as a
means to compare the BTA results%
```

```
        index=stats(obj).PixelIdxList;  % this command assigns the PixelIdxList values
from the variable stats corresponding to the 1st object in it%
        indexmatrix(obj)=mean(g(index)); % the variable intensity is created in order to
store the mean of all the green pixel values in each object for each image and is output
into the main program%
            end
            for obj=1:len
                y(obj,t)=(indexmatrix(obj)/indexmatrix(len));
            end
            subplot(2,1,1)
            imagesc(mask)
            subplot(2,1,2)
            imagesc(im)
            pause(2)
            close all
        end
        intensity = y; %the values obtained here are then processed, colour change points
are obtained and interpolated with the standard curve to obtain mean PE CFU/ml
        end
```

APPENDIX D
POLYMERASE CHAIN REACTION DATA, GRAPHS AND GEL RESULTS

Graph in Figure 4-32 was used to obtain the data, given in Table D-1 below for the qPCR results with SA biofilm formation.

Table D-1 Real-time PCR quantification data – SH1000 qPCR

| Pattern | CT Mean | CT SD | SQ Mean | SQ SD |
|---|---|---|---|---|
| 2µm Pits | 19.38 | 0.37 | 0.09 | 0.03 |
| 7µm Pits | 19.24 | 0.45 | 0.11 | 0.05 |
| 17µm Pits | 19.26 | 0.52 | 0.11 | 0.04 |
| 5µm Pillars | 20.02 | 0.49 | 0.05 | 0.02 |
| 11µm Pillars | 18.74 | 1.54 | 0.27 | 0.22 |
| 21µm Pillars | 18.05 | 0.53 | 0.34 | 0.18 |
| 2µm Cross | 17.26 | 0.52 | 0.71 | 0.32 |
| Sharklet$^{TM}$ | 19.80 | 0.15 | 0.06 | 0.01 |
| Smooth PDMSe | 20.09 | 0.62 | 0.05 | 0.02 |

Calculations for DNA start quantity to total number of cells is performed as follows.The argument follows from the accepted fact that 1µg of 1000 base pairs of DNA is equivalent to 1.52picomoles (*216*). Thus assuming 1000 base pairs is 1 DNA unit,

1µg of 1 DNA unit = 1.52pmole

1 DNA unit = $1.0925 \times 10^{-12}$µg

Given:

1 SA genome molecule = 2.821 million base pairs

1 PA genome molecule = 6.264 million base pairs

Thus,

1 SA genome molecule = $2.821 \times 10^3$ DNA units = 3.082 x 10-9 µg

1 PA genome molecule = $6.264 \times 10^3$ DNA units = 6.843 x 10-9µg

All calculations for total cell counts were based on these unit quantities.

LIST OF REFERENCES


1. H. Ceri, M. E. Olson, C. Stremick, R. R. Read, D. Morck, A. Buret, The Calgary Biofilm Device: New technology for rapid determination of antibiotic susceptibilities of bacterial biofilms. *Journal of Clinical Microbiology* **37**, 1771 (Jun, 1999).

2. J. W. Costerton, P. S. Stewart, E. P. Greenberg, Bacterial biofilms: A common cause of persistent infections. *Science* **284**, 1318 (May, 1999).

3. R. M. Donlan, J. W. Costerton, Biofilms: Survival mechanisms of clinically relevant microorganisms. *Clinical Microbiology Reviews* **15**, 167 (Apr, 2002).

4. J. W. Costerton, Z. Lewandowski, D. E. Caldwell, D. R. Korber, H. M. Lappinscott, Microbial Biofilms. *Annual Review of Microbiology* **49**, 711 (1995).

5. M. E. Callow, Callow J.A., Marine biofouling: a sticky problem. *Biologist* **49**, 10 (2002).

6. K. E. Cooksey, B. Wigglesworthcooksey, Adhesion of bacteria and diatoms to surfaces in the sea - a review. *Aquatic Microbial Ecology* **9**, 87 (1995).

7. R. M. Klevens, J. R. Edwards, C. L. Richards, T. C. Horan, R. P. Gaynes, D. A. Pollock, D. M. Cardo, Estimating health care-associated infections and deaths in US hospitals, 2002. *Public Health Reports* **122**, 160 (Mar-Apr, 2007).

8. K. S. Reed D., Infection control and prevention: a review of hospital-acquired infections and the economic implications. *Ochsner Journal* **9**, 27 (2009).

9. L. A. Mermel, Prevention of intravascular catheter-related infections. *Annals of Internal Medicine* **132**, 391 (Mar, 2000).

10. A. I. Hidron, J. R. Edwards, J. Patel, T. C. Horan, D. M. Sievert, D. A. Pollock, S. K. Fridkin, S. Natl Healthcare Safety Network Tea; Participating Natl Healthcare, Antimicrobial-Resistant Pathogens Associated With Healthcare-Associated Infections: Annual Summary of Data Reported to the National Healthcare Safety Network at the Centers for Disease Control and Prevention, 2006-2007. *Infection Control and Hospital Epidemiology* **29**, 996 (Nov, 2008).

11. J. L. Vincent, Y. Sakr, C. L. Sprung, V. M. Ranieri, K. Reinhart, H. Gerlach, R. Moreno, J. Carlet, J. R. Le Gall, D. Payen, P. Sepsis Occurrence Acutely Ill, Sepsis in European intensive care units: Results of the SOAP study. *Crit. Care Med.* **34**, 344 (Feb, 2006).

12. J. C. Tiller, C. J. Liao, K. Lewis, A. M. Klibanov, Designing surfaces that kill bacteria on contact. *Proceedings of the National Academy of Sciences of the United States of America* **98**, 5981 (May, 2001).

13. M. Hentzer, H. Wu, J. B. Andersen, K. Riedel, T. B. Rasmussen, N. Bagge, N. Kumar, M. A. Schembri, Z. J. Song, P. Kristoffersen, M. Manefield, J. W. Costerton, S. Molin, L. Eberl, P. Steinberg, S. Kjelleberg, N. Hoiby, M. Givskov, Attenuation of Pseudomonas aeruginosa virulence by quorum sensing inhibitors. *Embo Journal* **22**, 3803 (Aug, 2003).

14. M. Hentzer, K. Riedel, T. B. Rasmussen, A. Heydorn, J. B. Andersen, M. R. Parsek, S. A. Rice, L. Eberl, S. Molin, N. Hoiby, S. Kjelleberg, M. Givskov, Inhibition of quorum sensing in Pseudomonas aeruginosa biofilm bacteria by a halogenated furanone compound. *Microbiology-Sgm* **148**, 87 (Jan, 2002).

15. M. Manefield, T. B. Rasmussen, M. Henzter, J. B. Andersen, P. Steinberg, S. Kjelleberg, M. Givskov, Halogenated furanones inhibit quorum sensing through accelerated LuxR turnover. *Microbiology-Sgm* **148**, 1119 (Apr, 2002).

16. P. Kingshott, J. Wei, D. Bagge-Ravn, N. Gadegaard, L. Gram, Covalent attachment of poly(ethylene glycol) to surfaces, critical for reducing bacterial adhesion. *Langmuir* **19**, 6912 (Aug, 2003).

17. K. K. Chung, J. F. Schumacher, E. M. Sampson, R. A. Burne, P. J. Antonelli, A. B. Brennana, Impact of engineered surface microtopography on biofilm formation of Staphylococcus aureus. *Biointerphases* **2**, 89 (Jun, 2007).

18. D. G. Maki, P. A. Tambyah, Engineering out the risk for infection with urinary catheters. *Emerging Infectious Diseases* **7**, 342 (Mar-Apr, 2001).

19. W. R. Jarvis, W. J. Martone, Predominant pathogens in hospital infections. *Journal of Antimicrobial Chemotherapy* **29**, 19 (Apr, 1992).

20. T. Monson, C. M. Kunin, Evaluation of a polymer-coated indwelling catheter in prevention of infection. *Journal of Urology* **111**, 220 (1974).

21. N. S. Morris, D. J. Stickler, R. J. C. McLean, The development of bacterial biofilms on indwelling urethral catheters. *World J. Urol.* **17**, 345 (Dec, 1999).

22. T. Gilchrist, D. M. Healy, C. Drake, Controlled silver-releasing polymers and their potential for urinary-tract infection control. *Biomaterials* **12**, 76 (Jan, 1991).

23. N. S. Morris, D. J. Stickler, C. Winters, Which indwelling urethral catheters resist encrustation by Proteus mirabilis biofilms? *Br. J. Urol.* **80**, 58 (Jul, 1997).

24. E. L. Lawrence, I. G. Turner, Materials for urinary catheters: a review of their history and development in the UK. *Med. Eng. Phys.* **27**, 443 (Jul, 2005).

25. T. Reiche, G. Lisby, S. Jorgensen, A. B. Christensen, J. Nordling, A prospective, controlled, randomized study of the effect of a slow-release silver device on the frequency of urinary tract infection in newly catheterized patients. *BJU Int.* **85**, 54 (Jan, 2000).

26. J. Nakada, M. Kawahara, S. Onodera, Y. Oishi, Clinical study of Silver Lubricath Foley catheter. *Hinyokika kiyo. Acta urologica Japonica* **42**, 433 (1996, 1996).

27. M. Talja, A. Korpela, K. Jarvi, Comparison of urethral reaction to full silicone, hydrogen-coated and siliconized latex catheters. *Br. J. Urol.* **66**, 652 (Dec, 1990).

28. N. Nakagawa, N. Yashiro, Y. Nakajima, W. H. Barnhart, M. Wakabayashi, Hydrogel-coated glide catheter - experimental studies and initial clinical-experience. *Am. J. Roentgenol.* **163**, 1227 (Nov, 1994).

29. C. D. Young, J. R. Wu, T. L. Tsou, High-strength, ultra-thin and fiber-reinforced pHEMA artificial skin. *Biomaterials* **19**, 1745 (Oct, 1998).

30. M. Gray, Does the construction material affect outcomes in long-term catheterization? *J. Wound Ostomy Cont. Nurs.* **33**, 116 (Mar-Apr, 2006).

31. H. Kumon, H. Hashimoto, M. Nishimura, K. Monden, N. Ono, Catheter-associated urinary tract infections: impact of catheter materials on their management. *Int. J. Antimicrob. Agents* **17**, 311 (Apr, 2001).

32. J. N. Nacey, A. G. S. Tulloch, A. F. Ferguson, Catheter-induced urethritis - a comparison between latex and silicone catheters in a prospective clinical-trial. *Br. J. Urol.* **57**, 325 (1985).

33. C. Allison, L. Emody, N. Coleman, C. Hughes, The role of swarm cell-differentiation and multicellular migration in the uropathogenicity of proteus-mirabilis. *Journal of Infectious Diseases* **169**, 1155 (May, 1994).

34. D. Stickler, N. Morris, M. C. Moreno, N. Sabbuba, Studies on the formation of crystalline bacterial biofilms on urethral catheters. *European Journal of Clinical Microbiology & Infectious Diseases* **17**, 649 (Sep, 1998).

35. A. Marmur, Underwater superhydrophobicity: Theoretical feasibility. *Langmuir* **22**, 1400 (Feb, 2006).

36. J. Genzer, K. Efimenko, Recent developments in superhydrophobic surfaces and their relevance to marine fouling: a review. *Biofouling* **22**, 339 (2006).

37. A. Tuteja, W. Choi, M. L. Ma, J. M. Mabry, S. A. Mazzella, G. C. Rutledge, G. H. McKinley, R. E. Cohen, Designing superoleophobic surfaces. *Science* **318**, 1618 (Dec, 2007).

38. R. Poetes, K. Holtzmann, K. Franze, U. Steiner, Metastable Underwater Superhydrophobicity. *Physical Review Letters* **105**, (Oct, 2010).

39. C. W. Extrand, Model for contact angles and hysteresis on rough and ultraphobic surfaces. *Langmuir* **18**, 7991 (Oct, 2002).

40. R. G. Harrison, On the stereotropism of embryonic cells. *Science* **34**, 279 (Jul-Dec, 1911).

41. P. Weiss, In vitro experiments on the factors determining the course of the outgrowing nerve fiber. *Journal of Experimental Zoology* **68**, 393 (Aug, 1934).

42. A. S. G. Curtis, M. Varde, Control of cell behavior - topological factors. *Journal of the National Cancer Institute* **33**, 15 (1964).

43. Y. A. Rovensky, I. L. Slavnaja, J. M. Vasiliev, Behaviour of fibroblast-like cells on grooved surfaces. *Experimental Cell Research* **65**, 193 (1971).

44. G. A. Dunn, J. P. Heath, New hypothesis of contact guidance in tissue-cells. *Experimental Cell Research* **101**, 1 (1976).

45. C. S. Izzard, L. R. Lochner, Cell-to-substrate contacts in living fibroblasts - interference reflection study with an evaluation of technique. *Journal of Cell Science* **21**, 129 (1976).

46. J. P. Heath, G. A. Dunn, Cell to substratum contacts of chick fibroblasts and their relation to microfilament system - correlated interference-reflection and high-voltage electron-microscope study. *Journal of Cell Science* **29**, 197 (1978).

47. P. T. Ohara, R. C. Buck, Contact guidance invitro - light, transmission, and scanning electron-microscopic study. *Experimental Cell Research* **121**, 235 (1979).

48. C. S. Izzard, L. R. Lochner, Formation of cell-to-substrate contacts during fibroblast motility - an interference-reflexion study. *Journal of Cell Science* **42**, 81 (1980).

49. M. Abercrombie, G. A. Dunn, Adhesions of fibroblasts to substratum during contact inhibition observed by interference reflection microscopy. *Experimental Cell Research* **92**, 57 (1975).

50. M. Abercrombie, G. Dunn, J. Heath, The shape and movement of fibroblasts in culture. *Society of General Physiologists series* **32**, 57 (1977).

51. J. R. Couchman, D. A. Rees, Behavior of fibroblasts migrating from chick heart explants - changes in adhesion, locomotion and growth, and in the distribution of actomyosin and fibronectin. *Journal of Cell Science* **39**, 149 (1979).

52. J. R. Couchman, M. Lenn, D. A. Rees, Coupling of cytoskeleton functions for fibroblast locomotion. *European Journal of Cell Biology* **36**, 182 (1985).

53. D. M. Brunette, Fibroblasts on micromachined substrata orient hierarchically to grooves of different dimensions. *Experimental Cell Research* **164**, 11 (May, 1986).

54. P. Clark, P. Connolly, A. S. G. Curtis, J. A. T. Dow, C. D. W. Wilkinson, Topographical control of cell behavior .1. simple step cues. *Development* **99**, 439 (Mar, 1987).

55. J. Meyle, K. Gultig, H. Wolburg, A. F. Vonrecum, Fibroblast anchorage to microtextured surfaces. *Journal of Biomedical Materials Research* **27**, 1553 (Dec, 1993).

56. P. Weissmanshomer, M. Fry, Chick-embryo fibroblasts senescence invitro - pattern of cell-division and life-span as a function of cell density. *Mechanisms of Ageing and Development* **4**, 159 (1975).

57. A. Atabek, T. A. Camesano, Atomic force microscopy study of the effect of lipopolysaccharides and extracellular polymers on adhesion of Pseudomonas aeruginosa. *Journal of Bacteriology* **189**, 8503 (Dec, 2007).

58. K. Anselme, P. Davidson, A. M. Popa, M. Giazzon, M. Liley, L. Ploux, The interaction of cells and bacteria with surfaces structured at the nanometre scale. *Acta Biomater.* **6**, 3824 (Oct, 2010).

59. M. L. Carman, T. G. Estes, A. W. Feinberg, J. F. Schumacher, W. Wilkerson, L. H. Wilson, M. E. Callow, J. A. Callow, A. B. Brennan, Engineered antifouling microtopographies - correlating wettability with cell attachment. *Biofouling* **22**, 11 (2006).

60. L. Hoipkemeier-Wilson, J. Schumacher, M. Carman, A. Gibson, A. Feinberg, M. Callow, J. Finlay, J. Callow, A. Brennan, Antifouling potential of lubricious, micro-engineered, PDMS elastomers against zoospores of the green fouling alga Ulva (Enteromorpha). *Biofouling* **20**, 53 (2004).

61. C. M. Magin, C. J. Long, S. P. Cooper, L. K. Ista, G. P. Lopez, A. B. Brennan, Engineered antifouling microtopographies: the role of Reynolds number in a model that predicts attachment of zoospores of Ulva and cells of Cobetia marina. *Biofouling* **26**, 719 (2010).

62. C. J. Long, J. F. Schumacher, P. A. C. Robinson, J. A. Finlay, M. E. Callow, J. A. Callow, A. B. Brennan, A model that predicts the attachment behavior of Ulva linza zoospores on surface topography. *Biofouling* **26**, 411 (2010).

63. J. F. Schumacher, M. L. Carman, T. G. Estes, A. W. Feinberg, L. H. Wilson, M. E. Callow, J. A. Callow, J. A. Finlay, A. B. Brennan, Engineered antifouling microtopographies - effect of feature size, geometry, and roughness on settlement of zoospores of the green alga Ulva. *Biofouling* **23**, 55 (2007).

64. I. Alcamo E., *Fundamentals of Microbiology*. (Benjamin/Cummings, 1997).

65. J. R. Lawrence, D. R. Korber, B. D. Hoyle, J. W. Costerton, D. E. Caldwell, Optical Sectioning of Microbial Biofilms. *Journal of Bacteriology* **173**, 6558 (Oct, 1991).

66. D. R. Korber, A. Choi, G. M. Wolfaardt, D. E. Caldwell, Bacterial plasmolysis as a physical indicator of viability. *Applied and Environmental Microbiology* **62**, 3939 (Nov, 1996).

67. J. R. Lawrence, T. R. Nie, G. D. W. Swerhone, Application of multiple parameter imaging for the quantification of algal, bacterial and exopolymer components of microbial biofilms. *Journal of Microbiological Methods* **32**, 253 (May, 1998).

68. M. S. Chae, H. Schraft, Comparative evaluation of adhesion and biofilm formation of different Listeria monocytogenes strains. *International Journal of Food Microbiology* **62**, 103 (Dec, 2000).

69. D. C. Ren, J. J. Sims, T. K. Wood, Inhibition of biofilm formation and swarming of Escherichia coli by (5Z)-4-bromo-5(bromomethylene)-3-butyl-2(5H)-furanone. *Environmental Microbiology* **3**, 731 (Nov, 2001).

70. H. Beyenal, C. Donovan, Z. Lewandowski, G. Harkin, Three-dimensional biofilm structure quantification. *Journal of Microbiological Methods* **59**, 395 (Dec, 2004).

71. A. Heydorn, A. T. Nielsen, M. Hentzer, C. Sternberg, M. Givskov, B. K. Ersboll, S. Molin, Quantification of biofilm structures by the novel computer program COMSTAT. *Microbiology-Uk* **146**, 2395 (Oct, 2000).

72. A. Heydorn, B. K. Ersboll, M. Hentzer, M. R. Parsek, M. Givskov, S. Molin, Experimental reproducibility in flow-chamber biofilms. *Microbiology-Uk* **146**, 2409 (Oct, 2000).

73. J. T. Walker, C. W. Keevil, Study of Microbial Biofilms Using Light-Microscope Techniques. *International Biodeterioration & Biodegradation* **34**, 223 (1994).

74. P. Phillips, Q. Yang, G. Schultz, Antimicrobial efficacy of negative pressure wound therapy (npwt) plus instillation of antimicrobial solutions against mature pseudomonas aeruginosa biofilm. *Wound Repair and Regeneration* **19**, A42 (Mar-Apr, 2011).

75. W. J. Drury, W. G. Characklis, P. S. Stewart, Interactions of 1 mu-m latex-particles with pseudomonas-aeruginosa biofilms. *Water Research* **27**, 1119 (Jul, 1993).

76. W. J. Drury, P. S. Stewart, W. G. Characklis, Transport of 1-mu-m latex-particles in pseudomonas-aeruginosa biofilms. *Biotechnol. Bioeng.* **42**, 111 (Jun, 1993).

77. O. Wanner, W. Gujer, A multispecies biofilm model. *Biotechnol. Bioeng.* **28**, 314 (Mar, 1986).

78. P. Stoodley, D. Debeer, Z. Lewandowski, Liquid flow in biofilm systems. *Applied and Environmental Microbiology* **60**, 2711 (Aug, 1994).

79. D. Debeer, P. Stoodley, Z. Lewandowski, Liquid flow in heterogeneous biofilms. *Biotechnol. Bioeng.* **44**, 636 (Aug, 1994).

80. F. L. Roe, Z. Lewandowski, T. Funk, Simulating microbiologically influenced corrosion by depositing extracellular biopolymers on mild steel surfaces. *Corrosion* **52**, 744 (Oct, 1996).

81. P. M. Armenante, D. Kafkewitz, G. Lewandowski, C. M. Kung, Integrated anaerobic-aerobic process for the biodegradation of chlorinated aromatic-compounds. *Environmental Progress* **11**, 113 (May, 1992).

82. S. Dikshitulu, B. C. Baltzis, G. A. Lewandowski, S. Pavlou, Competition between 2 microbial-populations in a sequencing fed-batch reactor - theory, experimental-verification, and implications for waste treatment applications. *Biotechnol. Bioeng.* **42**, 643 (Aug, 1993).

83. B. C. Baltzis, G. A. Lewandowski, J. H. Wang, Denitrification with a strain of pseudomonas denitrificans - fundamental kinetic-studies and their implications for bioreactor design. *Abstracts of Papers of the American Chemical Society* **205**, 26 (Mar, 1993).

84. P. Phillips, paper presented at the Wounds Internationl, South Africa, 25/05/2010 2010.

85. E. J. Bouwer, Theoretical investigation of particle deposition in biofilm systems. *Water Research* **21**, 1489 (Dec, 1987).

86. D. Lopez, H. Vlamakis, R. Kolter, Biofilms. *Cold Spring Harbor Perspect. Biol.* **2**, (Jul, 2010).

87. D. G. Davies, M. R. Parsek, J. P. Pearson, B. H. Iglewski, J. W. Costerton, E. P. Greenberg, The involvement of cell-to-cell signals in the development of a bacterial biofilm. *Science* **280**, 295 (Apr, 1998).

88. R. R. C. J.W. Costerton, *Eds. Native Aquatic Bacteria: Enumeration, Activity and Ecology*. (ASTM Press Philadelphia, 1979).

89. K. Sauer, A. K. Camper, G. D. Ehrlich, J. W. Costerton, D. G. Davies, Pseudomonas aeruginosa displays multiple phenotypes during development as a biofilm. *Journal of Bacteriology* **184**, 1140 (Feb, 2002).

90. A. D. Zobell CE, Observations on the multiplication of bacteria in different volumes of stored seawater and the influence of oxygen tension and solid surfaces. *Biological Bulletin* **71**, 324 (1936).

91. K. A. Jensen E T, Lam K, Costerton JW. , Human polymorphonuclear leukocyte response to *pseudomonas aeruginosa* biofilms. *Infect. Immun.* **58**, 2383 (1990).

92. S. J. Anwar H, Costerton JW, Establishment of aging biofilms: a possible mechanism of bacterial resistance to antimicrobial therapy. *Antimicrob. Agents Chemother.* **36**, 1347 (1992).

93. S. J. Anwar H, Costerton JW, Susceptibility of biofilm cells of pseudomonas aeruginosa to bactericidal actions of whole blodd and serum. *FEMS Microbiol. Lett.* **92**, 235 (1992).

94. W. P. Brown MRW, The influence of the environment on envelope properties affecting survival of bacteria in infections. *Annual Review of Microbiology* **39**, 527 (1985).

95. S. M. Boomer, K. L. Noll, G. G. Geesey, B. E. Dutton, Formation of Multilayered Photosynthetic Biofilms in an Alkaline Thermal Spring in Yellowstone National Park, Wyoming. *Applied and Environmental Microbiology* **75**, 2464 (Apr, 2009).

96. D. Meyer-Dombard, A. Dibbell, A. S. Bradley, E. L. Shock, R. E. Summons, Microbial diversity and SIP investigations of streamer biofilm communities in Yellowstone National Park. *Geochimica Et Cosmochimica Acta* **71**, A661 (Aug, 2007).

97. T. M. Salmassi, J. J. Walker, D. K. Newman, J. R. Leadbetter, N. R. Pace, J. G. Hering, Community and cultivation analysis of arsenite oxidizing biofilms at Hot Creek. *Environmental Microbiology* **8**, 50 (Jan, 2006).

98. J. G. Banwell, R. Howard, D. Cooper, J. W. Costerton, Intestinal microbial-flora after feeding phytohemagglutinin lectins (phaseolus-vulgaris) to rats. *Applied and Environmental Microbiology* **50**, 68 (1985).

99. C. Van Delden, B. H. Iglewski, Cell-to-cell signaling and Pseudomonas aeruginosa infections. *Emerging Infectious Diseases* **4**, 551 (Oct-Dec, 1998).

100. M. B. Miller, B. L. Bassler, Quorum sensing in bacteria. *Annual Review of Microbiology* **55**, 165 (2001).

101. M. J. Federle, B. L. Bassler, Interspecies communication in bacteria. *Journal of Clinical Investigation* **112**, 1291 (Nov, 2003).

102. D. T. Hughes, V. Sperandio, Inter-kingdom signalling: communication between bacteria and their hosts. *Nature Reviews Microbiology* **6**, 111 (Feb, 2008).

103. J. M. Yarwood, D. J. Bartels, E. M. Volper, E. P. Greenberg, Quorum sensing in Staphylococcus aureus biofilms. *Journal of Bacteriology* **186**, 1838 (Mar, 2004).

104. J. W. Warren, Catheter-associated urinary tract infections. *Infectious Disease Clinics of North America* **11**, 609 (Sep, 1997).

105. D. J. Stickler, Bacterial biofilms and the encrustation of urethral catheters. *Biofouling* **9**, 293 (1996).

106. F. E. B. Foley, A self-retaining bag catheter - For use as an indwelling catheter for constant drainage of the bladder. *Journal of Urology* **38**, 140 (Jul, 1937).

107. D. R. Absolom, F. V. Lamberti, Z. Policova, W. Zingg, C. J. Vanoss, A. W. Neumann, Surface Thermodynamics of Bacterial Adhesion. *Applied and Environmental Microbiology* **46**, 90 (1983).

108. C. J. Van Oss, Interaction forces between biological and other polar entities in water - how many different primary forces are there. *Journal of Dispersion Science and Technology* **12**, 201 (1991, 1991).

109. R. Bos, H. C. van der Mei, H. J. Busscher, Physico-chemistry of initial microbial adhesive interactions - its mechanisms and methods for study. *Fems Microbiology Reviews* **23**, 179 (Apr, 1999).

110. J. L. Hutter, J. Bechhoefer, MANIPULATION OF VANDERWAALS FORCES TO IMPROVE IMAGE-RESOLUTION IN ATOMIC-FORCE MICROSCOPY. *Journal of Applied Physics* **73**, 4123 (May, 1993).

111. E. Arunan, G. R. Desiraju, R. A. Klein, J. Sadlej, S. Scheiner, I. Alkorta, D. C. Clary, R. H. Crabtree, J. J. Dannenberg, P. Hobza10, Definition of the hydrogen bond (IUPAC Recommendations 2011). *Pure Appl. Chem* **83**, 1637 (2011).

112. B. Deryagin, N. Churaev, Structure of water in thin layers. *Langmuir* **3**, 607 (1987).

113. C. J. Vanoss, M. K. Chaudhury, R. J. Good, Interfacial lifshitz-vanderwaals and polar interactions in macroscopic systems. *Chem. Rev.* **88**, 927 (Sep-Oct, 1988).

114. R. M. Pashley, J. N. Israelachvili, MOLECULAR LAYERING OF WATER IN THIN-FILMS BETWEEN MICA SURFACES AND ITS RELATION TO HYDRATION FORCES. *Journal of Colloid and Interface Science* **101**, 511 (1984).

115. W. A. Ducker, T. J. Senden, R. M. Pashley, MEASUREMENT OF FORCES IN LIQUIDS USING A FORCE MICROSCOPE. *Langmuir* **8**, 1831 (Jul, 1992).

116. A. Roosjen, H. J. Kaper, H. C. van der Mei, W. Norde, H. J. Busscher, Inhibition of adhesion of yeasts and bacteria by poly(ethylene oxide)-brushes on glass in a parallel plate flow chamber. *Microbiology-Sgm* **149**, 3239 (Nov, 2003).

117. C. J. v. Oss, *Interfacial Forces in Aqueous Media*. (Marcel Dekker,, New York, 1994).

118. M. Lampin, R. WarocquierClerout, C. Legris, M. Degrange, M. F. SigotLuizard, Correlation between substratum roughness and wettability, cell adhesion, and cell migration. *Journal of Biomedical Materials Research* **36**, 99 (Jul, 1997).

119. Y. Liu, Q. Zhao, Influence of surface energy of modified surfaces on bacterial adhesion. *Biophysical Chemistry* **117**, 39 (Aug, 2005).

120. M. Geoghegan, J. S. Andrews, C. A. Biggs, K. E. Eboigbodin, D. R. Elliott, S. Rolfe, J. Scholes, J. J. Ojeda, M. E. Romero-Gonzalez, R. G. J. Edyvean, L. Swanson, R. Rutkaite, R. Fernando, Y. Pen, Z. Y. Zhang, S. A. Banwart, The polymer physics and chemistry of microbial cell attachment and adhesion. *Faraday Discuss.* **139**, 85 (2008).

121. A. Roosjen, H. J. Busscher, W. Nordel, H. C. van der Mei, Bacterial factors influencing adhesion of Pseudomonas aeruginosa strains to a poly(ethylene oxide) brush. *Microbiology-Sgm* **152**, 2673 (Sep, 2006).

122. M. Katsikogianni, Y. Missirlis, Concise review of mechanisms of bacterial adhesion to biomaterials and of techniques used in estimating bacteria-material interactions. *Eur Cell Mater* **8**, 37 (2004).

123. H. C. van der Mei, R. Bos, H. J. Busscher, A reference guide to microbial cell surface hydrophobicity based on contact angles. *Colloids and Surfaces B-Biointerfaces* **11**, 213 (Jul, 1998).

124. W. Teughels, N. Van Assche, I. Sliepen, M. Quirynen, Effect of material characteristics and/or surface topography on biofilm development. *Clin. Oral Implant. Res.* **17**, 68 (Oct, 2006).

125. M. N. Bellonfontaine, N. Mozes, H. C. Vandermei, J. Sjollema, O. Cerf, P. G. Rouxhet, H. J. Busscher, A comparison of thermodynamic approaches to predict the adhesion of dairy microorganisms to solid substrata. *Cell Biophysics* **17**, 93 (Aug, 1990).

126. L. Ploux, S. Beckendorff, M. Nardin, S. Neunlist, Quantitative and morphological analysis of biofilm formation on self-assembled monolayers. *Colloids and Surfaces B-Biointerfaces* **57**, 174 (Jun, 2007).

127. R. Oliveira, Understanding adhesion: A means for preventing fouling. *Experimental Thermal and Fluid Science* **14**, 316 (May, 1997).

128. M. Quirynen, Bollen, C.M., Eyssen, H. & van Steenberghe, D., Microbial penetration along the implant components of the Branemark system. An in vitro study. *Clin. Oral Implant. Res.* **5**, 239 (1994).

129. M. B. Quirynen, C.M., The influence of surface roughness and surface-free energy on supra- and subgingival plaque formation in man. A review of the literature. *Journal of Clinical Periodontology* **22**, (1995).

130. M. Quirynen, Bollen, C.M., Papaioannou, W., Van Eldere, J. & van Steenberghe, D., The influence of titaniumabutment surface roughness on plaque accumulation and gingivitis: short-term observations. *International Journal of Oral & Maxillofacial Implants* **11**, 169 (1996).

131. A. I. Hochbaum, J. Aizenberg, Bacteria Pattern Spontaneously on Periodic Nanostructure Arrays. *Nano Letters* **10**, 3717 (Sep, 2010).

132. B. Pokroy, S. H. Kang, L. Mahadevan, J. Aizenberg, Self-Organization of a Mesoscale Bristle into Ordered, Hierarchical Helical Assemblies. *Science* **323**, 237 (Jan, 2009).

133. M. E. Davey, G. A. O'Toole, Microbial biofilms: from ecology to molecular genetics. *Microbiology and Molecular Biology Reviews* **64**, 847 (Dec, 2000).

134. L. Jin, Fabrication of microengineerd polymeric films and investigation of bioresponses of substrata, *Dissertation*, University of florida (2010).

135. J. A. Lichter, M. T. Thompson, M. Delgadillo, T. Nishikawa, M. F. Rubner, K. J. Van Vliet, Substrata mechanical stiffness can regulate adhesion of viable bacteria. *Biomacromolecules* **9**, 1571 (Jun, 2008).

136. C. Diaz, P. L. Schilardi, P. C. D. Claro, R. C. Salvarezza, M. de Mele, Submicron Trenches Reduce the Pseudomonas fluorescens Colonization Rate on Solid Surfaces. *ACS Applied Materials & Interfaces* **1**, 136 (Jan, 2009).

137. H. Beyenal, Z. Lewandowski, G. Harkin, Quantifying biofilm structure: Facts and fiction. *Biofouling* **20**, 1 (Feb, 2004).

138. R. D. Waite, A. Papakonstantinopoulou, E. Littler, M. A. Curtis, Transcriptome analysis of Pseudomonas aeruginosa growth: Comparison of gene expression in planktonic cultures and developing and mature biofilms. *Journal of Bacteriology* **187**, 6571 (Sep, 2005).

139. P. J. Antonelli, E. M. Sampson, C. Ojano-Dirain, Biofilm formation on silicone tympanostomy tubes with polyvinylpyrrolidone coating. *Archives of Otolaryngology-Head & Neck Surgery* **137**, 19 (Jan, 2011).

140. T. F. Mah, B. Pitts, B. Pellock, G. C. Walker, P. S. Stewart, G. A. O'Toole, A genetic basis for Pseudomonas aeruginosa biofilm antibiotic resistance. *Nature* **426**, 306 (Nov, 2003).

141. X. M. Yang, H. Beyenal, G. Harkin, Z. Lewandowski, Quantifying biofilm structure using image analysis. *Journal of Microbiological Methods* **39**, 109 (Jan, 2000).

142. H. J. Busscher, A. H. Weerkamp, H. C. Vandermei, A. W. J. Vanpelt, H. P. Dejong, J. Arends, Measurement of the surface free-energy of bacterial-cell surfaces and its relevance for adhesion. *Applied and Environmental Microbiology* **48**, 980 (1984, 1984).

143. S. McEldowney, M. Fletcher, Effect of growth-conditions and surface characteristics of aquatic bacteria on their attachment to solid-surfaces. *Journal of General Microbiology* **132**, 513 (Feb, 1986).

144. I. Williams, W. A. Venables, D. Lloyd, F. Paul, I. Critchley, The effects of adherence to silicone surfaces on antibiotic susceptibility in Staphylococcus aureus. *Microbiology-Uk* **143**, 2407 (Jul, 1997).

145. J. A. Wu, C. Kusuma, J. J. Mond, J. F. Kokai-Kun, Lysostaphin disrupts Staphylococcus aureus and Staphylococcus epidermidis biofilms on artificial surfaces. *Antimicrobial Agents and Chemotherapy* **47**, 3407 (Nov, 2003).

146. D. Campoccia, L. Montanaro, C. R. Arciola, The significance of infection related to orthopedic devices and issues of antibiotic resistance. *Biomaterials* **27**, 2331 (Apr, 2006).

147. S. S. Rogers, C. van der Walle, T. A. Waigh, Microrheology of Bacterial Biofilms In Vitro: Staphylococcus aureus and Pseudomonas aeruginosa. *Langmuir* **24**, 13549 (Dec, 2008).

148. S. Y. Hou, H. A. Gu, C. Smith, D. C. Ren, Microtopographic Patterns Affect Escherichia coil Biofilm Formation on Poly(dimethylsiloxane) Surfaces. *Langmuir* **27**, 2686 (Mar, 2011).

149. G. L. a. R. Pettipher, U.M., Semi-automated counting of bacteria and somatic cells in milk using epifluorescence microscopy and television image analysis. *J. Appl. Bacterial.* **53**, 323 (1982).

150. M. E. Sieracki, Johnson, P.W. and Sieburth, M., Detection, enumeration, and sizing of planktonic bacteria by image-analyzed epifluorescence microscopy. *Appl. Environ. Microb.* **49**, 799 (1985).

151. Y. H. An, R. J. Friedman, R. A. Draughn, E. A. Smith, J. H. Nicholson, J. F. John, Rapid quantification of staphylococci adhered to titanium surfaces using image analyzed epifluorescence microscopy. *Journal of Microbiological Methods* **24**, 29 (Nov, 1995).

152. R. F. Berlutti F, Bosso P, Giansanti F, Ajello M, De Rosa A, Quantitative evaluation of bacteria adherent to polyelectrolyte hema based hydrogels. *Journal of Biomedical Materials Research* **67A**, 18 (2003).

153. J. A. T. Sandoe, J. Wysome, A. P. West, J. Heritage, M. H. Wilcox, Measurement of ampicillin, vancomycin, linezolid and gentamicin activity against enterococcal biofilms. *Journal of Antimicrobial Chemotherapy* **57**, 767 (Apr, 2006).

154. F. Pantanella, P. Valenti, A. Frioni, T. Natalizi, L. Coltella, F. Berlutti, BioTimer Assay, a new method for counting Staphylococcus spp. in biofilm without sample manipulation applied to evaluate antibiotic susceptibility of biofilm. *Journal of Microbiological Methods* **75**, 478 (Dec, 2008).

155. G. S. Chen FC, Comparison of rapid ATP bioluminiscence assay and standard plate count methods for assessing microbial contamination of consumers' refrigerators. *Journal of Food Prot.* **69**, 2534 (2006).

156. L. Silbert, I. Ben Shlush, E. Israel, A. Porgador, S. Kolusheva, R. Jelinek, Rapid chromatic detection of bacteria by use of a new biomimetic polymer sensor. *Applied and Environmental Microbiology* **72**, 7339 (Nov, 2006).

157. J. L. Connell, A. K. Wessel, M. R. Parsek, A. D. Ellington, M. Whiteley, J. B. Shear, Probing Prokaryotic Social Behaviors with Bacterial "Lobster Traps". *Mbio* **1**, (Sep-Oct, 2010).

158. W. Barthlott, C. Neinhuis, Purity of the sacred lotus, or escape from contamination in biological surfaces. *Planta* **202**, 1 (May, 1997).

159. X. F. Gao, L. Jiang, Water-repellent legs of water striders. *Nature* **432**, 36 (Nov, 2004).

160. W. Lee, M. K. Jin, W. C. Yoo, J. K. Lee, Nanostructuring of a polymeric substrate with well-defined nanometer-scale topography and tailored surface wettability. *Langmuir* **20**, 7665 (Aug, 2004).

161. K. Koch, B. Bhushan, W. Barthlott, Diversity of structure, morphology and wetting of plant surfaces. *Soft Matter* **4**, 1943 (2008).

162. A. Marmur, The lotus effect: Superhydrophobicity and metastability. *Langmuir* **20**, 3517 (Apr, 2004).

163. E. Martines, K. Seunarine, H. Morgan, N. Gadegaard, C. D. W. Wilkinson, M. O. Riehle, Superhydrophobicity and superhydrophilicity of regular nanopatterns. *Nano Letters* **5**, 2097 (Oct, 2005).

164. M. L. Ma, R. M. Hill, Superhydrophobic surfaces. *Current Opinion in Colloid & Interface Science* **11**, 193 (Oct, 2006).

165. X. M. Li, D. Reinhoudt, M. Crego-Calama, What do we need for a superhydrophobic surface? A review on the recent progress in the preparation of superhydrophobic surfaces. *Chemical Society Reviews* **36**, 1350 (2007).

166. B. Bhushan, Biomimetics: lessons from nature - an overview. *Philos. Trans. R. Soc. A-Math. Phys. Eng. Sci.* **367**, 1445 (Apr, 2009).

167. S. H. Hsu, W. M. Sigmund, Artificial Hairy Surfaces with a Nearly Perfect Hydrophobic Response. *Langmuir* **26**, 1504 (Feb, 2010).

168. B. Bhushan, Y. C. Jung, Natural and biomimetic artificial surfaces for superhydrophobicity, self-cleaning, low adhesion, and drag reduction. *Prog. Mater. Sci.* **56**, 1 (Jan, 2011).

169. P. van der Wal, U. Steiner, Super-hydrophobic surfaces made from Teflon. *Soft Matter* **3**, 426 (2007).

170. M. T. Khorasani, H. Mirzadeh, Z. Kermani, Wettability of porous polydimethylsiloxane surface: morphology study. *Applied Surface Science* **242**, 339 (Apr, 2005).

171. H. Y. Erbil, A. L. Demirel, Y. Avci, O. Mert, Transformation of a simple plastic into a superhydrophobic surface. *Science* **299**, 1377 (Feb, 2003).

172. X. Y. Lu, C. C. Zhang, Y. C. Han, Low-density polyethylene superhydrophobic surface by control of its crystallization behavior. *Macromolecular Rapid Communications* **25**, 1606 (Sep, 2004).

173. H. Liu, L. Feng, J. Zhai, L. Jiang, D. B. Zhu, Reversible wettability of a chemical vapor deposition prepared ZnO film between superhydrophobicity and superhydrophilicity. *Langmuir* **20**, 5659 (Jul, 2004).

174. S. Shibuichi, T. Onda, N. Satoh, K. Tsujii, Super water-repellent surfaces resulting from fractal structure. *J. Phys. Chem.* **100**, 19512 (Dec, 1996).

175. M. L. Ma, R. M. Hill, J. L. Lowery, S. V. Fridrikh, G. C. Rutledge, Electrospun poly(styrene-block-dimethylsiloxane) block copolymer fibers exhibiting superhydrophobicity. *Langmuir* **21**, 5549 (Jun, 2005).

176. P. Muthiah, S. H. Hsu, W. Sigmund, Coaxially Electrospun PVDF-Teflon AF and Teflon AF-PVDF Core-Sheath Nanofiber Mats with Superhydrophobic Properties. *Langmuir* **26**, 12483 (Aug, 2010).

177. R. Scheffler, N. S. Bell, W. Sigmund, Electrospun Teflon AF fibers for superhydrophobic membranes. *Journal of Materials Research* **25**, 1595 (Aug, 2010).

178. S. D. Bhagat, C. S. Oh, Y. H. Kim, Y. S. Ahn, J. G. Yeo, Methyltrimethoxysilane based monolithic silica aerogels via ambient pressure drying. *Microporous and Mesoporous Materials* **100**, 350 (Mar, 2007).

179. A. Balmert, H. F. Bohn, P. Ditsche-Kuru, W. Barthlott, Dry Under Water: Comparative Morphology and Functional Aspects of Air-Retaining Insect Surfaces. *Journal of Morphology* **272**, 442 (Apr, 2011).

180. N. J. Shirtcliffe, G. McHale, M. I. Newton, The Superhydrophobicity of Polymer Surfaces: Recent Developments. *Journal of Polymer Science Part B-Polymer Physics* **49**, 1203 (Sep, 2011).

181. J. Bico, C. Marzolin, D. Quere, Pearl drops. *Europhysics Letters* **47**, 220 (Jul, 1999).

182. D. Quere, M. Reyssat, Non-adhesive lotus and other hydrophobic materials. *Philos. Trans. R. Soc. A-Math. Phys. Eng. Sci.* **366**, 1539 (May, 2008).

183. L. L. Cao, H. H. Hu, D. Gao, Design and fabrication of micro-textures for inducing a superhydrophobic behavior on hydrophilic materials. *Langmuir* **23**, 4310 (Apr, 2007).

184. A. Tuteja, W. Choi, J. M. Mabry, G. H. McKinley, R. E. Cohen, Robust omniphobic surfaces. *Proceedings of the National Academy of Sciences of the United States of America* **105**, 18200 (Nov, 2008).

185. A. Marmur, Super-hydrophobicity fundamentals: implications to biofouling prevention. *Biofouling* **22**, 107 (2006).

186. A. Kosar, C. J. Kuo, Y. Peles, Boiling heat transfer in rectangular microchannels with reentrant cavities. *International Journal of Heat and Mass Transfer* **48**, 4867 (Nov, 2005).

187. H. Kubo, H. Takamatsu, H. Honda, Effects of size and number density of micro-reentrant cavities on boiling heat transfer from a silicon chip immersed in degassed and gas-dissolved FC-72. *Journal of Enhanced Heat Transfer* **6**, 151 (1999).

188. W. Choi, A. Tuteja, J. M. Mabry, R. E. Cohen, G. H. McKinley, A modified Cassie-Baxter relationship to explain contact angle hysteresis and anisotropy on non-wetting textured surfaces. *Journal of Colloid and Interface Science* **339**, 208 (Nov, 2009).

189. A. B. D. Cassie, S. Baxter, Wettability of porous surfaces. *Transactions of the Faraday Society* **40**, 0546 (1944).

190. L. C. Gao, T. J. McCarthy, Contact angle hysteresis explained. *Langmuir* **22**, 6234 (Jul, 2006).

191. T. Young, An essay on the cohesion of fluids. *Philos. Trans. R. Soc.* **95**, 65 (1805).

192. R. N. Wenzel, Resistance of solid surfaces to wetting by water. *Industrial and Engineering Chemistry* **28**, 988 (1936).

193. D. C. Pease, The significance of the contact angle in relation to the solid surface. *J. Phys. Chem.* **49**, 107 (1945).

194. L. C. Gao, T. J. McCarthy, Reply to "Comment on How Wenzel and Cassie Were Wrong by Gao and McCarthy". *Langmuir* **23**, 13243 (Dec, 2007).

195. L. C. Gao, T. J. McCarthy, How Wenzel and Cassie were wrong. *Langmuir* **23**, 3762 (Mar, 2007).

196. M. V. Panchagnula, S. Vedantam, Comment on how Wenzel and Cassie were wrong by Gao and McCarthy. *Langmuir* **23**, 13242 (Dec, 2007).

197. G. McHale, Cassie and Wenzel: Were they really so wrong? *Langmuir* **23**, 8200 (Jul, 2007).

198. E. Mckenna, An investigation into wetting and two phase heat transfer on reetrant textured surfaces, *Dissertation*, University of Florida (2011).

199. Y. T. Cheng, D. E. Rodak, Is the lotus leaf superhydrophobic? *Applied Physics Letters* **86**, (Apr, 2005).

200. L. C. Gao, T. J. McCarthy, An Attempt to Correct the Faulty Intuition Perpetuated by the Wenzel and Cassie "Laws". *Langmuir* **25**, 7249 (Jul, 2009).

201. F. E. Bartell, G. B. Hatch, The wetting characteristics of galena. *J. Phys. Chem.* **39**, 11 (Jan, 1935).

202. J. J. Bikerman, Surface roughness and contact angle. *Journal of Physical and Colloid Chemistry* **54**, 653 (1950).

203. R. E. Johnson, R. H. Dettre, Contact angle hysteresis .3. study of an idealized heterogeneous surface. *J. Phys. Chem.* **68**, 1744 (1964).

204. J. F. Joanny, P. G. Degennes, A model for contact-angle hysteresis. *Journal of Chemical Physics* **81**, 552 (1984).

205. C. A. Curtis J., in *Biomaterials science: an introduction to materials in medicine,* B. D. Ratner, Hoffman A.S., Schoen F.J., Lemons J.E. , Ed. (Elsevier, San Diego, 2004), pp. p. 697-707.

206. A. J. O'Neill, Staphylococcus aureus SH1000 and 8325-4: comparative genome sequences of key laboratory strains in staphylococcal research. *Letters in Applied Microbiology* **51**, 358 (Sep, 2010).

207. K. E. Beenken, P. M. Dunman, F. McAleese, D. Macapagal, E. Murphy, S. J. Projan, J. S. Blevins, M. S. Smeltzer, Global gene expression in Staphylococcus aureus biofilms. *Journal of Bacteriology* **186**, 4665 (Jul, 2004).

208. L. L. Pelletier, C. B. Baker, OXACILLIN, CEPHALOTHIN, AND VANCOMYCIN TUBE MACRODILUTION MBC RESULT REPRODUCIBILITY AND EQUIVALENCE TO MIC RESULTS FOR METHICILLIN-SUSCEPTIBLE AND REPUTEDLY TOLERANT STAPHYLOCOCCUS-AUREUS ISOLATES. *Antimicrobial Agents and Chemotherapy* **32**, 374 (Mar, 1988).

209. A. F. Stalder, G. Kulik, D. Sage, L. Barbieri, P. Hoffmann, A snake-based approach to accurate determination of both contact points and contact angles. *Colloids and Surfaces A: Physicochemical and Engineering Aspects* **286**, 92 (2006).

210. K. Lewis, Persister cells, dormancy and infectious disease. *Nature Reviews Microbiology* **5**, 48 (Jan, 2007).

211. R. A. Proctor, C. von Eiff, B. C. Kahl, K. Becker, P. McNamara, M. Herrmann, G. Peters, Small colony variants: a pathogenic form of bacteria that facilitates persistent and recurrent infections. *Nature Reviews Microbiology* **4**, 295 (Apr, 2006).

212. R. Singh, P. Ray, A. Das, M. Sharma, Role of persisters and small-colony variants in antibiotic resistance of planktonic and biofilm-associated Staphylococcus aureus: an in vitro study. *Journal of Medical Microbiology* **58**, 1067 (Aug, 2009).

213. D. Campoccia, L. Montanaro, H. Agheli, D. S. Sutherland, V. Pirini, M. E. Donati, C. R. Arciola, Study of Staphylococcus aureus adhesion on a novel nanostructured surface by chemiluminometry. *International Journal of Artificial Organs* **29**, 622 (Jun, 2006).

214. W. Choi, Micro-Textured Surfaces for Omniphobicity and Drag-Reduction, *Dissertation*, Massachusetts Institute of Technology (2009).

215. J. F. Schumacher, Control of marine biofouling and medical biofilm formation with engineered topography, *Dissertation*, University of Florida (2007).

216. O. Kurauchi, T. Furui, A. Itakura, H. Ishiko, M. Sugiyama, Y. Ohno, H. Ando, A. Tanamura, T. Ishida, A. Nawa, S. Nomura, S. Mizutani, Y. Tomoda, Studies on transmission of hepatitis-c virus from mother-to-child in the perinatal-period. *Archives of Gynecology and Obstetrics* **253**, 121 (Sep, 1993).

# BIOGRAPHICAL SKETCH

Ravikumar Vasudevan was born to Vasumathi and Vasudevan in 1985, in Madras, Tamil Nadu, India. He completed the first 14 years of his education at Vidya Mandir Senior Secondary School, Mylapore, Madras, and spent a lot of his time playing outdoor sports including badminton and cricket. During this time, he discovered his interest in all things scientific and chemistry in particular, through Dr. Nagarajan's mentoring and Seetharaman's support.

To equip him for the opportunity (problem) filled world, he received his bachelor's degree in chemical engineering, through a 4 year program at Sri Venkateswara College of Engineering, from Anna University in August 2006, where he met his future wife to be, Sowmya.

Following his dream of pursuing a career in research, he applied to and was accepted in to the doctoral program for materials science and engineering at the University of Florida. In the 5 years spent at UF, he worked on areas ranging from the study of wetting, its effects on biofilm formation, gastropod behavior and relaxed with his "Looti Gumbal", fun group. Subsequently, he received his PhD from the University of Florida in the fall of 2011.

Aside from his main interest in solving research problems, he enjoys sports, exercising, reading, practicing music and spending time with his family and friends. He also happens to be a "Zubaan ka Gulaam" meaning a slave to good food.